Norwegian University
of Life Sciences

Master's Thesis 2023 45 ECTS
Faculty of Chemistry, Biotechnology and Food Science

Investigating the effects of methanol on ammonia-oxidising archaea in marine sediment microcosms

Julie Martin
Master's in Technology - Chemistry and Biotechnology

Summary

Ammonia-oxidising archaea (AOA) are dominant in nutrient-scarce marine sediments and are important primary producers sustaining the activity of other microorganisms. They are also assumed to be globally important producers of vitamin B12, which is essential to all living organisms. Previous research has shown that AOA are inhibited by various organic compounds, including methanol. Therefore, we aimed to assess how AOA are affected by the presence of methanol in concentrations corresponding to treated wastewater.

The aim was addressed by enriching AOA in marine sediments using a microcosm approach. Sediments enriched with AOA were thereafter exposed to methanol in concentrations simulating treated wastewater. The microbial activity was monitored by measuring the pH, ORP, and concentration of nitrogen species in the microcosms. Metabarcoding and qPCR were employed to assess the microbial diversity and metabolic potential in the microcosm sediments. To ensure proper targeting of archaeal DNA, a preliminary primer evaluation was carried out.

We did observe signs of ammonia-oxidising activity, although we could not attribute it to AOA. While the relative abundance of AOA decreased in the presence of methanol, there were little signs of an absolute decrease in their abundance. Altogether, we did not observe a direct inhibition of AOA by methanol, possibly due to the initially low concentration of methanol. Unexpectedly, the main archaeal response to methanol was the enrichment of *Methanosarciniales*, which might have contributed to keeping the concentration of methanol at a minimum by converting it to methane. We conclude that the interplay between AOA and methane-producing archaea might be an interesting aspect for further investigation.

Sammendrag

Ammoniumoksiderende arker (AOA) er dominerende mikroorganismer i næringsfattige marine sedimenter. AOA produserer viktige næringsstoffer som opprettholder veksten til andre mikroorganismer. Det antas også at AOA er globalt viktige produsenter av vitamin B12, som er essensielt for alle levende organismer. Tidligere studier har imidlertid vist at AOA hemmes av forskjellige organiske forbindelser, deriblant metanol. Vi ønsket derfor å undersøke hvordan marine AOA påvirkes av metanol i konsentrasjoner tilsvarende det som er tillatt i renset avløpsvann.

For å undersøke dette, startet vi med å anrike AOA i mikrokosmos av marine sedimenter. Sedimenter som viste tegn til å være anriket med AOA ble deretter utsatt for metanol i konsentrasjoner tilsvarende det som er tillatt i renset avløpsvann. Den mikrobielle aktiviteten i sedimentene ble overvåket med pH- og redoksmålinger, samt kvantitering av ulike nitrogenforbindelser. For å få innsyn i hvilke mikroorganismer som var til stede i mikrokosmaene, benyttet vi oss av qPCR og metabarcoding. Siden disse metodene er primer-avhengige, gjorde vi også en evaluering av arke-spesifikke primere.

Vi observerte tegn på ammoniumoksiderende aktivitet, men den kunne ikke med sikkerhet tilskrives AOA. Selv om den relative forekomsten av AOA sank i nærvær av metanol, var det lite som tydet på en reduksjon i absolutt forekomst. Vi observerte altså ikke at metanol hemmet AOA i mikrokosmaene. Dette kan muligens henge sammen med at metanol ble tilsatt i relativt lav konsentrasjon. Den største responsen på metanol observert i arkeriket, var den uventede anrikningen av *Methanosarciniales*, som kan ha bidratt med å holde metanolkonsentrasjonen lav ved å omdanne metanol til metan. Vi konkluderer derfor med at samspillet mellom AOA og metanproduserende arker kan være et interessant aspekt for videre forskning.

Acknowledgements

I would like to express my deepest gratitude to my supervisors Knut and Inga, for their invaluable guidance and feedback. Thank you for generously sharing your knowledge and expertise, and for always having your door open.

I also could not have undertaken this journey without the patience and advice from the rest of the MiDiv group, who welcomed me warmly from the first day. Thank you, Else, Morten, Ida, Tonje, Karen, Oda, Ewelina, and Lars.

I am also grateful to Johanne and Jenny, for your proofreading help and advice, and for always believing in me. I would be remiss in not mentioning Ole-Kristian, Fanny, Emilie, and Marte, for their emotional support. Lastly, I would like to thank my dog Whisky, for tirelessly keeping me company and taking me out for relaxing walks.

Abbreviations and definitions

16S rRNA: A highly conserved gene encoding the small ribosomal subunit in bacteria and archaea. The gene is a widely used marker gene for PCR- and sequencing-based analyses of environmental samples, because of its variable and conserved regions.

***amoA*:** The gene encoding the A subunit of the ammonia monooxygenase enzyme, which catalyses the first step in the oxidation of ammonia. *amoA* is a widely used marker gene for AOA and AOB and differs in sequence between the two domains.

AMO: The ammonia monooxygenase enzyme, which catalyses the first step of ammonia oxidation in AOA and AOB.

AOA: Ammonia-oxidising archaea.

AOB: Ammonia-oxidising bacteria.

C_q: The qPCR cycle at which the fluorescent signal of a DNA or RNA sequence surpasses the background noise and can be quantified. The C_q can be used to estimate the initial number of the target sequence in a sample.

Electron donor and electron acceptor: Cells can exploit the energy released when electron donors transfer electrons to an electron acceptor. The amount of energy released increases with the increasing difference in oxidation state between the electron donor and the terminal electron acceptor. Therefore, highly reduced electron donors, such as ammonia, and highly oxidised electron acceptors, such as oxygen, are energetically favourable.

***In situ*:** "in the original place", i.e., measurements taken in the natural context of the phenomenon of interest.

***In silico*:** "in silicon", i.e., experiments conducted on a computer.

***In vitro*:** "in glass", i.e., experiments conducted with cells or molecules in a test tube. This term signifies that the experiment in question is performed outside the normal biological context of the biological material analysed.

MGI: Marine Group I Archaea is a subgroup of *Nitrososphaerota* living in marine dark zones, including sediments.

N_0: The efficiency-corrected initial target quantity (N_0) of an amplified sequence of DNA or RNA, as estimated by qPCR. N_0 takes into account the amplification efficiency and the quantification threshold of the qPCR, thereby accommodating more nuanced information than raw C_q values. N_0 is expressed in relative fluorescence units (RFU).

ORP: The oxidation reduction potential (ORP) defines which energy-generating reactions are most likely to take place in a system where energy generation occurs through the transfer of electrons from electron donors to electron acceptors. The ORP determines which microorganisms can generate enough energy to grow, depending on which electron donors and acceptors they are able to use. A low ORP indicates that sulphate reduction and methanogenesis are more feasible, while a high ORP indicates that oxygen is available as a terminal electron acceptor for aerobic energy generation.

Table of contents

1 Introduction

Marine microorganisms play a crucial role in the global cycling of elements (Arrigo, 2005). It is estimated that microorganisms account for ≈ 70% of the total marine biomass (Bar-On et al., 2018), and their activity forms the basis of marine food webs. The marine bottoms represent an important part of marine ecosystems and harbours a vast diversity of unknown microorganisms. Microorganisms living in the marine bottom sediments are in charge of storing substantial amounts of organic carbon, but might also have global importance for the cycling of other elements, such as nitrogen and sulphur (Cavicchioli et al., 2019; Orcutt et al., 2011).

1.1 Anthropogenic impact on marine environments

The marine bottoms are recipients of sedimentation and diffusion from the overlying water. Sedimentation is a result of erosion from land as well as primary production in the water column and surface water (Smith et al., 1999). Primary production involves the production of organic compounds from CO_2 using energy from light or chemical compounds. In the water column and surface, primary production is carried out by autotrophic organisms including phytoplankton and macroalga. The organic compounds from autotrophic activity represent sources of carbon and energy for heterotrophic microorganisms, that are unable to fixate CO_2. Heterotrophic degradation of organic compounds requires available terminal electron acceptors[1], of which oxygen is the most energetically favourable. As the organic compounds are degraded, carbon is remineralised, meaning that CO_2 or other inorganic forms of carbon are regenerated. Organic compounds that are not remineralised are stored in the marine floors, which represent a carbon sink that removes carbon from the active carbon cycle (Munn, 2019).

Marine primary producers are often limited by the availability of nitrogen (Elser et al., 2007). Although the atmosphere consists of ≈ 80% of nitrogen gas (N_2), this form of nitrogen is inaccessible to most organisms. However, some microorganisms can convert nitrogen gas to ammonia (NH_3) through a process called nitrogen fixation. Ammonia is the most reduced form

[1] To produce energy that can be used in cellular processes, electrons are transferred from an electron donor to a terminal electron acceptor. Each transfer releases energy that is used by the cell to fuel energy-demanding processes. The amount of energy released increases with the increasing oxidation state of the terminal electron acceptor. Therefore, oxygen is often a preferred terminal electron acceptor.

of nitrogen, making it an essential electron donor[2] in marine habitats. Its bioavailability is evident by its many possible pathways in the nitrogen cycle (Figure 1), and microorganisms can assimilate it into organic compounds or oxidise it to obtain energy. Organic nitrogen is demineralised back to ammonia through ammonification, which is performed by degraders. Ammonia can also be oxidised through a two-step process called nitrification (Figure 1). It is carried out in two strictly aerobic steps, where oxygen is used as the terminal electron acceptor. The first step of nitrification involves the oxidation of ammonia to nitrite (NO_2^-) and is mostly carried out by ammonia-oxidising archaea (AOA) in the open ocean. The second step of nitrification is performed by nitrite-oxidising bacteria and involves the oxidation of nitrite to nitrate (NO_3^-). Nitrate is a favourable terminal electron acceptor in the absence of oxygen, due to its highly oxidised state. Therefore, a wide range of microorganisms can switch to reducing nitrate when oxygen is depleted, which is illustrated by the many possible cycling pathways of nitrate (Figure 1). Assimilatory and dissimilatory reduction of nitrate keeps the nitrogen in a bioavailable state. On the other hand, denitrification and anammox are two strictly anaerobic processes converting bioavailable nitrogen into gaseous forms of nitrogen, ultimately returning the bioavailable forms of nitrogen to the atmosphere (Hutchins & Capone, 2022).

Anthropogenic activities including agriculture, combustion, and wastewater disposal have caused a substantial increasing input of nitrate and ammonia to terrestrial and aquatic environments (Smith et al., 1999). Because these forms of bioavailable nitrogen are usually limited in marine environments, the increased supply results in an excessive enrichment of planktonic organisms, known as algal blooms. The sedimentation of dead alga and organic compounds fuels the heterotrophic activity in the water columns and marine bottoms, resulting in seasonal or permanent oxygen depletion killing fish and sedimentary animals (Munn, 2019).

In marine bottom sediments, the abundance of bacteria is largely controlled by the availability of organic nutrients (Danovaro et al., 2016), to which sedimentation contributes substantially. Because eutrophication is strongly affected by anthropogenic activity, there is more organic material available heterotrophic activity closer to land. The degradation of organic compounds

[2] To produce energy that can be used in cellular processes, electrons are transferred from an electron donor to an electron acceptor. Each transfer releases energy that is used by the cell to fuel energy-demanding processes. The amount of energy released increases with the decreasing oxidation state of the electron donor. Therefore, highly reduced electron donors, such as ammonia, are the most energetically favourable electron donors.

quickly consumes oxygen, leaving the bottom sediments anoxic. Marine bottoms impacted by high sedimentation rates are dominated by anaerobic microorganisms, such as sulphate-reducing bacteria, methanogenic and methanotrophic archaea, and fermentative microorganisms. As the distance to land increases, more oxygen is left in the sediments, allowing aerobic microorganisms to thrive (Orsi, 2018). Oxic top layer sediments are characterised by a high bacterial diversity including the alpha, delta, and gamma subclasses of *Proteobacteria, Acidobacteria, Actinobacteria,* and *Planctomycetes*, while the archaea are mainly represented by ammonia-oxidising archaea belonging to *Nitrososphaerota* (Orcutt et al., 2011). Therefore, the microbial composition and activity in marine bottom sediments are highly affected by anthropogenic activity.

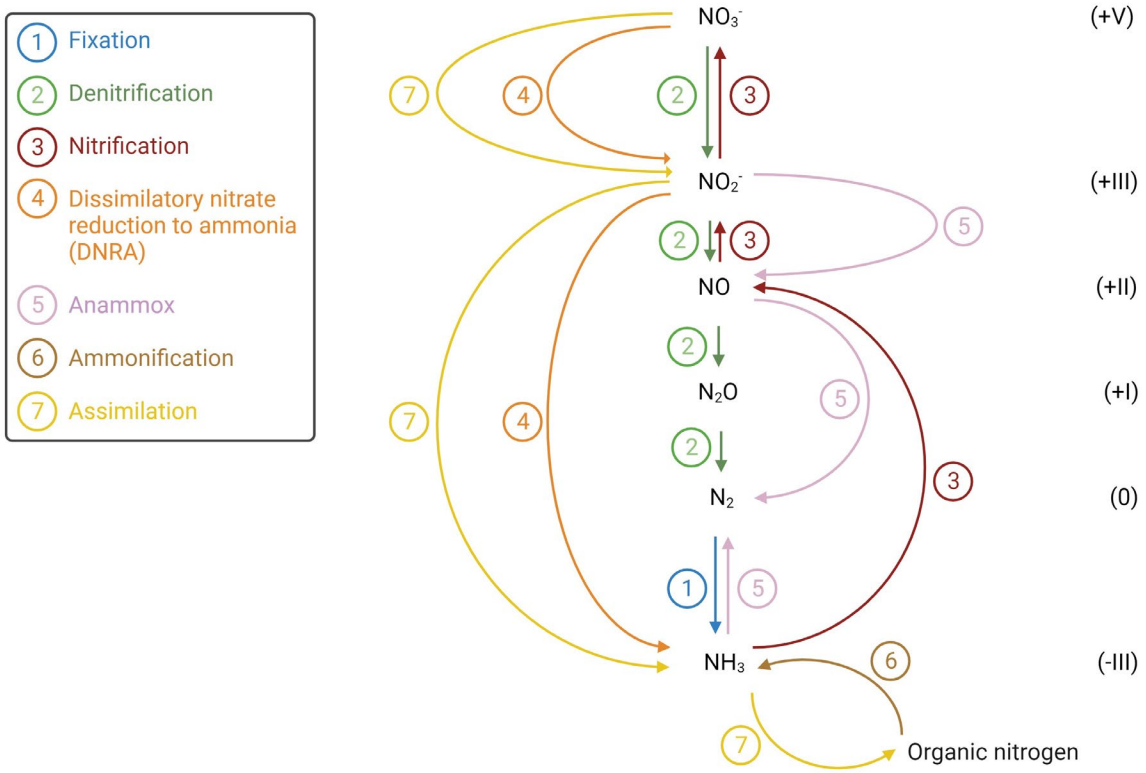

Figure 1: The nitrogen cycle. The different pathways of nitrogen cycling are separated by colours and numbering. The oxidation state of the different nitrogen species is indicated in roman numerals to the right in the figure. The figure was made with BioRender.

1.2 Wastewater treatment

Wastewater treatment plants release purified wastewater in rivers, lakes, and marine environments. However, little is known about the impact of these discharges on the aquatic

microorganisms. The discharge of preliminary treated wastewater has been shown to increase the concentrations of organic matter, ammonia, and other nutrients, affecting the community composition in the water and bottom sediments of the recipient ecosystem (Nogales et al., 2011; Ruprecht et al., 2021; Zhang et al., 2008). However, there are still major holes in our understanding of the cause and effect of these observations.

The production of wastewater from human industry and households is unavoidable. To minimise the contribution of wastewater disposal to eutrophication, nutrients can be removed biologically. Organic compounds are first removed by heterotrophic microorganisms. Thereafter, ammonia is oxidised to nitrate and nitrite. Both steps take place in tanks supplied with oxygen to enhance the efficiency of the organic degradation and because nitrification is strictly aerobic. The last treatment step is denitrification, which is performed in anaerobic conditions. Here, nitrogen is removed from the wastewater by reducing nitrate and nitrite to gaseous forms of nitrogen (Figure 1) (Pepper et al., 2011).

The removal of nitrogen by denitrification is a heterotrophic process that requires available organic carbon. The chemical oxygen demand (COD) is an indirect measure of the organic content of the wastewater and describes the amount of oxygen required to oxidise the organic matter chemically. Stoichiometrically, the requirement of organic carbon for denitrification is 2.86 g COD per gram of nitrate (Pelaz et al., 2018). However, up to 11 g COD per gram of nitrate is required to obtain an efficient nitrogen removal in the wastewater treatment process (Ruscalleda Beylier et al., 2011). Because the organic matter is degraded in the first step of wastewater purification, an external source of organic carbon is added to enhance the nitrifying process in the third step. Methanol is often used, because it is cost-effective and highly efficient in terms of increasing the denitrifying activity (Lu et al., 2014; Nyberg et al., 1992; Park & Yoo, 2009).

The excess of methanol added to drive the last step of wastewater purification raises the question of how much methanol remains in the wastewater after the final treatment step. While the total nitrogen, including organic nitrogen, ammonia, nitrate, and nitrite, in treated wastewater should not exceed 15 mg L^{-1}, the maximum permitted COD of purified wastewater is 125 mg O_2 L^{-1} (Forurensningsforskriften, 2004). The considerable difference between the permitted emissions of organic compounds and nitrogen reflects our objective to avoid eutrophication, which is usually linked to the anthropogenic emissions of bioavailable nitrogen

and not to organic carbon. Moreover, it suggests that there might be a considerable amount of methanol left in the treated wastewater.

1.3 Ammonia-oxidising archaea (AOA)

Below the sediment surface, the microorganisms are largely represented by archaea (Biddle et al., 2006; Lipp et al., 2008). Archaea constitute one of the three domains of life alongside Bacteria and Eukaryotes. They were initially separated into two phyla, the *Euryarchaeota* and *Crenarchaeota*, which were thought to thrive only in extreme environments. However, the development of molecular techniques contributed to discovering formerly unknown mesophilic[3] ammonia-oxidising archaea. These archaea were recognised as a separate archaeal phylum, *Thaumarchaeota* (Brochier-Armanet et al., 2008), later renamed *Nitrososphaerota* (Oren & Garrity, 2021; Whitman et al., 2018).

The Marine Group I (MGI) is a subgroup of *Nitrososphaerota* living in marine dark zones. The MGI represents more than half of the archaea in oxic top layer sediments (Danovaro et al., 2016) and outnumber bacteria in the dark zones of the ocean (Karner et al., 2001). Previous findings suggest that MGI are the predominant ammonia-oxidisers in marine environments (Wuchter et al., 2006) playing a vital role in the marine cycling of nitrogen. In the following, the more general term "ammonia-oxidising archaea" (AOA) will mostly be used, for simplicity.

AOA are chemolithotrophs, obtaining their energy by oxidising ammonia (NH_3) (Könneke et al., 2005). Because the energy yield from the oxidation of inorganic compounds, such as ammonia, is low, AOA must oxidise large amounts of ammonia to obtain enough energy for growth. Therefore, the metabolism of AOA contributes substantially to the cycling of nitrogen (Munn, 2019). Moreover, AOA are autotrophic microorganisms, transforming CO_2 to organic compounds by primary production (Könneke et al., 2005; Orsi, 2018). The primary production by AOA supports up to 19 % of the heterotrophic production in marine sediments (Orsi, 2018) with a supply of various organic compounds, including vitamin B12 (Doxey et al., 2015; Law et al., 2021). Because vitamin B12 is produced by a limited selection of microorganisms

[3] Thriving at moderate temperatures.

(Kräutler, 2005), the vitamin B12 produced by AOA might potentially be of great importance to a complex food web.

Because ammonia oxidation is strictly aerobic, AOA were previously believed to live only in oxic environments. Oxic sediments are characterized by little or no sedimentation of organic matter through the water columns, resulting in a limited amount of nutrients (Orsi, 2018). The nutrient depletion reduces the overall microbial growth, leaving oxygen available throughout the water column, from where it diffuses into the sediments (D'Hondt et al., 2015). As a result, oxic sediments tend to have low cell concentrations. The aerobic nature of nitrification therefore suggests that AOA only live in oligotrophic, deep-sea environments. However, a recent study found that AOA can produce their own oxygen when subjected to anoxic environments (Kraft et al., 2022), implying that AOA might be adaptable to various conditions. The ability of AOA to live in low-ammonium and low-oxygen environments and fixate carbon may reflect adaptations that make them successful in competition with other microorganisms in nutrient-depleted environments.

A recent study found that the ammonia monooxygenase (AMO) enzyme of a terrestrial AOA was inhibited by methanol. The AMO enzyme is essential to the ammonia-oxidising activity of AOA. When methanol is present in concentrations from 20 μM, it prevents ammonia from binding to AMO. However, the study did not conclude on whether AOA oxidise the methanol (Oudova-Rivera et al., 2023). To the writer's knowledge, little is known about the effect of methanol on marine AOA, which makes it an interesting subject to investigate.

1.4 Methanol-consuming microorganisms

Methanol is suggested an important source of energy in anoxic sediments and is consumed by methanotrophic microorganisms. Marine sources of methanol include the *in-situ* degradation of organic matter and oxidation of methane, as well as the deposition of terrestrial methanol. Methanol levels are higher in sediments than in the overlaying water, and the concentration of methanol increases with increasing sediment depth. However, it is unclear whether methanol produced and deposited in the water columns can reach the sediments (Fischer et al., 2021).

In marine sediments, methanol can be converted through methanogenesis, oxidation to CO_2, and acetogenesis. Although little is known about marine microorganisms performing the latter, the three processes can coexist. However, the oxidation of methanol to CO_2 has been suggested

the dominant methanol-consuming process in sediments (King et al., 1983). Methanol can be oxidised anaerobically by sulphate reducers and nitrate reducers (Fischer et al., 2021) and aerobically by methanotrophs (Bowman, 2014). On the other hand, the reduction of methanol to methane is strictly anaerobic. It is carried out by methanogenic archaea affiliated with the genera *Methanococcoides, Methanosarcinia,* and *Methanolobus*, among others (Liu & Whitman, 2008).

Methanol consumption is also linked to the nitrogen cycle. It was previously shown that *Methylophilaceae* can oxidise methanol using nitrate as an electron acceptor, thereby linking methanol consumption to denitrification (Kalyuhznaya et al., 2009). Another study found that methanol inhibits the anaerobic oxidation of ammonia (anammox) performed by sedimentary microorganisms (Jensen et al., 2007). Finally, ammonia-oxidising bacteria (AOB) are able to oxidise, but not grow on, methanol, suggesting that methanol is a competitive and reversible inhibitor of bacterial ammonia-oxidation (Hooper & Terry, 1973; Prosser, 2004). The inhibitory effect of methanol on bacterial ammonia-oxidation is analogous to the previously mentioned effect of methanol on AOA (Oudova-Rivera et al., 2023).

1.5 Analytical strategies

1.5.1 Microcosm experiments

Sediment microcosms are widely used to investigate sedimentary microorganisms (Li & Gu, 2013; Wu et al., 2013; Zeng et al., 2014). A microcosm is an artificial and simplified ecosystem enabling simulations of the natural ecosystem and its response to factors of interest. Sediment microcosms enable the exposure of sedimentary microbial communities to various factors, such as temperature, pollutants or other factors that can be difficult to control *in situ*. Moreover, the microcosms allow close monitoring of the microbial communities and their activity using techniques that are not restricted to field study equipment, because the microcosms can be maintained in the laboratory.

1.5.2 Marker genes

Marker genes are genes that enable the identification of individual species or taxonomic lineages in a sample. The genes to target are carefully chosen depending on the group of organisms to target (Pepper & Pillai, 1994). The gene encoding the AMO subunit A (*amoA*) is a widely used functional marker gene for AOA, because it encodes an enzyme essential to their activity (Mincer et al., 2007; Sintes et al., 2013; Treusch et al., 2005; Wuchter et al., 2006).

Another widely used marker gene is the 16S rRNA gene, which is present in most, if not all, microbial species, because cells cannot function without it. The 16S rRNA gene is a special marker gene, due to its conserved and variable regions. The conserved regions are nearly identical in all microorganisms, allowing the molecular targeting of most microorganisms simultaneously. Other regions of the gene are specific to taxonomic lineages. These regions are called variable regions in the 16S rRNA gene and enable assigning a taxonomy to the sequence (Pepper et al., 2011).

1.5.3 Primers targeting archaeal sequences.

Primers are short, single-stranded oligonucleotides complementing the sequences flanking the DNA region of interest. Primers are used to amplify specific DNA regions by PCR. Primers are designed based on conserved regions across gene sequences from known species (Bahram et al., 2019; Baker et al., 2003), which results in yet unknown species being easily overlooked. Recent findings revealed that primers targeting the whole archaeal 16S rRNA gene miss 28-77% of the operational taxonomic units in sediments (Karst et al., 2018). Moreover, the sequences used for primer design also influence the target coverage and specificity (Wei et al., 2019). In a recent study, 16S rRNA molecules were reverse-transcribed and sequenced to generate SSU sequences without primer bias (Karst et al., 2018). This approach resulted in more archaeal 16S rRNA sequences than what was available in the SILVA SSU reference database[4], which illustrates how primers may exclude substantial parts of microbial communities. Primer-dependent community composition analyses may therefore differ depending on the primer pair used for the purpose.

1.5.4 Polymerase chain reaction (PCR) and quantitative PCR (qPCR)

The polymerase chain reaction (PCR) is a method used to amplify nucleic acid sequences *in vitro*. The PCR exploits a heat-stable polymerase to efficiently amplify a specified nucleic acid sequence in the presence of a large molecular excess of primers and deoxyribonucleotide triphosphates. The primer sequences complement the sequences flanking the DNA region of interest, which is amplified by PCR through repeated cycles of denaturation, annealing, and elongation. The newly synthesised DNA strands are also used as templates in the following

[4] The SILVA SSU reference database is a web resource for high-quality databases of small subunit rRNA sequences from the bacterial, archaeal and eukaryotic domains (https://www.arb-silva.de/).

cycles. Therefore, the repeated cycles of denaturation, annealing, and elongation result in an exponential accumulation of the sequence of interest (Mullis & Faloona, 1987).

Quantitative PCR (qPCR) quantifies a sample's initial amount of a target DNA sequence. The technique uses PCR to amplify a target sequence. Upon each qPCR amplification cycle, the amount of double-stranded DNA (dsDNA) is quantified from the signal emitted by dyes that fluoresce when bound to dsDNA (Higuchi et al., 1993). Because dsDNA dyes bind unspecifically to dsDNA, signals emitted after the initial cycles largely depend on the template DNA, including non-target DNA. However, as the qPCR progresses, the amount of PCR product becomes detectable. The cycle at which the fluorescent signal reaches a threshold exceeding the noise from the non-target binding is called the quantification cycle (C_q). The C_q value can be related to the initial number of target sequence copies, which is associated with the number of organisms harbouring the target sequence in their genomes (Bustin et al., 2009).

1.5.5 Nanopore sequencing and metabarcoding.

Metabarcoding uses DNA sequencing of specific gene sequences to rapidly assess the organisms present in a sample. DNA sequencing is the process of determining the sequence of bases in a strand of DNA, and has enabled the discovery, study and taxonomical classification of microorganisms that cannot easily be cultivated in the laboratory. The Oxford Nanopore sequencing technology offers a cheap and efficient way of sequencing large amounts of DNA in one run, at the expense of lower read quality. To recognise the origin of the sequence reads, unique barcode oligonucleotides are integrated at the ends of the sequences. The resulting sequence libraries are inserted on a flow cell, where nanopores are arranged in multiple channels. As the DNA passes through the nanopores, nucleotide-specific changes in an ionic current are generated. These changes are recorded by sensors in the channels and subsequently decoded to infer the ssDNA sequence (Magi et al., 2018). The decoding process of raw Nanopore sequencing signals is called basecalling. Modern basecallers use neural networks trained on real data. The training data should ideally be as similar to the experimental data as possible to ensure high-quality results. However, most basecallers do not have fully disclosed information on the training data available (Wick et al., 2019). After basecalling, the reads are demultiplexed, meaning that reads are sorted by their barcodes. Demultiplexing ensures the separation of sequences originating from different samples.

1.6 Aims

Previous findings indicate that marine AOA are restrained by pollution (Pettersen et al., 2022; Ruprecht et al., 2021). However, the mechanisms behind this remain unclear. AOA thrive in nutrient-poor environments with available oxygen (Orsi, 2018), while being inhibited by organic compounds (Könneke et al., 2005; Oudova-Rivera et al., 2023; Qin et al., 2016). Organic compounds, especially methanol, are extensively used in biological wastewater treatment. Therefore, we aimed to assess how AOA are affected by the presence of methanol in the concentrations permitted in treated wastewater. The subgoals to achieve the main aim are as follows:

- Establish a Nanopore metabarcoding pipeline for archaea.
- Enrichment of AOA using a microcosm approach.
- Pollution experiment with methanol as an organic pollutant.
- Characterize the response to the enrichment and the pollution experiment.

The Nanopore metabarcoding pipeline was established by evaluating long-range primers targeting the archaeal 16S rRNA gene using *in silico* and *in vitro* approaches. These primers were used to generate an archaeal 16S rRNA library for Nanopore sequencing of the microcosm sediments. To enrich AOA, microcosms composed of artificial seawater and marine sediment samples were established in microaerophilic and dark conditions. The sediments from a microcosm displaying signs of nitrification were used assess the effects of methanol pollution on AOA. To monitor the response to the enrichment experiment and the pollution experiment, the abundance and composition of AOA and other relevant microbes were assessed using qPCR and the established Nanopore pipeline. The pH, ORP, and concentration of nitrogen species were also recorded to monitor the microbial activity.

2 Materials and methods

2.1 Overview

To enrich AOA from marine sediments, two sediment samples were used to make a total of eight marine sediment microcosms with artificial seawater medium (Figure 2-1a). While half of the microcosms were inoculated with pure sediments. the other half were inoculated with a mixture of sediments and sterile sand. The latter will hereafter be referred to as diluted sediments. Half of the microcosms were incubated at room temperature, while the other half were incubated at 10˚C (Figure 2-1a). Samples of the liquid medium and the sediments were taken in two-week intervals (Figure 2-3b and 2-3c). Upon each sampling, pH and ORP measurements were used to assess the potential microbial activity occurring in the microcosms (Figure 2-3a). Nitrite, nitrate, and ammonia concentrations were determined spectrophotometrically to look for signs of nitrification (Figure 2-4b).

The pH, ORP, and nitrogen measurements were used to assess if the enrichment of AOA had been successful. The sediments from a microcosm, in which signs of nitrifying activity had been recorded, was used as the inoculum for a pollution experiment (Figure 2-2b). The treatment microcosm, which hereafter will be referred to as the polluted microcosm, was exposed to methanol and nitrate in concentrations corresponding to the permitted COD and total nitrogen in purified wastewater. A control microcosm, which did not receive nitrate and methanol, was included. The polluted microcosm and the control microcosm were incubated for four weeks and sampled with 2-3 days intervals as previously described (Figure 2-3a, 2-3b. and 2-3c).

The sediment samples from the pollution experiment and the enrichment of AOA were processed simultaneously after the end of the pollution experiment. DNA was extracted from the sediment samples (Figure 2-4c). Thereafter, qPCR and Nanopore metabarcoding were employed to get an insight into the microbial diversity and metabolic potential of all the microcosms.

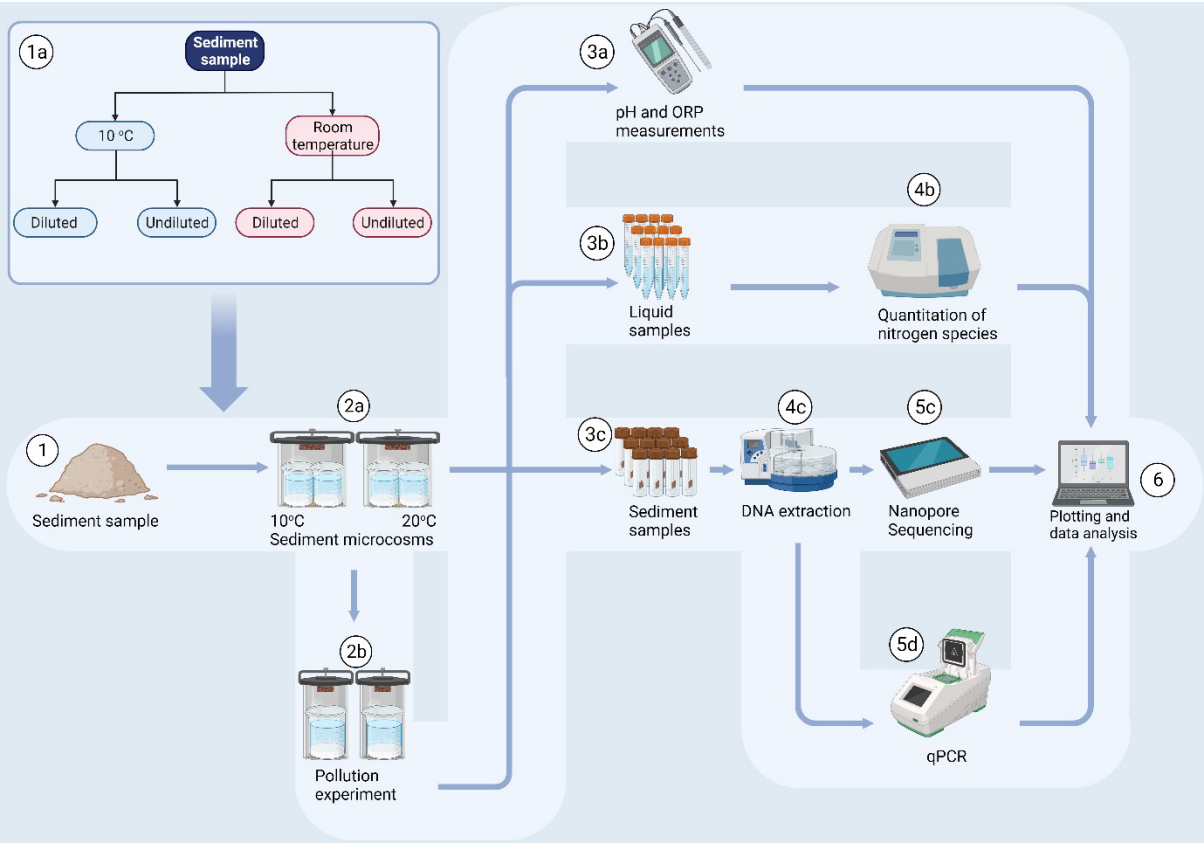

Figure 2: Overview of the methods. Two sediment samples were used as inoculum to enrich AOA **(1)**. Four different microcosms were established per sediment sample **(1a)** and incubated in microaerophilic conditions **(2a)**. The sediments from a microcosm displaying signs of nitrification were used as inoculum for a pollution experiment **(2b)**. The pH and ORP were measured in the microcosms regularly **(3a)**. Liquid samples were taken from the microcosms regularly **(3b)** and the concentration of nitrate, nitrite, and ammonium was measured **(4b)**. Sediments were sampled from the microcosms **(3c)**. DNA was extracted from the sediment samples **(4c)** and used to investigate the archaeal and bacterial composition by Nanopore sequencing **(5c)**. The DNA extractions were also used to assess the gene copy number of the bacterial and archaeal *amoA* and 16S rRNA genes **(5d)**. All the recordings and generated data was processed bioinformatically **(6)**. The figure was made with BioRender.

2.2 Sediment samples

Sediments were sampled at the coast of Norland and from the inner Oslo Fjord (Figure 3). Nordland is a Norwegian county with seven inhabitants per square kilometre (Statistisk sentralbyrå, 2023). In contrast, the inner Oslo Fjord is surrounded by the city Oslo and the county Viken, which have 1,643 and 56 inhabitants per square kilometre, respectively (Statistisk sentralbyrå, 2023). The sediments from the inner Oslo Fjord were, therefore, assumed to be more impacted by anthropogenic pollution than the sediments sampled by Nordland.

These sediments from Nordland were sampled at 83 m depth, but their exact sampling location is not publicly available (Figure 3B). Therefore, the sediments sampled in Nordland will be referred to as Cref hereafter. On the other hand, the sediments from the inner Oslo Fjord were sampled outside Håøygrunnen (Figure 3A) at 30 m depth.

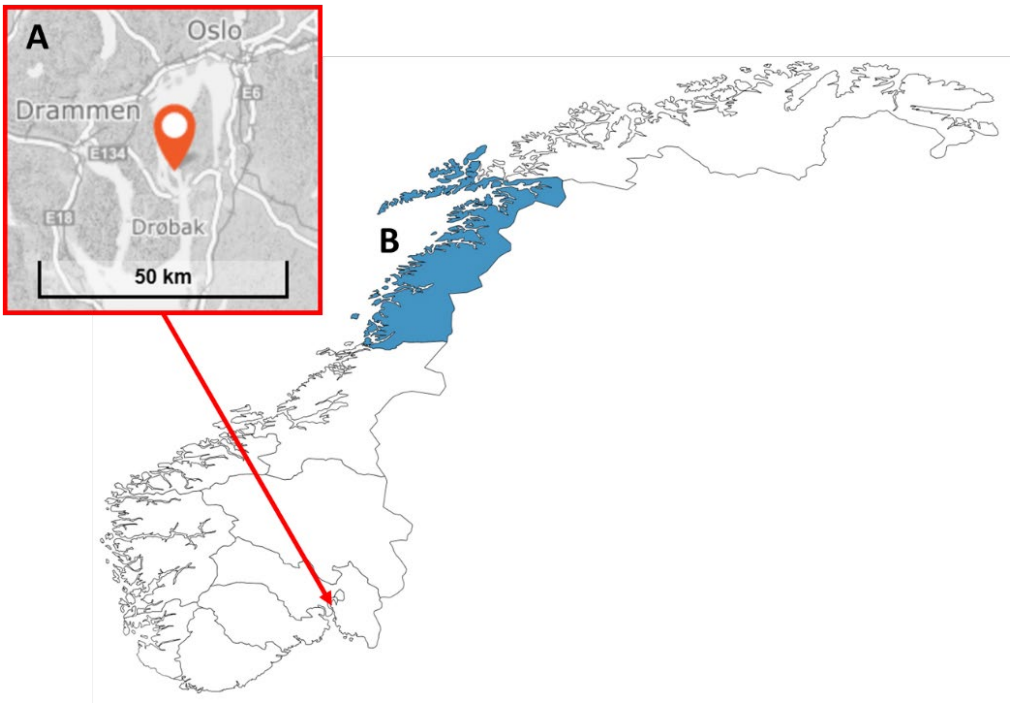

Figure 3: Sampling location of the sediments used for the microcosm experiments. The Oslo Fjord sediments were sampled at a 30 m depth in the inner Oslo Fjord southwest of Håøygrunnen **(A)**. This region is within the seafood warning area of the inner Oslo Fjord, due to pollution from industrial and domestic wastewater and microplastics (Norwegian Ministry of Climate and Environment, 2021). The Cref sediments were sampled at 83 m depth somewhere along the coast of the less densely populated Norland, but the exact sampling location is not publicly available **(B)**. The figure was made with https://mapchart.net and https://norgeskart.no.

2.3 Enriching AOA from marine sediment samples.

2.3.1 Enrichment conditions.

The microcosms were established under different conditions to enrich AOA. Firstly, two different sediment samples were inoculated. Moreover, the microcosms were incubated at different temperatures. Lastly, half of the microcosms were inoculated with sediments diluted with sterile sand. The microcosms were named after their inoculum, incubation temperature,

and sediment dilution (Table 1). The microcosms inoculated with the Oslo Fjord sediments were named OF, while those inoculated with the Cref sediments were named Cref. The incubation temperature of the microcosms is indicated by the number 10 (i.e., 10 ˚C) or 20 (room temperature). Furthermore, the microcosms in which the inoculum was diluted with sterile sand have the letter S in their names. As an example, the microcosm named OF-20-S was inoculated with Oslo Fjord sediments diluted with sterile sand and incubated at 20 ˚C.

Table 1: Overview of the microcosms. The name of each microcosm reflects the inoculum, the incubation temperature, and whether the inoculum was diluted with autoclaved sand or not. The column with sediment dilutions lists the ratio of inoculum to sterile sand in the microcosms.

Microcosm name	Inoculum	Incubation temperature (˚C)	Sediment dilution (w/w)
Cref-10	Cref sediments	10	
Cref-10-S			1:1
Cref-20		20	
Cref-20-S			1:1
OF-10	Oslo Fjord (OF) sediments	10	
OF-10-S			1:2
OF-20		20	
OF-20-S			1:2

2.3.2 Preparing a medium favouring the enrichment of AOA.

Artificial seawater medium was prepared as described by Könneke et al. (2005). The basal medium contained 26 g L^{-1} of NaCl, 5 g L^{-1} of $MgSO_4 \cdot 7H_2O$, 5 g L^{-1} of $MgCl_2 \cdot 6H_2O$, 1.5 g L^{-1} of $CaCl_2 \cdot 2H_2O$ and 0.1 g L^{-1} of KBr. A portion of the basal medium was used to soak the sand 1:1 (w/w) before autoclaving because we assumed the liquid would increase the reliability of the sterilisation. The basal medium and the soaked sand were autoclaved at 121˚ C for 15 minutes, and stored for up to 3 months at 10˚C. The day before each microcosm experiment was initiated, the following solutions were added to one litre of basal medium: 3 mL of $NaHCO_3$ (1M), 5 mL of KH_2PO_4 (0.4 g L^{-1}), 1 mL of FeNaEDTA (7.5 mM), 0.2 mL of NH_4Cl (1 M), 0.1 mL of α-ketoglutaric acid (100 mM), 0.25 mL of catalase (≈20,000 u mL^{-1}), 1 mL of $Na_2S_2O_3$ (100 mM) , and 1 mL of modified trace element solution. A portion of the artificial seawater medium was kept ammonium-free to serve as a blank for the later spectrophotometric quantitation of nitrogen species. The liquid stock solutions used to prepare the medium were stored at 4 ˚C in the dark for up to 12 months. The catalase had expired but was still used because it displayed the desired activity when tested with hydrogen peroxide.

The modified trace element solution (Martens-Habbena et al., 2009; Widdel & Bak, 1992) was prepared by lab personnel for a previous experiment and had been stored in dark conditions at 4 ˚C for 9 months. One litre of trace element solution contained 8 mL of concentrated HCl (approx. 12.5 M), 30 mg of H_3BO_3, 100 mg of $MnCl_2 \cdot 4H_2O$, 190 mg of $CoCl_2 \cdot 6H_2O$, 24 mg of $NiCl_2 \cdot 6H_2O$, 2 mg of $CuCl_2 \cdot 2H_2O$, 144 mg of $ZnSO_4 \cdot 7H_2O$, and 36 mg $Na_2MoO_4 \cdot 2H_2O$.

2.3.3 Preparing, incubating, and sampling the microcosms.

Four 500 mL glass beakers containing 250 mL of artificial seawater medium were inoculated with the Cref sediments (Figure 2-1a). In two of the beakers, the Cref sediments were diluted 1:1 (w/w) with autoclaved sand to a final weight of 150 g. The remaining two beakers received 150 g of undiluted sediments. Similarly, four 600 mL glass beakers containing 430 mL of artificial seawater medium were inoculated with the Oslo Fjord sediments (Figure 2-1a). Two beakers received a 1:2 (w/w) dilution of the Oslo Fjord sediments with autoclaved sand to a final weight of 150 g. The remaining two beakers received 150 g of undiluted sediments. The following procedure was identical for both sets of microcosms.

Null samples were taken in triplicates from the inoculum, the sterile sand, and the liquid medium, as described below. The liquid pH was adjusted to 8.0-8.2 using NaOH (1 M). The microcosms were incubated in a microaerophilic environment using GasPak 150 jars (BBL Microbiology Systems, USA) with CampyGen 3.5 L sachets (Thermo Fisher Scientific, USA). Because light exposure moderately inhibits the growth of some AOA (Qin et al., 2014), the GasPak jars were wrapped in aluminium foil to ensure dark conditions. The microcosms were incubated at room temperature during the first 24 hours after sealing the anaerobic jars, to ensure the microaerophilic conditions were reached at equal rates. Thereafter, one pair of microcosms was incubated in a microaerophilic environment in the dark at 10 ˚C. Similarly, the two remaining microcosms, one with diluted sediments and the other with undiluted sediments, were incubated under the same conditions, but at room temperature (19.5-21.5 ˚C).

At 0, 2 and 4 weeks, sediments and liquid media were sampled from the microcosms in triplicates. Sediment samples were mixed 1:3 with STAR buffer (Roche Diagnostics, USA) and stored at -18 ˚C until further processing (Section 2.6). Liquid samples were filtered (0.2 μm) and stored at 4˚C for up to three days until further analyses (Section 2.5). After sampling, the sediment ORP and pH were measured using a Combo pH/ORP/Temperature Tester

(HannaNorden AB, Sweden), followed by an adjustment of the liquid pH to 8.0-8.2 using NaOH (1 M). The initial pH of the liquid medium was recorded.

2.4 The pollution experiment

2.4.1 Preparing, incubating, and sampling the pollution experiment.

Two batches of artificial seawater medium were prepared as previously described (Section 2.3.2). One batch was supplemented with 15 mg L^{-1} of $NaNO_3$ and 100 mg L^{-1} of CH_3OH to simulate the effluent from a wastewater treatment plant, hereafter called the polluted medium. The second batch remained identical to the medium previously used to enrich AOA.

Because our main interest was to investigate the effects of methanol as an organic pollutant on AOA, the sediments from Cref-20-S were used as inoculum for the pollution experiment. Cref-20-S displayed signs of nitrification, as evidenced by ammonium consumption and nitrate or nitrite production (Figure 6). The inoculum was diluted 2:3 (w/w) with sterile sand. In a 500 mL beaker, 250 mL of synthetic seawater medium was inoculated with 200 g of diluted sediments. Similarly, in another 500 mL beaker, 250 mL of polluted medium was inoculated with 200 g of diluted sediments. Sampling, ORP and pH measurements, and pH adjustments were done as described previously (Section 2.3.3). Additionally, the ORP in the liquid medium was measured. The beakers were sealed in a GasPak jar (9.5 L) with 3 CampyGen sachets (3.5 L) and incubated at room temperature. Samples were collected with 2-3 days intervals, as described previously (Section 2.3.3).

2.4.2 Converting the permitted COD in treated wastewater to the corresponding concentration of methanol.

The permitted emission of chemical oxygen demand (COD) in urban wastewater effluents is 125 mg/L (Forurensningsforskriften, 2004). This can be translated into a stoichiometric quantity of methanol, assuming a complete combustion (Equation 1). The complete combustion of methanol requires three moles of oxygen gas per two moles of methanol, which results in a COD of 1.5 moles of oxygen per mole of methanol (Equation 2). This corresponds to a COD of 1.5 grams of oxygen per gram of methanol (Equation 3). Thus, a COD of 125 mg corresponds to 83 mg of methanol (Equation 4). Forurensningsforskriften (2004) limits the effluent COD to exceed 125 mg L^{-1} with up to 100%, although the limitation is disregarded in periods with high precipitation or other anormal conditions affecting the wastewater

purification efficiency. Therefore, the concentration of methanol in the simulated wastewater was rounded to 100 mg/L.

$$2\,CH_3OH + 3\,O_2 \rightarrow 4\,H_2O + 2\,CO_2 \quad (1)$$

$$COD_{n(CH_3OH)} = \frac{n(O_2)}{n(CH_3OH)} = \frac{3\,mol}{2\,mol} = 1.5 \quad (2)$$

$$COD_{m(CH_3OH)} = \frac{m(O_2)}{m(CH_3OH)} = \frac{n(O_2)\cdot[O_2]}{n(CH_3OH)\cdot[CH_3OH]} = \frac{1.5\,mol\cdot 32.0\frac{g}{mol}}{1.0\,mol\cdot 32.0\frac{g}{mol}} = 1.5 \quad (3)$$

$$m(CH_3OH) = \frac{COD_{\text{effluent}}}{COD_{m(CH_3OH)}} = \frac{125\frac{mg}{L}}{1.5} = 83\frac{mg}{L} \quad (4)$$

2.5 Spectrophotometric quantitation of nitrogen species in the liquid samples.

Stock solutions of KNO_3, KNO_2, and NH_4Cl (all 1 M) were employed to make dilution series of the nitrogen species. The stock solutions were diluted with ammonium-free artificial seawater medium. The resulting dilutions were treated as samples, and their corresponding absorbance readings were used to construct standard curves for ammonium (0, 0.025, 0.1, and 0.25 mM), nitrate (0, 0.1, 0.25, and 0.5 mM), and nitrite (0, 0.001, 0.025, and 0.1 mM). The spectrophotometer was calibrated using the 0 mM standards as blanks, which were included in every round of analysis. For each instance of reagent depletion and subsequent replacement with a freshly prepared batch, new standard curves were generated. The standard curves were used to convert the recorded absorbance values to concentrations.

The following protocols (Sections 2.5.1-2.5.3) were applied to all the liquid samples taken from the microcosms.

2.5.1 Quantitation of nitrate.

In an Eppendorf tube, 18 µl of the sample was mixed with 4.5 µl of saturated H_3NSO_3. Subsequently, 90 µl of salicylic acid in concentrated H_2SO_4 (5%, w/v) was added to the mixture After thorough mixing, the tube was incubated in the dark at room temperature for 10 minutes. Following this, 900 µl of NaOH (4 M) was introduced to the tube, and the mixture was further incubated under the same conditions for an additional 20 minutes. The tube was vortexed before the mixture's absorbance at 420 nm was measured spectrophotometrically.

2.5.2 Quantitation of ammonium/ammonia.

An ortho-phtaldialdehyde (OPA) reagent consisting of 5.4 g L^{-1} of Ortho-phtaldialdehyde in a mixture of ethanol (10 %), phosphate buffer (360 nM), and β-mercaptoethanol (0.5‰) was prepared by lab personnel. In an Eppendorf tube, 975 µl of the OPA reagent was mixed thoroughly with 65 µl of the sample and subsequently incubated in the dark at room temperature for at least 20 minutes. The absorbance at 420 nm was then measured spectrophotometrically.

2.5.3 Quantitation of nitrite.

The Griess reagents used in the present study were prepared by lab personnel. Reagent A was composed of N-(1-naphthyl) ethylenediamine dihydrochloride (0.2 g L^{-1}) in HCl (1.5 M), while reagent B consisted of sulphanilic acid (10 g L^{-1}) in HCl (1.5 M). Reagents A and B were stored separately and combined 1:1 (v/v) within an hour before the spectrophotometric quantitation of nitrite. For each sample, 850 µl of the Griess reagents mixture was thoroughly mixed with 170 µl of the sample, followed by incubation in a light-protected environment for a minimum of 10 minutes. Finally, the absorbance at 543 nm was measured using a spectrophotometer.

The reagents and stock solutions used for the quantitation of nitrogen species were prepared by experienced lab personnel and stored in light-protected environments. The nitrite and ammonium stocks were stored at 4˚C. The same applied to the Griess reagent A and the reagents used to quantitate nitrite, except the NaOH solution. The remaining stock and reagents were stored at room temperature.

2.6 DNA methods.

2.6.1 Extracting DNA from the sediment samples.

The sediment samples were thawed on ice and homogenised using a vortex. All the lysis preparation work was performed on ice. The samples and controls were mixed 1:3 (v/v) with BashingBead Buffer (Zymo Research, USA) in separate BashingBead Lysis Tubes (Zymo Research, USA). STAR buffer was used as a negative control, while the positive control consisted of ZymoBIOMICS Microbial Community Standard (Zymo Research, USA) mixed 3:7 (v/v) with STAR buffer. Cells were lysed using a TissueLyser high-speed disruptor at 30 Hz for 2 × 2.5 minutes. Upon lysis, samples were centrifuged at 10,000 g for 1 min and stored at 4˚C overnight.

DNA was separated from the cell components and purified using a KingFisher Flex robot (Thermo Fisher Scientific, USA) and the Quick-DNA Fecal/Soil Microbe 96 Magbead Kit (Zymo Research, USA) in accordance with the manufacturer's recommendations. The sample lysate (200 µl) was mixed with 600 µl of Quick DNA Mag Binding Buffer and 25 µl of Mag Binding Beads. gDNA was purified using 900 µl of Pre-Wash Buffer and 2 × 900 µl of gDNA Wash Buffer, before it was eluted in 60 µl of Elution Buffer. To assess the general DNA content in eluates, gDNA concentrations in 10-15 samples were measured using a Qubit dsDNA HS kit (Invitrogen, USA), following the manufacturer's protocol.

2.6.2 Gradient PCR for optimisation of annealing temperatures.

Each gradient PCR reaction contained 1× HOT FIREPol Blend Master Mix RTL (Solis BioDyne, Estonia), 0.2 µM of forward primer, 0.2 µM of reverse primer, and 1 ng of template DNA from the Cref extraction (Table 2). Nuclease-free water was used as a negative control for all primer pairs. Reactions were amplified in a Mastercycler ® gradient (Eppendorf, USA) at 95°C for 15 min, followed by 32 cycles of 95°C for 30 sec, 55-64°C for 30 sec, and 72°C for 30 sec (qPCR primers) or 1 min 20 sec (long-range primers), and one final elongation at 72°C for 10 min. The products were stored at 4°C.

2.6.3 Quantitative PCR (qPCR)

Reactions contained 1× HOT FIREPol® EvaGreen® qPCR supermix (Solis BioDyne, Estonia), 0.2 µM forward primer (Table 3), 0.2 µM reverse primer (Table 3) and 0.1-10 ng of template DNA. Nuclease-free water was used as a negative control for all primer pairs. All reactions were amplified using a C1000 Touch Thermal Cycler CFX96 Real-Time System (Bio-Rad, USA) at 95°C for 15 min, followed by 40 cycles of 95°C for 30 sec, annealing temperature (Table 3) for 30 sec, and 72°C for the specified elongation time (Table 3). Melt curve analyses were performed for all reactions. The products were stored at 4°C.

2.6.3.1 Quantifying the **amoA** *and 16S rRNA genes of archaea and bacteria in the sediment samples.*

The abundance of marine AOA, AOB, eukaryotes, and bacteria in the sediment extractions were assessed using qPCR as described previously (Section 2.6.4). Marine AOA were quantified using the MCGI-391F/MCGI-554R and Cren-amoA-Q-F/Cren-amoA-mod-R primer pairs. AOB and bacteria were quantified using the amoA-1F/amoA-2R primer pair targeting the bacterial *amoA* gene and the 341f /806r (Appendix Table A1) primer pair targeting

the bacterial 16S rRNA gene, respectively. Eukaryotes were quantified using the 3NDF/V4_Euk_R2 primer pair targeting the 18S rRNA gene, but not in the pollution experiment samples. The C_q values were processed as described (Section 2.7).

2.6.4 Evaluation of archaeal primer pairs

2.6.4.1 DNA templates used to test the primers in vitro.

The DNA templates used to evaluate the archaeal primers were extracted from sediments sampled along the Norwegian coast. The Cref and DigiMiBa high-diversity sediments were expected not to be impacted by anthropogenic pollution. The unimpacted sediments harboured diverse microorganisms, including AOA (Table 2). In contrast, the C1 and DigiMiBa low-diversity sediments were assumed to be impacted by anthropogenic pollution. The impacted sediments harboured microbial communities with less diversity where little or no AOA was present (Table 2). The DigiMiBa sediment samples had previously been mixed 1:3 (v/v) with Stool Recovery and Transport (STAR) buffer (Roche Diagnostics, USA) for stabilisation of the nucleic acids and stored at -18˚C. The Cref and C1 samples had been stored in air-tight containers at 4˚C in the dark since December 2022.

Table 2: An overview of the DNA templates used to evaluate the specificity and performance of archaeal primers are listed below. Some sediments were impacted by pollution and displayed lower microbial diversity than the less impacted sediments. The less impacted sediments were previously found to be abundant in AOA, while the impacted sediments either contained less or no AOA (Rudi, personal communication).

Template name	Template origin	Use
Cref	DNA extracted from less impacted sediments.	Positive control for AOA
C1	DNA extracted from impacted sediments.	Bacterial control
DigiMiBa High diversity	DNA extracted from less impacted sediments.	Positive control for AOA
DigiMiBa Low diversity	DNA extracted from impacted sediments sampled.	Bacterial control
Zymo Community Standard	DNA extracted from the ZymoBIOMICS Microbial Community Standard (Zymo Research, USA).	Bacterial and eukaryotic control

2.6.4.2 Evaluating long-range primer pairs targeting the archaeal 16S rRNA gene

A total of 10 long-range primers were retrieved from the literature (Appendix Table A3). The candidate long-range primers were combined to produce amplicons with a minimum of 800 bp length. Gradient PCR was employed to find the optimal annealing temperatures for all the primer combinations (Section 2.6.3), and the gradient PCR products were separated on a 2 %

agarose gel at 80 V for 40 min (details in Appendix). The performance of the primer pairs at different temperatures was assessed by looking for signs of unspecific targeting or primer dimer formation.

The primer pairs that produced clear, single gel bands after gradient PCR were evaluated for archaeal specificity using regular PCR. Each PCR reaction contained 1× HOT FIREPol Blend Master Mix RTL (Solis BioDyne, Estonia), 0.2 µM of forward primer, 0.2 µM of reverse primer, and 4 ng of template DNA from the Cref, C1, and Zymo community standard extractions (Table 2). Nuclease-free water was used as a negative control for all primer pairs. Reactions were amplified in a 2720 Thermal Cycler (Applied Biosystems, USA) at 95°C for 15 min, followed by 32 cycles of 95°C for 30 sec, 55˚C (Table 3) for 30 sec, and 72°C for 1 min 20 sec (Table 3), and one final elongation at 72°C for 10 min. The products were stored at 4°C. The PCR products were separated using gel electrophoresis on a 2 % agarose gel at 80 V for 40 min (details in Appendix). The primer pairs' specificity to archaea was assessed by analysing the visualised gel.

The primer pairs that produced clear, single gel bands after gradient PCR were also evaluated *in silico* using the SILVA TestProbe 3.0 probe match and evaluation tool with full-length 16S rRNA sequences (https://www.arb-silva.de/search/testprobe/). Each primer was evaluated separately, with a maximum number of mismatches set to 1. The results were downloaded and plotted using ggplot2 (Wickham, 2016) in RStudio v2022.07.2+576 (R Core Team, 2022) to assess the primers' coverage of the archaeal domain and specificity to archaea.

2.6.4.3 Evaluating short-range primer pairs targeting the archaeal 16S rRNA and amoA genes.

A total of nine primer pairs were assessed during the present project, of which four targeted the archaeal *amoA* gene and five targeted the archaeal 16S rRNA gene (Appendix table A1). The candidate qPCR primer pairs' general performance and optimal annealing temperatures were assessed using gradient PCR (Section 2.6.3) and gel electrophoresis using a 2 % agarose gel at 80 V for 35 min (details in Appendix).

The primer pairs that produced amplicons during gradient PCR were analysed further by qPCR (Section 2.6.4) using all the templates extracted specifically for primer evaluation (Table 2). The 341f/806r primer pair (Appendix Table A1) targeting the bacterial 16S rRNA gene was

used for comparison. The qPCR products were analysed for PCR artefacts using gel electrophoresis on a 1 % gel at 80 V for 35 min (details in Appendix). The resulting melting curves were used to assess the primer pairs' specificity and the production of PCR artefacts.

Table 3: Overview of the primer pairs used in the present project, and their optimal annealing temperatures (OATs). The OATs for the archaeal primer pairs were determined by gradient PCR, while OATs for primer pairs targeting other domains were established before the initiation of the present project. Primer sequences and references are available in the appendix (Appendix Tables A1 and A3).

Use	Forward primer	Reverse primer	OAT (˚C)	Elongation (seconds)
Long-range primer evaluation	SSU1ArF	Arch-1000R	55	80
		SSU1000ArR	55	
		Arch-1017R	55	
		AU1204R		
		U1392R		
		U1492R	55	
	Arch-21F	Arch-1000R	55	
		SSU1000ArR	55	
		Arch-1017R	55	
		AU1204R		
		U1392R		
		U1492R		
	Arch-349F	U1392R		
		U1492R		
	THAUM-494F	U1392R		
		U1492R		
Short-range primer evaluation	MCGI-391f	MCGI-554r	60	30
	340f	806rB	55	45
	SSU1ArF	SSU520ArR	55	45
	Arch-519F	Arch-915R	55	45
	THAUM-494F		55	30
	Arch-Amoa-for	Arch-Amoa-rev	60	30
		Arch-Amoa-rev-New		30
	Cren-AmoA-Q-F	Cren-AmoA-mod-R	55	30
	Arch-amo-196F	Arch-amo-227R		30
qPCR	341F	806R	55	45
	Amo-1F	Amo-2R	55	30
	3NDF	V4_Euk_R2	55	30
Nanopore	Mangala-F1	16SUR	55	80

2.6.5 Nanopore sequencing

Because of the limitations in time and capacity, only a subset of the sediment samples was sequenced. Namely, the null, midpoint, and endpoint samples from the sediments of all microcosms and the pollution experiment were treated according to the following protocol.

First-step PCR: Archaeal and bacterial 16S rRNA genes from the microcosms and pollution experiment were amplified using the SSU1ArF/Arch-1017R and Mangala-F1/16SUR primer pairs, respectively (Appendix Table A3). The reactions contained 1× HOTFirePol, 0.2 µM forward primer, 0.2 µM reverse primer and 0.1-10 ng template DNA. Reactions were amplified in a 2720 Thermal Cycler (Applied Biosystems, USA) at 95˚C for 15 min, followed by 30 cycles of 95˚C for 30 sec, 55˚C for 30 sec, and 72˚C for 1 min 20 sec. PCR products were checked using gel electrophoresis on a 1% gel at 80 V for 35 min (details in Appendix). The amplicons were stored at 4˚C until further use.

Ampure clean-up: To remove PCR artefacts, the 16S rRNA amplicons were purified using 0.6× Ampure. Room-tempered Ampure beads were added to the DNA and incubated for 5 min. The samples were placed on a magnetic stand for the Ampure beads to aggregate. The supernatants were removed, and the beads were washed twice with 80% ethanol while keeping the samples on the magnetic stand. The beads were allowed to dry for 15 minutes on the magnetic stand before they were resuspended in nuclease-free water. After 3 min of incubation, the samples were placed on the magnetic stand until all beads had aggregated. The supernatants were transferred to clean recipients and kept on ice. For storage overnight, purified DNA was kept at 4˚C in the dark.

Qubit quantitation*:* DNA was quantitated using the Qubit™ 1X dsDNA HS Assay Kit (Thermo Fischer Scientific, USA) following the manufacturer's protocol. Namely, 10 µl of the kit standards were mixed with 190 µl of the working solution in Qubit™ tubes, and 2 µl of the purified DNA was mixed with 198 µl of the working solution in Qubit™ tubes. The tubes were incubated in the dark for 2 minutes. The standards were used to calibrate the Qubit™ fluorometer before measuring the DNA concentration in the samples.

Barcoding PCR: The barcoding PCR reactions contained 1×HOTFirePol, < 70 ng purified template amplicon and 0.2 µM barcode from the PCR Barcoding Expansion 96 kit (Oxford Nanopore Technologies, UK). Volumes were adjusted to 50 µl using nuclease-free water. The

samples were barcoded using the following cycling conditions: 95˚C for 15 min followed by 12 cycles of 95˚C for 30 sec, 62˚C for 15 sec, and 65˚C for 2 min, and one final elongation at 65˚C for 10 min. The resulting libraries were checked using a 1% gel at 80 V for 35 min.

Library pooling: Archaeal and bacterial 16S rRNA libraries were pooled in separate sequencing libraries. The gel results were used to quantify the barcoded samples relative to each other. Bands from bacterial 16S rRNA amplicons were similar in strength and therefore assumed to contain approximately equimolar amplicon concentrations. Bacterial libraries were therefore pooled using identical volumes of each library. Some archaeal 16S rRNA libraries produced weak bands and were therefore pooled 2:1 (v/v) compared to the archaeal libraries with stronger bands. Both pooled libraries were purified using 1× Ampure and quantified using Qubit, as previously described.

DNA repair and end-prep: The Ligation Sequencing Kit V14 (Oxford Nanopore Technologies, UK) was used to end-prep and repair the pooled 16S rRNA libraries. Each reaction contained 1 µg of pooled libraries adjusted to a total volume of 47 µl with nuclease-free water, 3.5 µl of NEBNext FFPE DNA Repair Buffer, 2 µl of NEBNext FFPE DNA Repair mix, 3.5 µl of Ultra II End-Prep Reaction Buffer, and 3 µl of Ultra II End-Prep Enzyme Mix. The reactions were incubated on a thermal cycler at 20˚C for 5 min and 65˚C for 5 min. The end-prepped products were purified using 1×Ampure as described previously, except the air drying was shortened to 30 sec. The purified DNA was eluted in 60 µl of nuclease-free water.

Adapter ligation: To 60 µl of the end-prepped and purified libraries, 25 µl of Ligation Buffer and 5 µl of Adapter Mix H were added from the Ligation Sequencing Kit V14 (Oxford Nanopore Technologies, UK). Finally, 10 µl of Quick T4 DNA Ligase (New England Biolabs Inc., USA) was added to each reaction. The reactions were mixed by pipetting and incubated for 10 min at room temperature. The products were purified using 0.4×Ampure as follows: the mixture was incubated for 5 min on a rotator at room temperature before the beads were pelleted on a magnet and washed and resuspended twice in 250 µl of Short Fragment Buffer from the Ligation Sequencing Kit. The beads were air-dried for 30 sec and resuspended in 15 µl of elution buffer. After pelleting the beads, the supernatant was removed, retained in a clean recipient tube, and quantified using Qubit as described previously.

Priming and loading the flow cell: The priming and loading was done following the *Ligation sequencing V14-PCR Barcoding (SQK-LSK114 with EXP-PBC096)* ver. PBC_9182_v114_revG_07Mar2023 last updated 25/05/2023 (Oxford Nanopore Technologies, UK). The reagents were from the Ligation Sequencing Kit V14 (Oxford Nanopore Technologies, UK).

The flow cell was checked on the MinION device and displayed 1467 available nanopores. The flow cell priming mix (without BSA) was prepared by adding 30 µl of Flow Cell Tether to a tube with 1170 µl of Flow Cell Flush. A small volume (20-30 µl) of buffer was removed from the sensor array through the priming port of the flow cell before 800 µl of the priming mix was loaded through the priming port. The flow cell was allowed to rest for 5 min. Meanwhile, the library was prepared as follows: 37 µl of sequencing buffer was mixed with 25.5 µl of library beads and 12 µl of 16S library (corresponding to 10 ng of archaeal and 20 ng of bacterial 16S amplicon). After 5 min, the flow cell priming was completed by loading 200 µl of the priming mix into the flow cell priming port, followed by 75 µl of the prepared library via the SpotON sample port dropwise. The ports were closed, and the flow cell was placed in the sequencing device. The libraries were sequenced for 50 hours, and the minimal read length was set to 200 bp.

Both sequencing libraries were prepared simultaneously, but only one library could be sequenced at a time. As a result, the archaeal library was sequenced immediately after the end-prep, during which the bacterial library was stored at 4˚C. Loading the flow cell requires some experience and finesse, and was, therefore, carried out by the author's co-supervisor.

2.7 Data handling and statistical analyses

2.7.1 Processing the qPCR data.

The qPCR raw data was uploaded to Bio-Rad CFX Maestro 2.2 version 5.2.008.0222 (Hercules, USA), where the baseline settings were set to "no baseline subtraction". The resulting fluorescence data was further processed in LinRegPCR ver. 2021.2 (Ruijter et al., 2009), where the individual amplification curves were employed to determine each reaction's quantification threshold and amplification efficiency. The mean efficiency and the common quantification threshold for the assay were calculated and used to estimate the initial concentration of target sequence (N_0) in each sample (Equation 5). The efficiency-corrected initial target quantity (N_0) takes into account the amplification efficiency (E) and the

quantification threshold (N_q), thereby accommodating more nuanced information than raw C_q values. N_0 values were expressed in arbitrary fluorescence units (RFU), because standards with known concentrations of the target sequences were not employed in the qPCR analysis.

$$N_0 = \frac{N_q}{E^{C_q}} \tag{5}$$

The null samples were taken from the inoculum sediments and sterile sand separately. Their N_0 were combined into one value per null sample. This was done by adjusting the inoculum N_0 and the sterile sand N_0 by their dilution factors and summing the resulting values. Thereafter, the N_0 per gram of sediment was calculated for the remaining samples. Upon the comparison of N_0 mean and median values per sample to assess normality, the natural logarithms of the mean N_0 values were plotted with the standard deviations. Melting peaks for each sample were also investigated manually to assess whether PCR artefacts had been generated.

The melting point analysis revealed that none of the archaeal or bacterial amplicons had melting points differing by more than ±0.3˚C. As a result, all the bacterial and archaeal N_0 values were included in the analysis. On the other hand, eukaryotic 18S rRNA sequences often had multiple melting points differing with up to 7˚C, mostly when the Oslo Fjord sediment extractions were used as the template. Therefore, the diverging melting points were not interpreted as primer dimers. Excluding all the samples with diverging 18S rRNA melting points would have resulted in the loss of almost all the 18S rRNA data from the Oslo Fjord microcosms, and they were therefore included despite the risk of including qPCR artefacts.

The AOA marker genes had Cq values ranging between 25 and 37 in all the sediment samples from the enrichments of AOA and the pollution experiment, and >40 in the negative control. The archaeal *amoA* gene generally displayed higher Cq values than the the MGI 16S rRNA gene. In contrast, the bacterial 16S rRNA gene had Cq values ranging between 17 and 23 in the sediment samples and between 35 and 38 in the negative control, while the bacterial *amoA* gene had Cq values ranging between 25 and 30 in the sediment samples and >40 in the negative control. Lastly, the eukaryotic 18S rRNA gene had Cq values ranging between 22 and 27 in all the Cref and the OF microcosm sediment samples and a Cq of 38 in the negative control (Appendix Table A5).

2.7.2 Data processing and statistical analyses of Nanopore data.

A total of 5.17 millions of archaeal and 14.8 millions of bacterial reads with a mode quality score (Qscore) of 10 were generated. All bases with a minimum Qscore of 8 were basecalled, resulting in a failure to basecall 35 % of the bases.

2.7.2.1 Data processing and taxonomic assignment.

The basecalling was performed by the MinION sequencing device using the Guppy basecaller. The sequencing device also carried out the demultiplexing. Thereafter, the basecalled and demultiplexed reads were processed using the SituSeq Stream 1 (Zorz et al., 2023) (accessed 21.06.23 at https://github.com/jkzorz/SituSeq) in RStudio v2022.07.2+576 (R Core Team, 2022) as follows: The fastq files resulting from the demultiplexing were concatenated into one file per barcode. To remove the parts of the reads that did not originate from the native 16S rRNA gene sequences, i.e., the barcode and primer sequences, 120 bp were trimmed from both ends of all sequences. Reads having a length below 700 bp or above 1500 bp were then removed to exclude possible artefacts. Each sample was subsampled to 3000 reads, and the DADA2 assignTaxonomy function (Callahan et al., 2016) was used to assign taxonomy to all subsamples with a minimum bootstrap support of 50. The database used for the purpose was the SILVA 138.1 prokaryotic taxonomic training data formatted for DADA2 (Callahan et al., 2016; Quast et al., 2013; Yilmaz et al., 2014) (accessed 21.06.23 from https://zenodo.org/record/4587955). Finally, the resulting taxa were counted in terms of relative abundance for each sample, and the top 13 taxa for each sample were displayed using stacked bar plots.

The relative abundance of archaeal sequences that were not assigned a taxonomy increased as the taxonomic rank decreased, from approximately 1-5 % at phylum level to approximately 59-82 % at genus level. The same trend was observed for bacterial sequences, of which the number of unassigned sequences increased from 7-13 % at phylum level to 57-67 % at genus level (Appendix).

2.7.2.2 Statistical analysis.

Statistical analyses were performed using the taxonomic output from SituSeq. The SituSeq output included summary tables with relative abundances for bacterial and archaeal reads at five taxonomic levels (phylum, order, class, family, and genus). To simplify the statistical analyses, any lacking numbers (NAs, meaning “no detected read represents the given taxon in

the given sample") were replaced with zero (0, meaning "the given taxon did not occur in the given sample").

The microcosms: Due to the low amount of data, it was difficult to assess whether the data followed a parametric distribution. Therefore, the nonparametric Wilcoxon rank sum test was used to assess if the relative abundance of AOA in the Cref and Oslo Fjord microcosms was affected by sediment dilution or temperature. The tests were performed separately at the midpoint and end-point samples because we assumed the microbial compositions would differ at the two sampling times. The median relative abundances of Nitrosopumilus-related taxa were plotted as box plots to accompany the test results.

The pollution experiment: Because the amount of data was too little to assess its distribution, a nonparametric Wilcoxon rank sum test and PCoA were used to investigate the effect of methanol pollution on the relative abundance of any bacterial or archaeal taxon. The midpoint and end-point samples were tested together as one group, although we assumed there would be differences in microbial compositions at the two sampling times. The choice was made due to the low number of sequenced samples troubling the statistical testing.

The Nanopore sequencing data provided relative abundances. To assess the effect of pollution on the absolute abundance of AOA, the Pearson correlation coefficient between the relative sequence abundances in the polluted and control sediments were calculated. This was done for archaeal relative abundance data at the order rank.

A principal coordinate analysis (PCoA) was done using the Morisita-Horn distance metric, suitable for relative abundances. The two principal coordinates explaining most variation were plotted, and the groups (polluted vs control) with their 95% confidence intervals were indicated using the *stat_ellipse()* function from the *ggplot2* package (Wickham, 2016). Approximate loadings were calculated using two different approaches: The approach suitable for plotting involved using the *wascores()* function from the *vegan* package (Oksanen et al., 2017), while the other approach involved calculating the correlations between the principal coordinates and the Morisita-Horn distances in the distance matrix.

3 Results

3.1 Short-range primer evaluation

All short-range qPCR primer pairs except Arch-amoA-for/Arch-amoA-rev-New and Arch-amo-196F/Arch-amo-227R produced amplicon during gradient PCR (Appendix Figure A1). However, the Arch-amoA-for/Arch-amoA-rev, MCGI-391F/MCGI-554R, and 340F/806rB primer pairs produced multiple PCR products at lower annealing temperatures. Therefore, their optimal annealing temperatures were set to 60˚C, while the optimal annealing temperatures of Cren-amoA-Q-F/Cren-amoA-mod-R, Arch-519F/Arch-915R, SSU1ArF/SSU520ArR, and THAUM-494F/Arch-915R were set to 55˚C (Table 3).

During qPCR, Arch-amoA-for/Arch-amoA-rev produced products of approximately 100 bp regardless of the template, including the negative control (Appendix Table A2). On the other hand, Cren-amoA-Q-F/Cren-amoA-mod-R only produced amplicons with the templates from sediments known to harbour AOA (Appendix Table A2). The melting curve analysis revealed that Cren-amoA-Q-F/Cren-amoA-mod-R produced one main melt peak with multiple shoulders, although signs of multiple amplicons were not observed after gel electrophoresis (data not shown).

MCGI-391F/MCGI-554R only produced amplicons with the templates known to harbour AOA (Appendix Table A2). In contrast, the other primer pairs targeting the archaeal 16S rRNA gene either produced amplicons with the bacterial control or did not produce amplicons in templates with DNA from AOA. Moreover, the primer pair Arch-519F/Arch-915R produced amplicons with the negative control (Appendix Table A2). Similar results were observed for the primer pair targeting bacterial 16S rRNA, and its C_q values correlated 95% with the C_q values produced by Arch-519F/Arch-915R (Appendix Figure A2).

3.2 Long-range primer evaluation

The forward primers Arch-21F and SSU1ArF in combination with the archaeal reverse primers Arch-1000R, Arch-1017R and SSU1000ArR produced one amplicon in the reactions across the whole annealing temperature gradient (Appendix Table 3). Arch-21F also produced amplicons in combination with the universal reverse primer U1492R, although at a more limited range of annealing temperatures (Appendix Table 3). Because we already had six primer combinations performing well across the entire annealing temperature gradient, the Arch-21F/U1492 primer combination was not tested further.

During the *in vitro* specificity evaluation, all the primer pairs produced amplicons with the template containing DNA from AOA, and none produced amplicons with the negative control (Appendix Figure A3). All primer combinations with the forward primer SSU1ArF produced amplicons with the Zymo community standard, which contained only bacterial and eukaryotic DNA (Appendix Figure A3). The amplicons produced with the bacterial control template were longer and produced weaker bands during gel electrophoresis than those generated with the template containing DNA from AOA. In contrast, the primer combinations with the forward primer Arch-21F did not target bacterial DNA.

The *in silico* primer evaluation revealed that although the Arch-21F forward primer was highly specific to archaea, it only covered 5.9% of the full-length archaeal 16S rRNA sequences in the SILVA database (Appendix Table A4). Accordingly, Arch-21F displayed a poor coverage of only a few archaeal phyla (Figure 4). In contrast, the SSU1ArF forward primer covered 75.6% of the archaea at the price of slightly poorer specificity. That is, SSU1ArF covered 0.3% of the eukaryotes in the database (Appendix Table A4). Moreover, SSU1ArF displayed >50% coverage of almost all the archaeal phyla, except *Nanoarchaeota, Iainarchaeota* and *Altiarchaeota*.

The reverse primers displayed a similar coverage of and specificity to archaea. Namely, they all covered ≈ 97% of the archaeal sequences, ≈ 3% of the bacterial sequences, and ≈ 80% of the eukaryotic sequences in the database (Appendix Table A4). Nevertheless, the reverse primer Arch-1017R got slightly fewer bacterial and eukaryotic hits than the other reverse primers. All the archaeal phyla except *Iainarchaeota* were covered at ≈100% by the reverse primers. SSU1ArF displayed a higher coverage of *Iainarchaeota* than the other reverse primers (Figure 4).

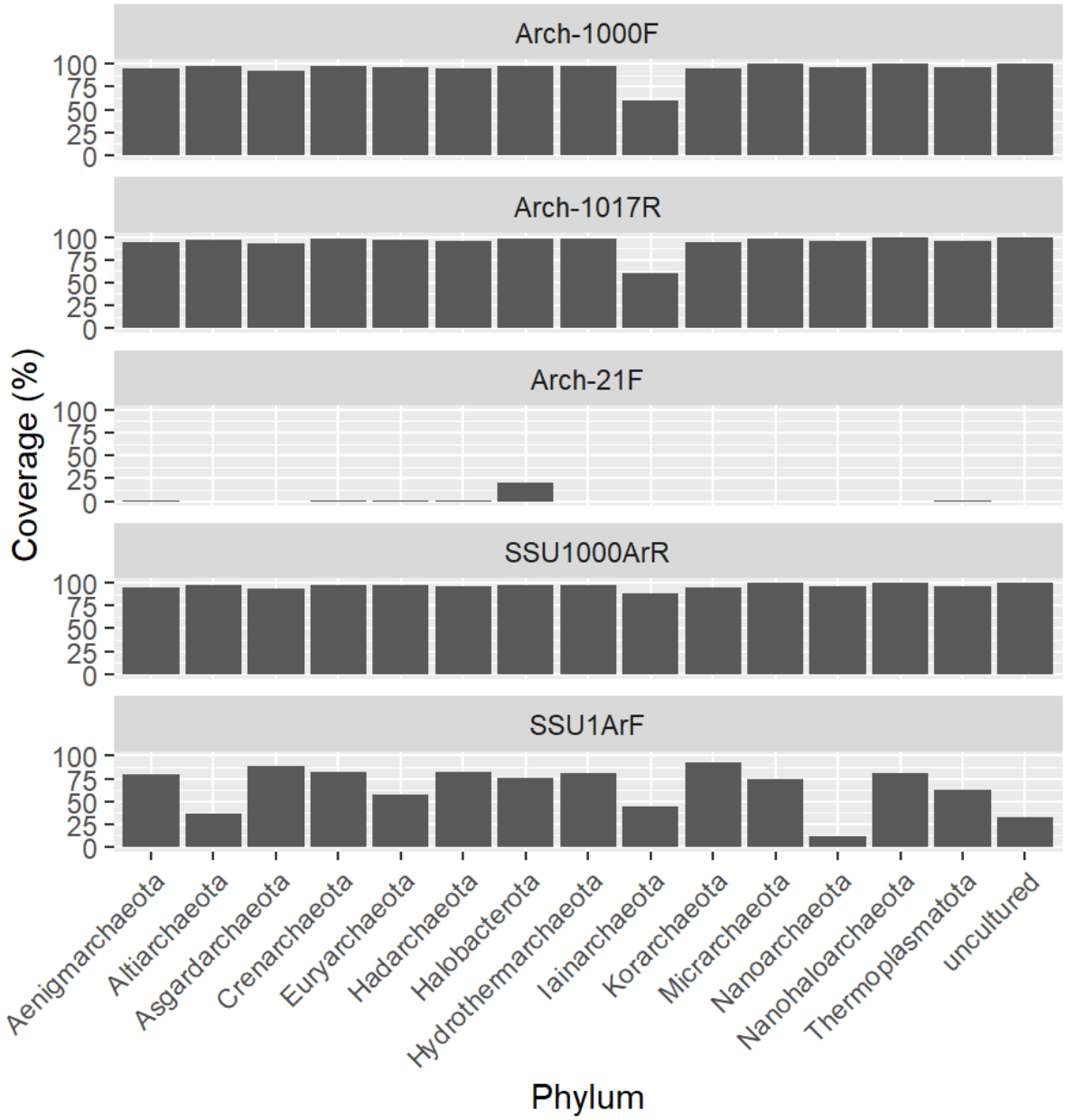

Figure 4: Archaeal phyla covered by long-range 16S rRNA primers, according to the results from SILVA TestProbe 3.0. The three reverse primers evaluated were Arch-1000R, Arch-1017R, and SSU1000ArR. They displayed a similar coverage of the archaeal phyla, but SSU1000ArR displayed a better coverage of *Iainarchaeota* compared to the other reverse primers. Of the two evaluated forward primers, SSU1ArF displayed a higher coverage of all the archaeal phyla. The other forward primer, Arch-21F, poorly covered most of the archaeal phyla.

3.3 The microcosm enrichment of AOA.

We attempted to enrich *Nitrosopumilus* and other AOA from two different sediment samples using an artificial seawater medium with ammonium (0.2 mM). A total of four microcosms per sediment sample were prepared. Samples were taken from the sediments and the liquid medium at zero, two, and four weeks, upon measuring the sediment ORP and pH (Figure 5). Potential nitrifying activity was monitored using spectrophotometric quantitation of ammonium, nitrite, and nitrate in the liquid samples. DNA was extracted from the sediments, followed by a qPCR analysis of various marker genes as well as archaeal and bacterial 16S rRNA gene sequencing, both of which were employed to assess the abundance and composition of microorganisms in the sediment samples.

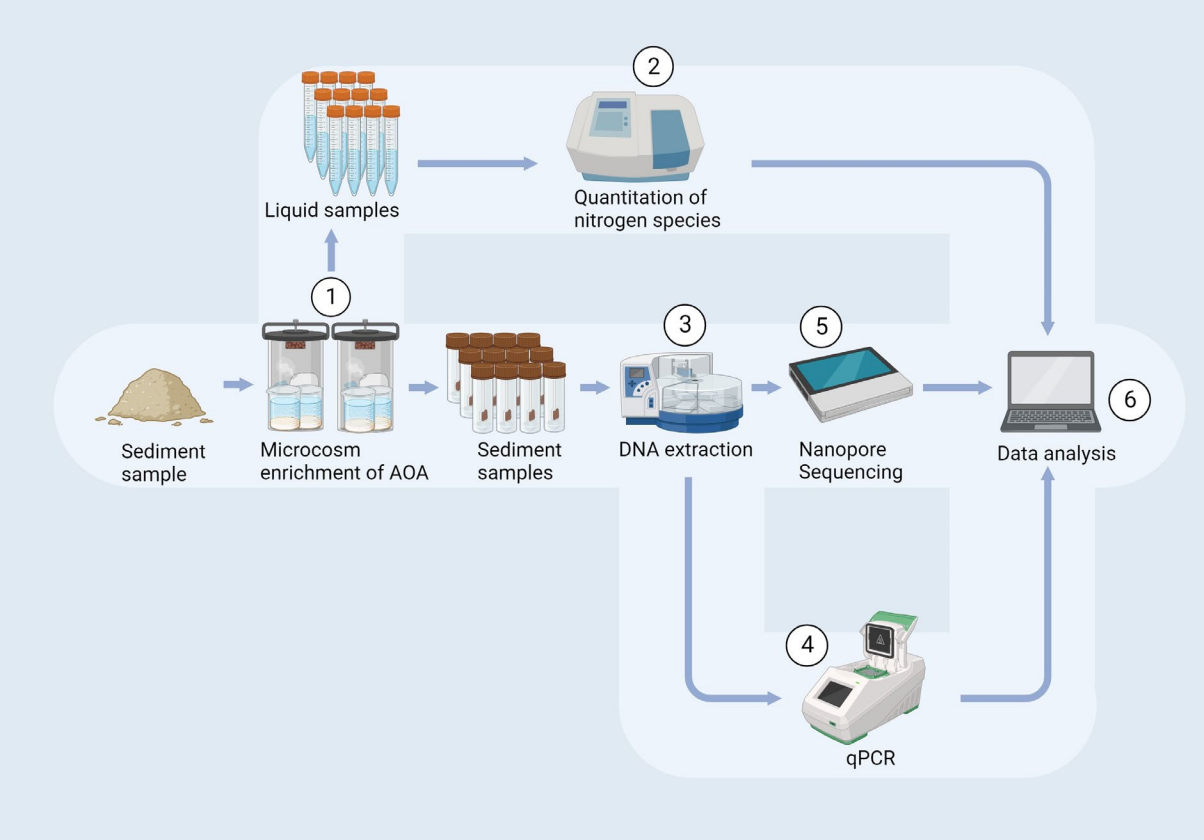

Figure 5: An overview of the workflow for the enrichment of AOA. **(1)** A microcosm approach was used to enrich AOA from sediments sampled in the Oslo Fjord and along the coast of Nordland. The microcosm sediments and liquid were sampled at zero, two, and four weeks. **(2)** The concentrations of ammonium, nitrate, and nitrite in the liquid samples were determined spectrophotometrically. **(3)** DNA was extracted from the sediment samples. **(4)** The numbers of AOA, AOB, bacteria, and eukaryotes were inferred using qPCR. **(5)** The bacterial and archaeal compositions of the sediments were inferred using 16S rRNA Nanopore sequencing. **(6)** The data from the chemical and molecular analyses were processed and analysed bioinformatically. The figure was created in BioRender.com.

3.3.1 The pH and ORP decreased during the first two weeks of incubation.

The pH in all the microcosm sediments seemed to stabilise below pH 7, although the liquid pH was adjusted to 8-8.2 after each sampling (Figure 6). All the microcosms displayed an initial reduction in sediment pH and ORP during the first two weeks of incubation, at which point the microcosms incubated at room temperature displayed a lower sediment ORP than the microcosms incubated at 10 ˚C. During the last two weeks, the sediment pH and ORP increased in all microcosms except OF-10 and Cref-10, in which the sediment ORP continued to decrease. After four weeks of incubation, the sediment ORPs in microcosms with diluted sediments were generally between -100 and -200 mV, and between -150 and -250 mV in microcosms with undiluted sediments.

3.3.2 Increasing ammonium levels in all the enrichments.

The lower limits of detection for nitrogen were 0.025 mM for ammonium, 0.1 mM for nitrate, and 0.001 mM for nitrite. The nitrite levels never increased above the limit of detection in any of the microcosms (Figure 6). In contrast, all the microcosms displayed increasing levels of nitrate and ammonium during the first two weeks of incubation. While the concentration of nitrate continued to increase in the Cref microcosms after the first two weeks, nitrate could not be detected in the Oslo Fjord microcosms after four weeks. On the other hand, the concentration of ammonium stopped increasing in the Cref microcosms after two weeks (Figure 6A), while continuing to increase in the Oslo Fjord microcosms (Figure 6B).

All the Cref microcosms displayed an increase in ammonium and nitrate concentrations during the first two weeks of incubation (Figure 6A). During the two last weeks, nitrate levels continued to increase at a steeper rate in all the microcosms except Cref-10. The largest increase in nitrate concentration was observed in Cref-20-S. The ammonium levels started to decrease after two weeks in all the Cref microcosms except Cref-20, where ammonium levels continued to increase during the third and fourth week of incubation.

In the Oslo Fjord microcosms, the nitrate levels started out below the detection limit, increased to approximately 0.25 mM after two weeks, and returned to below the detection limit after four weeks of incubation (Figure 6B). On the other hand, the concentration of ammonium continued to increase during the third and fourth week of incubation. The OF-20 microcosm displayed a substantial increase in ammonium concentration throughout the incubation, but especially during the first two weeks.

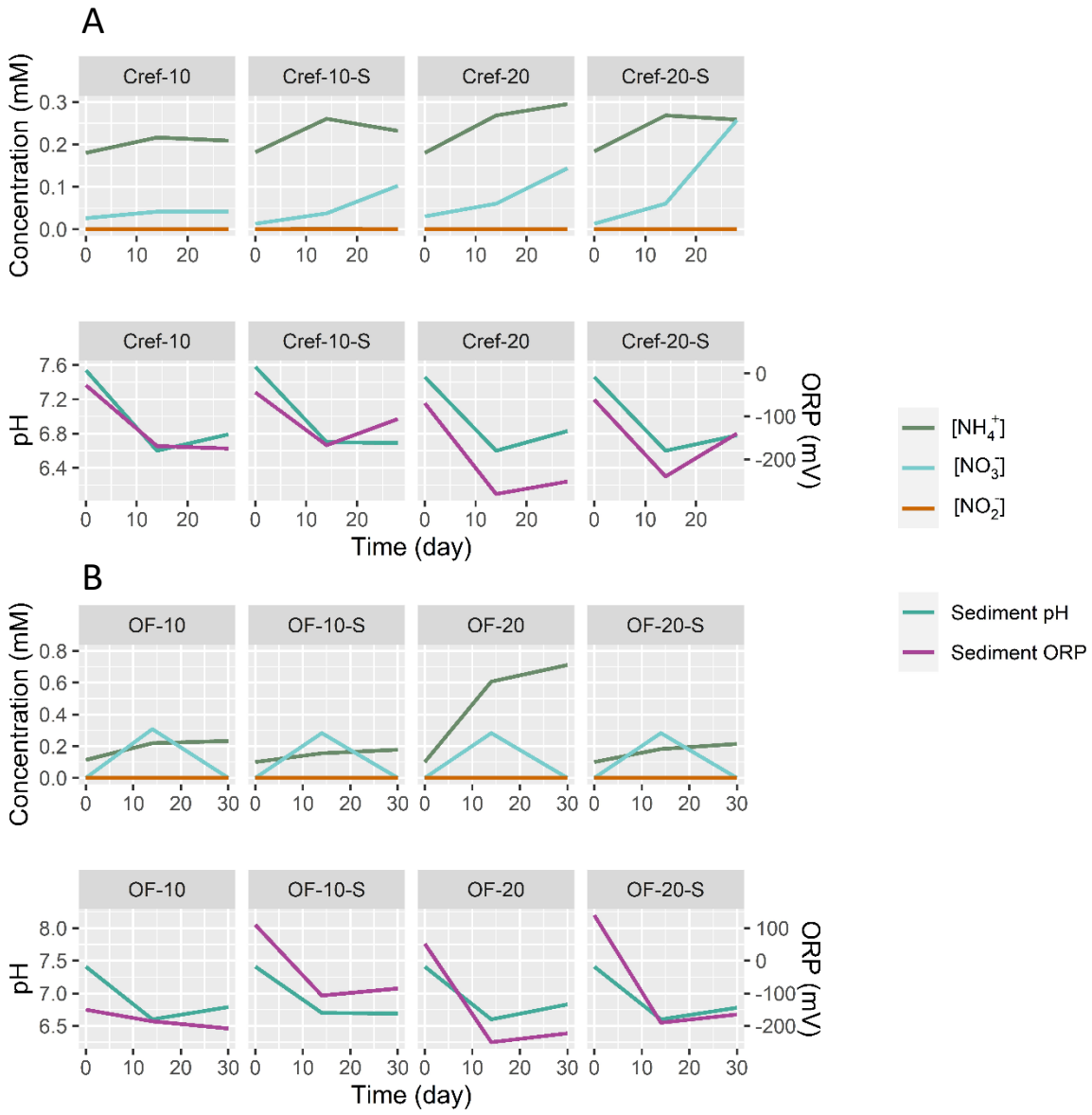

Figure 6: The pH, ORP, and concentration of nitrogen species in the **Cref (A)** and **Oslo Fjord (B)** microcosms at zero, two, and four weeks of incubation. The data points are means of triplicate measurements. The standard deviations were excluded from the plots because they were too small for visualisation. The upper panels display the concentrations of ammonium (NH_4^+), nitrate (NO_3^-), and nitrite (NO_2^-) in the liquid samples. Sediment pH and ORP measurements are displayed in the lower panels. Liquid pH measurements were not included, because they were similar to the sediment pH measurements. There is one plot per microcosm, indicated in the grey box above the graphs. The names of the microcosms indicate the origin of the sediment inoculum, the incubation temperature, and whether the inoculum was diluted or not (Table 1).

3.3.3 Archaeal marker genes were scarce compared to bacterial marker genes.

The qPCR analysis revealed that, of the targeted marker genes, the bacterial 16S rRNA gene was the most abundant in the microcosms, followed by the eukaryotic 18S rRNA gene (Figure 7). The bacterial *amoA* gene was the third most abundant of the targeted sequences in all the enrichments, while the archaeal *amoA* and MGI 16S rRNA genes occurred in low numbers in all the microcosms (Figure 7).

There was little difference in the N_0 (target copy number) of the individual genes between the different Cref microcosms, and the standard deviations largely overlapped (Figure 7A). Moreover, the individual target genes did not seem to increase in N_0 over time (Figure 7A).

The Oslo Fjord microcosms displayed changes in N_0 values over time (Figure 7B). The differences in N_0 between the microcosms were larger compared to the Cref microcosms, and the standard deviations did not completely overlap. After two weeks of incubation, the number of all targeted sequences had decreased in the microcosms with diluted sediments and increased in the microcosms with undiluted sediments (Figure 7B). After four weeks, the N_0 of all the marker genes had decreased in all the microcosms. The only exception was OF-20-S, in which all the marker genes besides the archaeal *amoA* gene displayed an increasing N_0.

3.3.4 Macroorganisms and fungi were observed in the Oslo Fjord sediments.

The sediment sample from the Oslo Fjord harboured various macroorganisms. Although attempts were made to remove most of them prior to inoculation, dark spots were observed around the cadavers of the remaining macroorganisms after incubation (Appendix Figure A4-A). These dark spots only appeared in the microcosms with undiluted sediments after two weeks and disappeared by four weeks. After four weeks, a white substance resembling several miniature clouds of 0.2-2 cm length were partially floating and resting on the sediments in all the Oslo Fjord microcosms except OF-10-S (Appendix Figure A4-B). Observations by light microscopy confirmed the assumption that the white substance was a fungus (Skaar, personal communication; Appendix Figure A4-C). Because we wanted to assess if the fungus or other macroorganisms in the Oslo Fjord sediments could have had an impact on the microcosms, we decided to quantify the eukaryotic 18S rRNA genes by qPCR. The mean number of eukaryotic 18S rRNA genes were higher in the microcosms where the fungus was observed (Figure 7B).

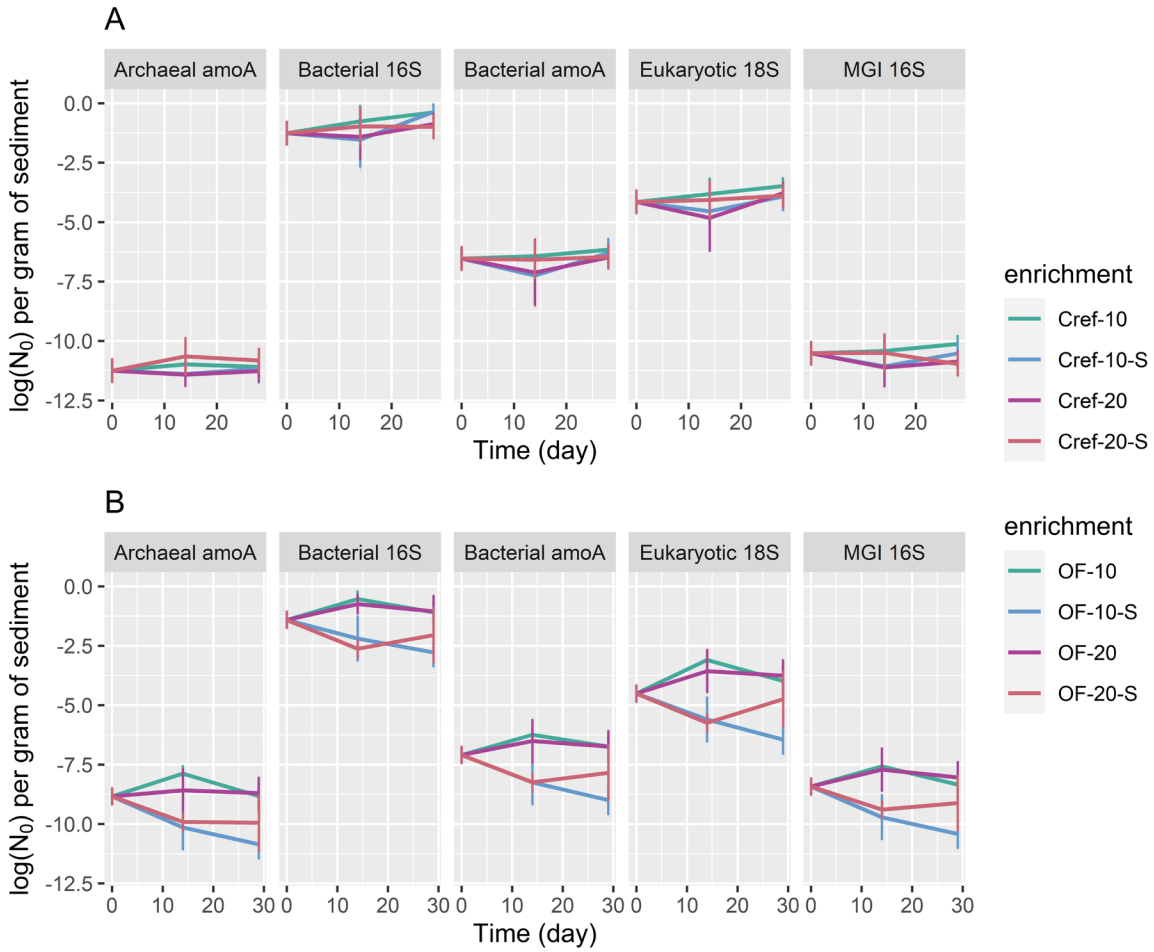

Figure 7: The log initial copy number (N_0) of various marker genes in the microcosm sediments expressed as arbitrary fluorescence units (RFU). The plotted N_0 values are based on mean C_q values of triplicate samples. The corresponding standard deviations are displayed as error bars. The Cref microcosms **(A)** are represented in the upper panels, while the Oslo Fjord microcosms **(B)** are represented below.

3.3.5 AOA dominated the archaeal communities in the Oslo Fjord microcosms.

According to the sequencing data, the archaeal communities in the microcosm sediments were largely similar among microcosms inoculated with the same sample. Namely, *Nitrososphaeria, Nanoarchaeia,* and *Thermoplasmata* were the most abundant archaeal classes in the Cref microcosm sediments (Figure 8A), while *Nitrososphaeria* and *Nanoarchaeia* seemed to be the dominant archaeal classes in the Oslo Fjord microcosms (Figure 8B). It is worth noticing that *Nitrososphaeria*, which is a class affiliated with AOA, seemed to represent a larger fraction of the archaeal community in the Oslo Fjord microcosms than the Cref microcosms.

Nitrososphaeria was represented by the genus *Candidatus* Nitrosopumilus (order *Nitrosopumilales*) in all the enrichments (Appendix Figures A7 and A10). Contrarily, the sequences that were assigned the class *Nanoarchaeia* were largely designated the order *Woesarchaeales* (Figure 9) but were not assigned any taxon at genus or family level. The same applies to the sequences which were designated the class *Thermoplasmata* and its orders SG8-5 and Marine Benthic Group D (Figure 9).

In all the microcosms, *Nitrosopumilales* (class *Nitrososphaeria*) was the only order affiliated with AOA (Figure 9). In the Cref inoculum, *Nitrosopumilales* represented 29 % of the archaeal 16S rRNA sequences. After two weeks of incubation, the relative sequence number of *Nitrosopumilales* had increased to 27-38 % in all the Cref microcosms, before decreasing to 19-28 % at four weeks. The sequence relative abundance of *Nitrosopumilales* was higher in Cref-20 than any other of the Cref microcosms after two weeks of incubation. After four weeks of incubations, Cref-20-S was the richest in *Nitrosopumilales* sequences (Figure 10A). These observations are consistent with the qPCR results (Figure 7A). Nevertheless, the standard deviations are large and overlapping, both in the qPCR results and the sequencing results.

On the other hand, *Nitrosopumilales* represented 56 % of the archaeal sequences in the Oslo Fjord inoculum. Analogous to the Cref microcosms, the relative sequence abundance of *Nitrosopumilales* had increased to 63-70 % after two weeks of incubation, while it decreased to 55-64 % after four weeks in the Oslo Fjord sediments (Figure 10B). OF-10-S harboured more *Nitrosopumilales* than any other microcosm during the whole microcosm experiment, which does not correspond to the qPCR results indicating that OF-20 was the richest in AOA (Figure 7B). However, the precision of the molecular techniques was relatively poor, as displayed by the standard deviations.

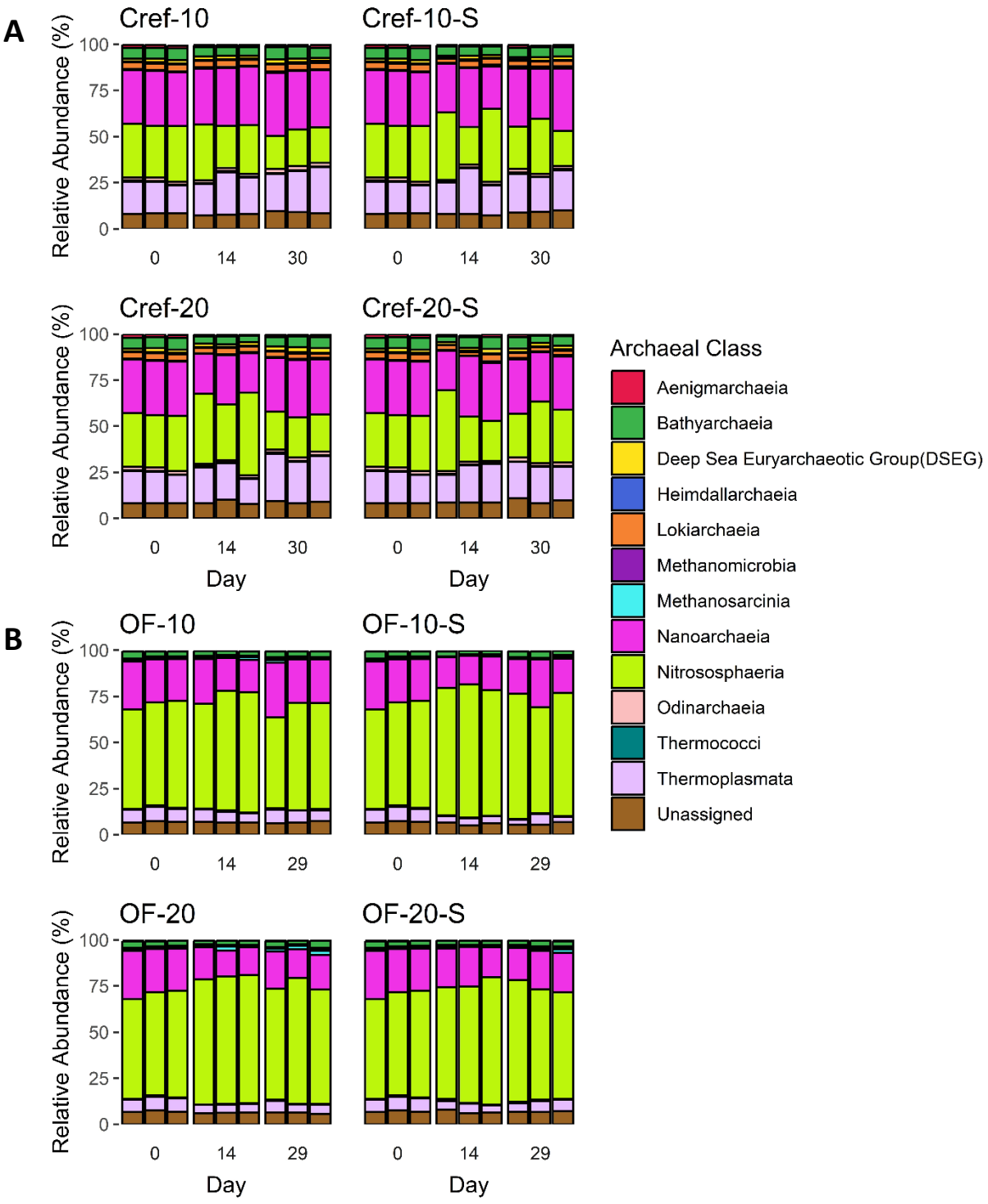

Figure 8: The top 13 archaeal classes in the Cref **(A)** and Oslo Fjord **(B)** microcosm sediments, according to the Nanopore sequencing of archaeal 16S rRNA sequences. The triplicate sediment samples from the inoculum are presented at day 0, while the triplicate sediment samples taken from the microcosm sediments are presented at day 15 and 30.

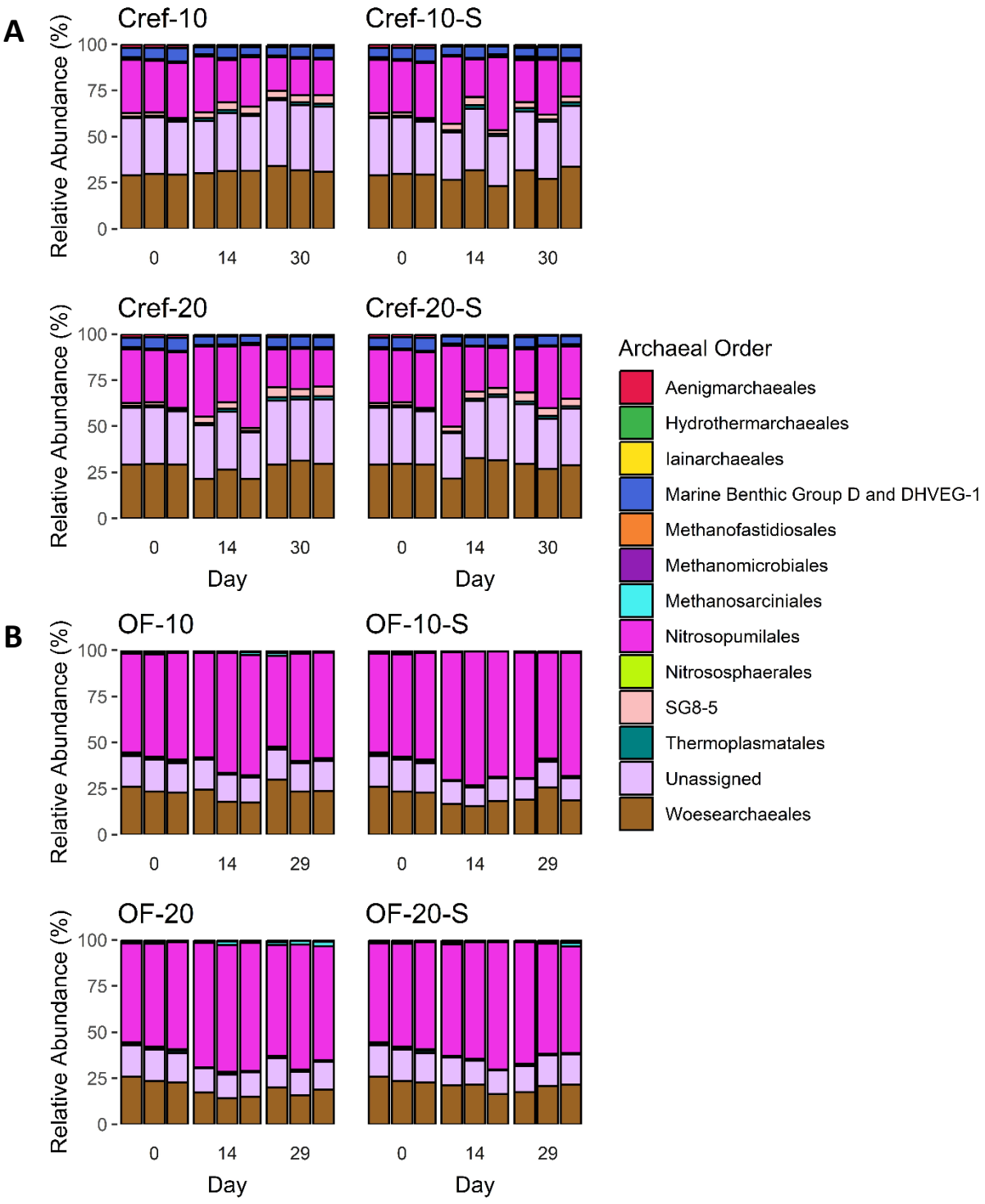

Figure 9: The top 13 archaeal orders in the Cref **(A)** and Oslo Fjord **(B)** microcosm sediments, according to the Nanopore sequencing of archaeal 16S rRNA sequences. The triplicate sediment samples from the inoculum are presented at day 0, while the triplicate sediment samples taken from the microcosm sediments are presented at day 15 and 30.

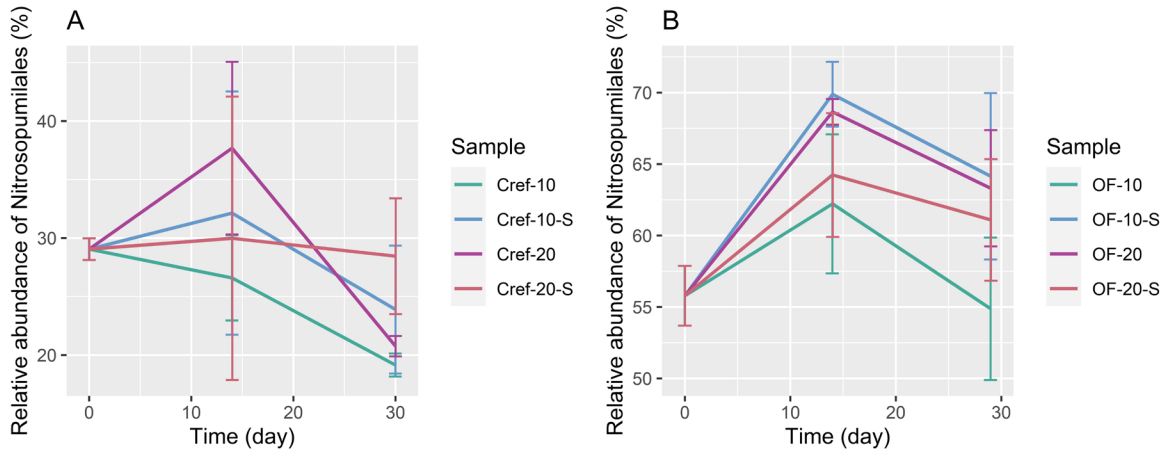

Figure 10: The mean relative abundances of *Nitrosopumilales* over time in the Cref (A) and Oslo Fjord (B) microcosms, according to the 16S rRNA sequencing results. The standard deviations are indicated with error bars.

3.3.5 Sediment dilution and incubation temperature did not affect the enrichment of AOA.

The sediment dilution did not seem to influence the enrichment of *Nitrosopumilales* in the Oslo Fjord microcosms (Wilcoxon p = 0.7, Figure 11C). However, the sediment the relative sequence abundance of *Nitrosopumilales* was higher in the Cref microcosms with diluted sediments than the microcosms with undiluted sediments after four weeks of incubation (Wilcoxon p = 0.06, Figure 11A). This trend was not apparent from the qPCR analyses (figure 7). Although the median relative abundance of *Nitrosopumilus* was generally higher in microcosms incubated at room temperature than at 10 ˚C (Figure 11B, Figure 11D), the incubation temperature did not significantly affect the relative abundance of *Nitrosopumilus* and its related AOA at any taxonomic rank investigated, neither after two nor four weeks (Wilcoxon p > 0.05).

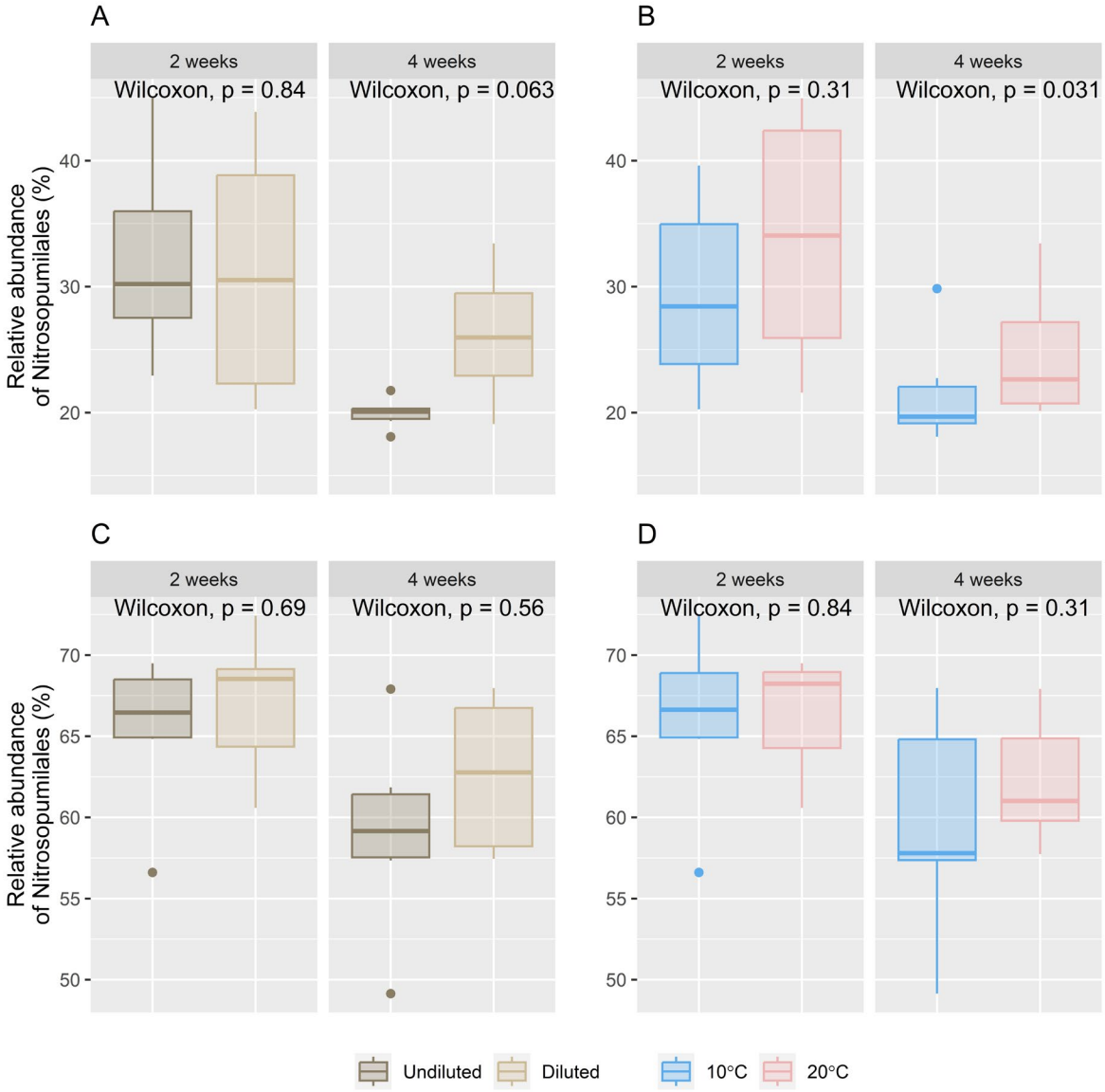

Figure 11: Boxplots of the relative abundances of *Nitrosopumilales* in the microcosm sediments determined by Nanopore 16S rRNA sequencing. All samples are grouped by temperature and sediment dilution, to assess whether any of the enrichment factors influenced the enrichment of AOA. The relative abundances were compared in the samples taken after two weeks and four weeks of incubation using the paired Wilcoxon rank sum test. Diagram **A** displays the difference between the microcosms with undiluted or diluted Cref sediments. Diagram **B** shows the difference between the Cref microcosms incubated at 10 ˚C and room temperature (20 ˚C). Diagram **C** displays the difference between the microcosms with diluted and undiluted Oslo Fjord sediments. Diagram **D** shows the difference between the Oslo Fjord microcosms incubated at 10 ˚C and room temperature (20 ˚C).

3.3.6 *Gammaproteobacteria* was the most abundant bacterial class.

Microcosms with the same inoculum displayed highly similar bacterial compositions. Aside from the unassigned sequences, the most abundant bacterial class in all the Cref and Oslo Fjord microcosms was the *Gammaproteobacteria*, followed by *Bacteroidia* and *Desulfobacteria* (Figure 12). *Alphaproteobacteria* was also among the 13 most abundant bacterial classes. Moreover, *Cyanobacteriia* was among the most abundant bacterial classes in the Oslo Fjord microcosm sediments (Figure 12B), although its relative abundance seemed to decrease over time. *Campylobacteria* was enriched in Cref-10 and OF-10 (Figure 12).

At the genus rank, *Algomarina,* which belongs to the class *Desulfobacteria*, was the most abundant genus in all the microcosms. The only exception were the Cref-10 and OF-10 microcosms, where *Poseidoniibacter* (class *Campylobacteria*) was enriched. *Nitrospira* (class *Nitrospiria*) was also among the 13 most abundant genera. However, up to 80% of the bacterial sequences were not assigned a genus (Appendix Figures A14 and A18).

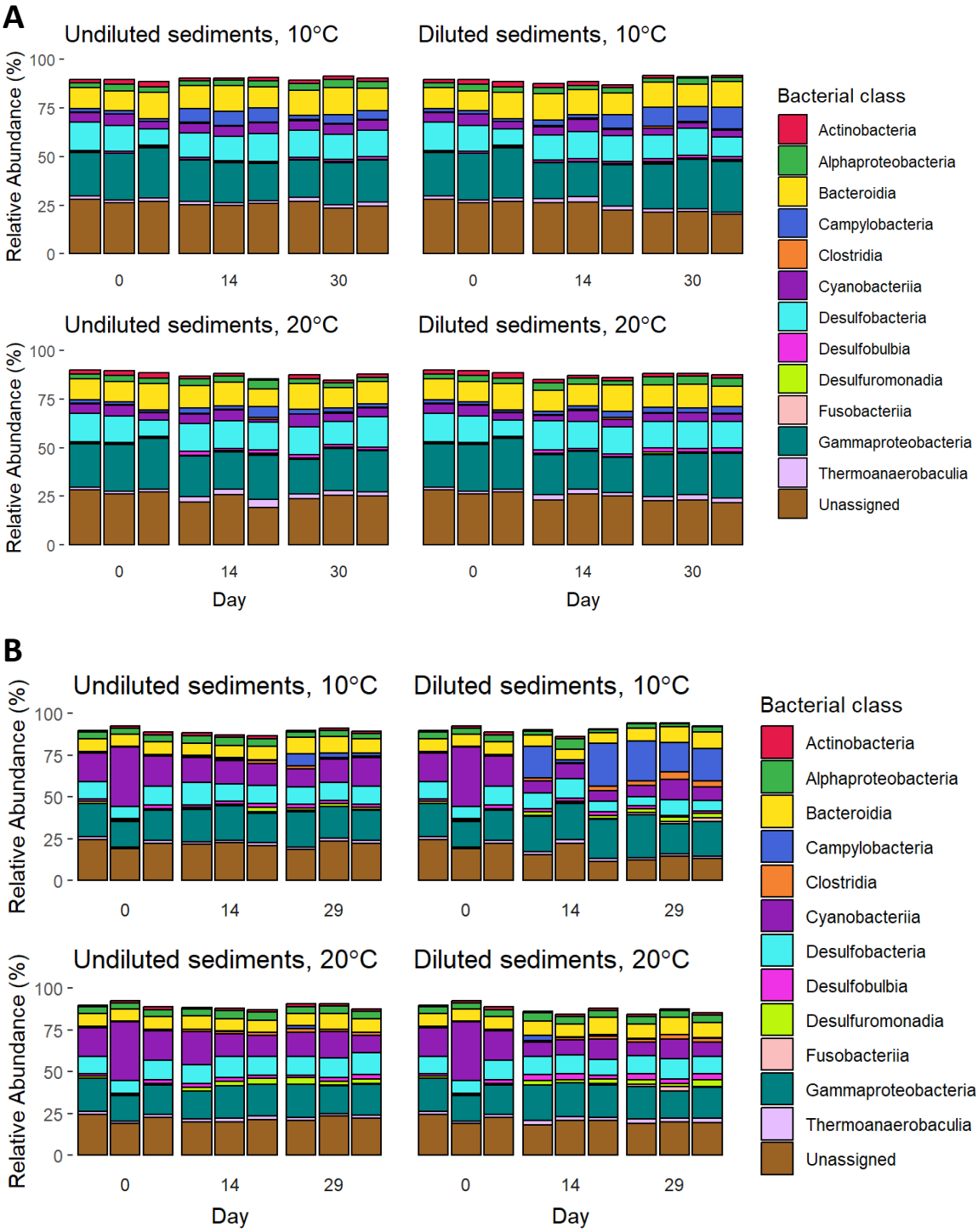

Figure 12: The 13 most abundant bacterial classes in the Cref (A) and Oslo Fjord (B) microcosms, according to the Nanopore 16S rRNA sequencing results. The triplicate sediment samples from the inoculum are presented at day 0, while the triplicate sediment samples taken from the microcosm sediments are presented at day 15 and 30.

3.4 The pollution experiment.

One of the aims of the present project were to assess how sedimentary microorganisms, especially AOA but also other archaea, are affected by pollution. Therefore, we aimed to enrich AOA from sediment samples and subsequently subject the AOA to a simulated pollution. Sediments enriched in AOA were diluted with sterile sediments and inoculated in two different media, one in regular artificial seawater medium and the other in artificial seawater medium with 100 mg/L of methanol and 15 mg/L of nitrate. The microcosms were incubated at 20˚C in a microaerophilic environment and sampled with 2-3 days intervals (Figure 13).

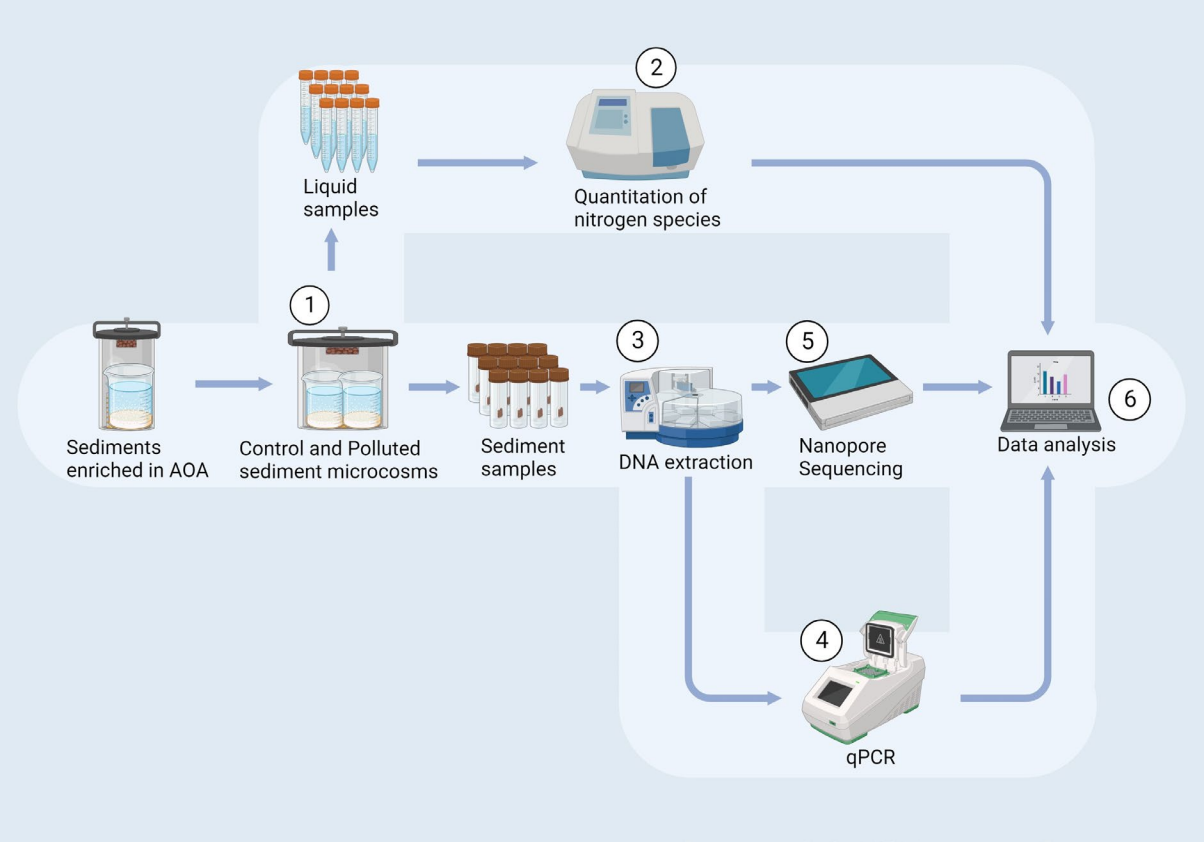

Figure 13: An overview of the pollution experiment workflow. **(1)** Because the Cref-20-S displayed signs of nitrifying activity, its sediments were inoculated in two separate beakers with artificial seawater and sterile sand. To assess the effect of wastewater effluent on AOA, methanol and nitrate were added to one of the microcosms. Samples were taken in 2-3 days intervals from the sediments and from the liquid medium. **(2)** The concentrations of ammonium, nitrate, and nitrite in the liquid samples were determined spectrophotometrically. **(3)** DNA was extracted from the sediment samples. **(4)** The numbers of AOA, AOB, bacteria, and eukaryotes were inferred using qPCR. **(5)** The bacterial and archaeal compositions of the sediments were inferred using 16S rRNA Nanopore sequencing. **(6)** The data from the chemical and molecular analyses were processed and analysed bioinformatically. The figure was created in BioRender.com.

3.4.1 Ammonium levels decreased faster in the polluted microcosm.

The polluted microcosm displayed a rapid decrease in ammonium concentration from 0.2 mM to 0.03 mM during the first four days of incubation. Simultaneously, the concentration of nitrite peaked at 0.02 mM. After this, the nitrite levels remained low and the ammonium levels did not surpass 0.05 mM, but stabilised around 0 mM at 21 days and throughout the remaining time of the experiment (Figure 14A). On the other hand, the ammonium concentration in the control microcosm decreased slowly, and even increased to a peak at seven days. However, a rapid decrease in ammonium was observed between days 18 and 21, after which the ammonium concentration stabilised around 0.06 mM throughout the last week of the experiment. The concentration of nitrite peaked between the second and seventh day, but was low throughout the remaining incubation (Figure 14B). The concentration of nitrate never surpassed the detection limit of 0.1 mM in any of the microcosms (Figure 14).

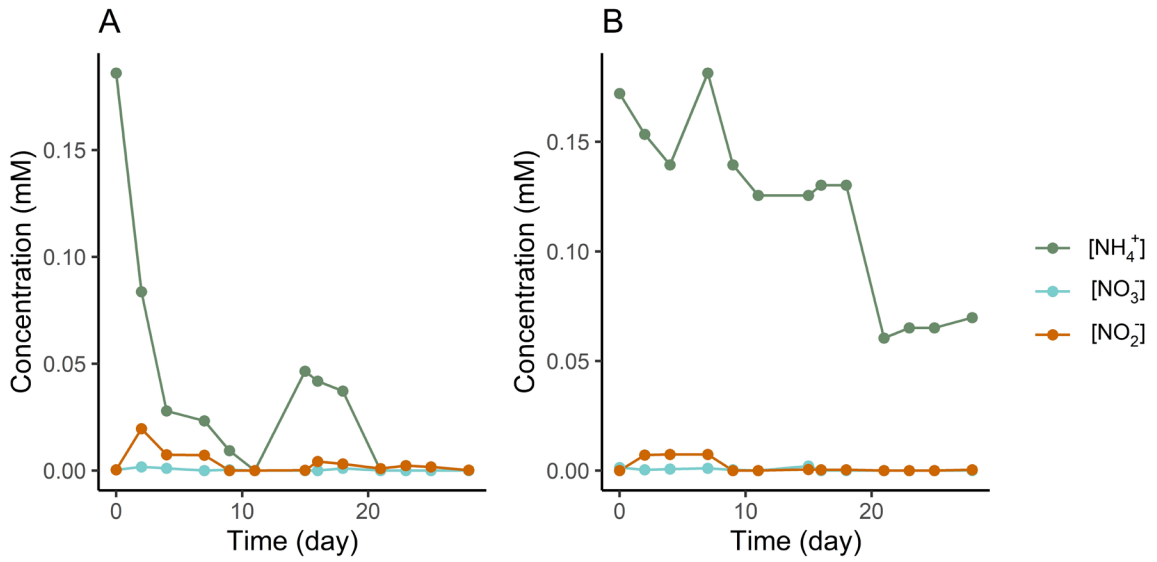

Figure 14: The concentrations of ammonium (NH_4^+), nitrate (NO_3^-), and nitrite (NO_2^-) in the liquid samples from the polluted microcosm **(A)** and the control microcosm **(B)**. The samples were taken in triplicates, and the figure displays their mean values. The standard deviations were too small to appear in the plot and were therefore negligible.

3.4.2 The ORP was lower in the polluted microcosm.

The liquid and sediment ORP were generally lower in the polluted microcosm than the control microcosm. However, the observed difference was larger in the liquid medium than the sediments. While the liquid pH was generally above 0 mV in both microcosms, the recorded ORP was consistently negative in the microcosm sediments. The liquid and sediment ORP were relatively stable over time, although short-term fluctuations were observed (Figure 15A and Figure 15B).

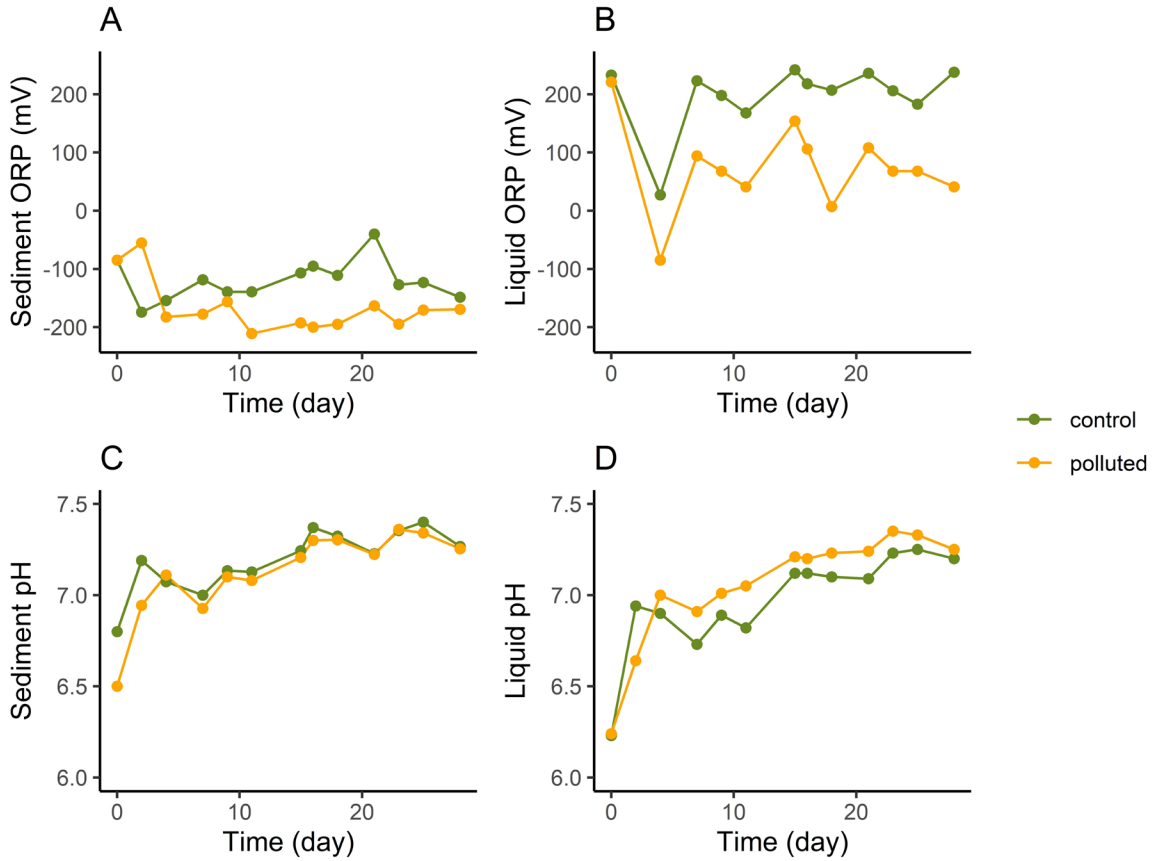

Figure 15: The pH and ORP recordings from the pollution experiment microcosms. The ORP was recorded in the sediments **(A)** and the liquid medium **(B)**. Similarly, the pH was recorded in the sediments **(C)** and the liquid medium **(D)** before the pH was adjusted to 8.0-8.2. Because the pH was consistently adjusted upon recording the liquid and sedimentary ORP and pH, the apparent increase in system pH indicates that the pH is reduced to a lower extent between each sampling.

3.4.3 The pH was consistently decreasing between the samplings.

Despite that the liquid pH was adjusted to 8-8.2 upon each sampling, the recorded pH measurements were consistently below pH 7.5. The sediment pH was similar in both microcosms throughout the pollution experiment (Figure 15C). Furthermore, the microcosms differed less in sediment pH than liquid pH (Figure 15C and 15D). The recorded pH was slightly lower in the polluted sediments than the control sediments until the fourth day, after which the difference in sediment pH was minor (Figure 15C). In contrast, the polluted microcosm had a higher liquid pH than the control microcosm at all sampling times except for the second day, at which the control microcosm had a higher liquid pH than the polluted microcosm. This difference in liquid pH was maintained throughout the remaining days of the experiment (Figure 15D).

3.4.4 The polluted microcosm sediments were enriched in bacterial 16S rRNA.

There seemed to be more bacterial 16S rRNA genes overall in the polluted microcosm than the control microcosm, although the standard deviations overlapped at days 18-23. The archaeal *amoA* gene also seemed to be slightly more abundant in the polluted sediments than the control sediments. However, the standard deviations were large, which resulted in at least partial overlap between the polluted and control samples.

AOA-related sequences were detected in lower nubers compared to the bacterial sequences in both microcosms. The two AOA marker genes, archaeal *amoA* and MGI 16S rRNA, were detected in similar abundances, although there seemed to be slightly more of the MGI 16S rRNA gene than the archaeal *amoA* gene (Figure 16).

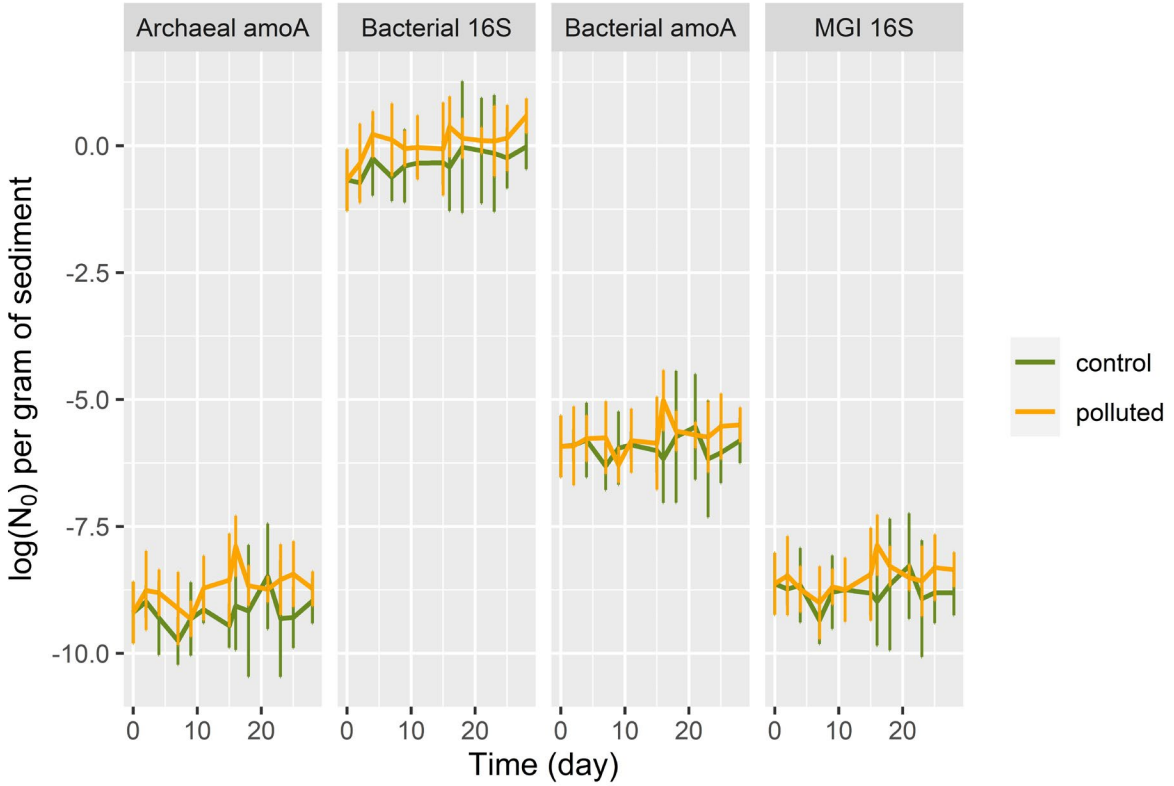

Figure 16: The initial log copy numbers of AOA and bacterial marker genes in the pollution experiment microcosms. The N_0 values are expressed in arbitrary fluorescence units (RFU). That is, the target sequences were not absolutely quantified, because standards with known concentrations of the target sequences were not employed in the qPCR analysis. The size of the standard deviation for each mean N_0 are indicated with vertical error bars. Generally, the standard deviations minimised the difference in N_0 between the polluted and control microcosms by overlapping, at least partially. Furthermore, the number of bacterial 16S rRNA sequences were tremendously higher than the number of any other targeted marker gene, while the N_0 of the two AOA marker genes, MGI 16S rRNA and archaeal *amoA*, generally corresponded well to each other. Finally, there seemed to be more AOB than AOA in both the polluted and control sediments.

3.4.5 *Methanosarciniales* were enriched in the polluted sediments.

The polluted sediments did not resemble the control sediments in terms of archaeal composition. Firstly, the sequence relative abundance of *Nitrosopumilales* was lower in the polluted sediments than the control sediments after two and four weeks of incubation (Wilcoxon $p = 0.008$). Secondly, the polluted sediments displayed an increased relative abundance of the order *Methanosarciniales* (class *Methanosarcinia*), which ultimately became the dominating archaeal order in the polluted sediments (Figure 17B). This trend was observed at all taxonomic ranks. That is, the families *Methanosarcinaceae* and *Methermicoccaceae*, both belonging to the class *Methanosarcinia*, displayed a high relative sequence abundance in the polluted sediments at two and four weeks (Appendix Figure A20). *Methanolobus* (family *Methanosarcinaceae,* order *Methanosarcinales*) was the most sequence abundant genus in the polluted microcosm at four weeks, accompanied by two less abundant genera of the same family, *Methanococcoides* and *Methanosalsum*. However, none of the sequences were assigned a genus affiliated with *Methermicoccaceae* (Appendix Figure A21).

On the other hand, the control sediments were similar to the inoculum in terms of archaeal sequence composition. Specifically, the control microcosm was dominated by the classes *Nitrososphaeria*, *Nanoarchaeia*, and *Thermoplasmata* (Figure 17A). At order level, *Nitrosopumilales* (class *Nitrososphaeria*) and *Woesearchaeales* (class *Nanoarchaeia*) were dominant in terms of sequence relative abundance (Figure 17B). Except for the AOA, most of the archaeal sequences were not assigned a genus or family. Hence, the sequences that were assigned a family or genus were mostly classified as *Nitrosopumilaceae* and *Candidatus* Nitrosopumilus, respectively (Appendix Figures A20 and A21).

The relationship between the abundance of archaeal orders in the polluted microcosm and the control microcosm was investigated using a simple Pearson correlation. When comparing the relative abundance of archaeal orders in the polluted and control sediments, the Pearson correlation coefficient was -0.021 ($p = 0.95$). In contrast, when *Methanosarciniales* was excluded from the data set, the Pearson correlation coefficient increased to 0.99 ($p = 1.7 \cdot 10^{-9}$).

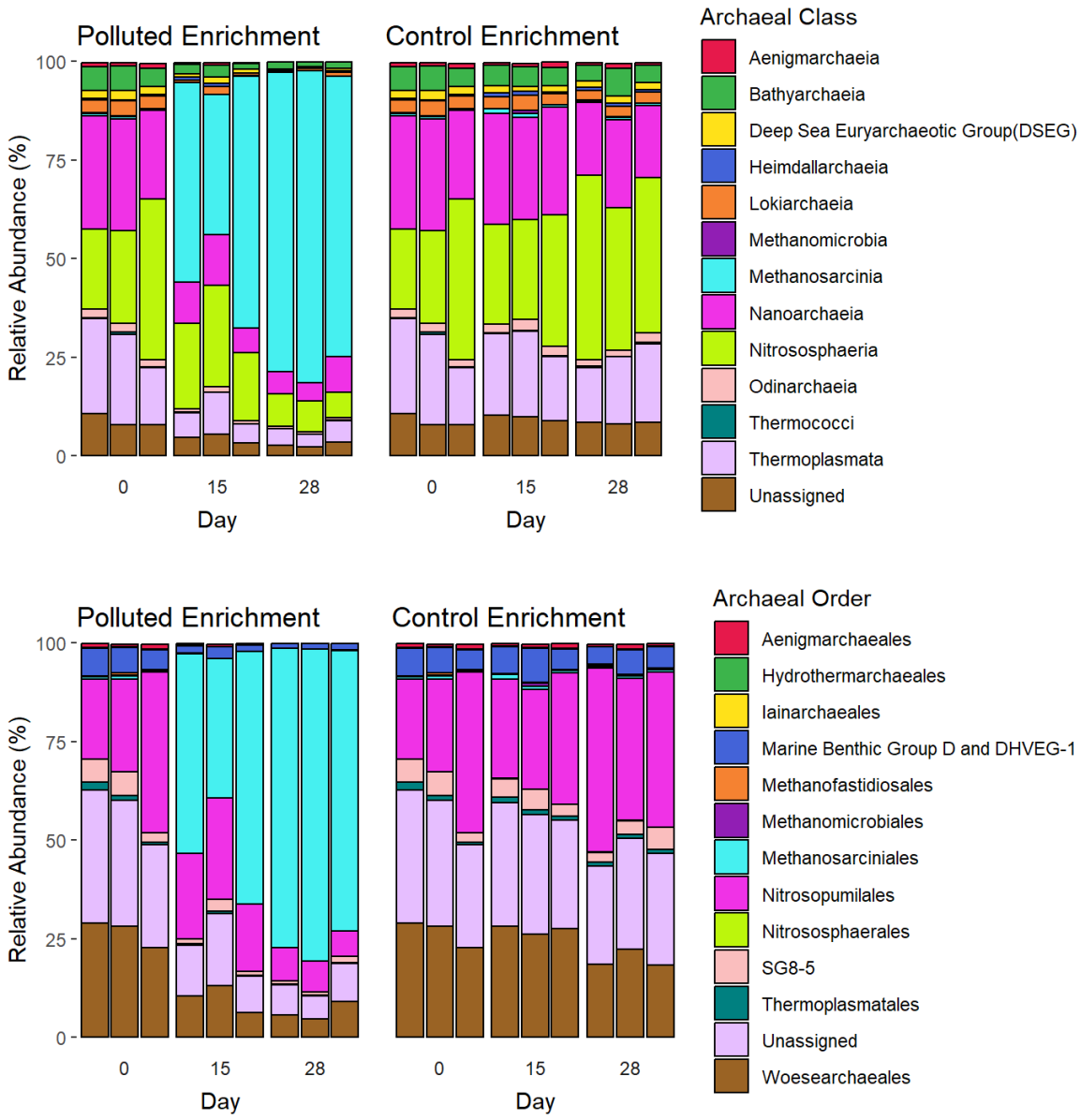

Figure 17: The 13 most abundant archaeal classes **(A)** and orders **(B)** in the pollution experiment microcosms, according to the Nanopore 16S rRNA sequencing results. Of the archaeal sequences, 3-11 % and 6-33 % were not assigned an archaeal class or order, respectively. All archaeal classes had different relative sequence abundances in the two microcosms (Wilcoxon $p < 0.03$), except *Halobacteria* and *Iainarchaeia* (Wilcoxon $p = 0.06$). The order *Nitrosopumilales* (class *Nitrososphaeria*) differed in relative abundance between the polluted and control sediments after two and four weeks of incubation (Wilcoxon $p = 0.008$). On the other hand, *Methanosarciniales* (class *Methanosarcinia*) was strongly enriched in the polluted sediments but barely present in the control sediments (Wilcoxon $p = 0.002$).

3.4.6 The polluted and control microcosms differed in terms of archaeal composition.

A principal coordinate analysis (PCoA) was performed to investigate if there was a difference between the control and polluted sediments in terms of relative sequence abundance of archaea and, if so, which archaea contributed to the difference. The PCoA showed that there was a clear separation between the sediment samples from the control and polluted sediments, and that *Methanosarciniales* was responsible for most of this variation. The 95 % confidence interval of the polluted samples did not overlap with the 95 % confidence interval of the control samples (Figure 18), indicating a clear distinction between the polluted sediments and the control sediments. Furthermore, *Methanosarciniales* correlated 99.9 % with principal coordinate 1 (PCo1), which explained 83 % of the variation in the data (Figure 18).

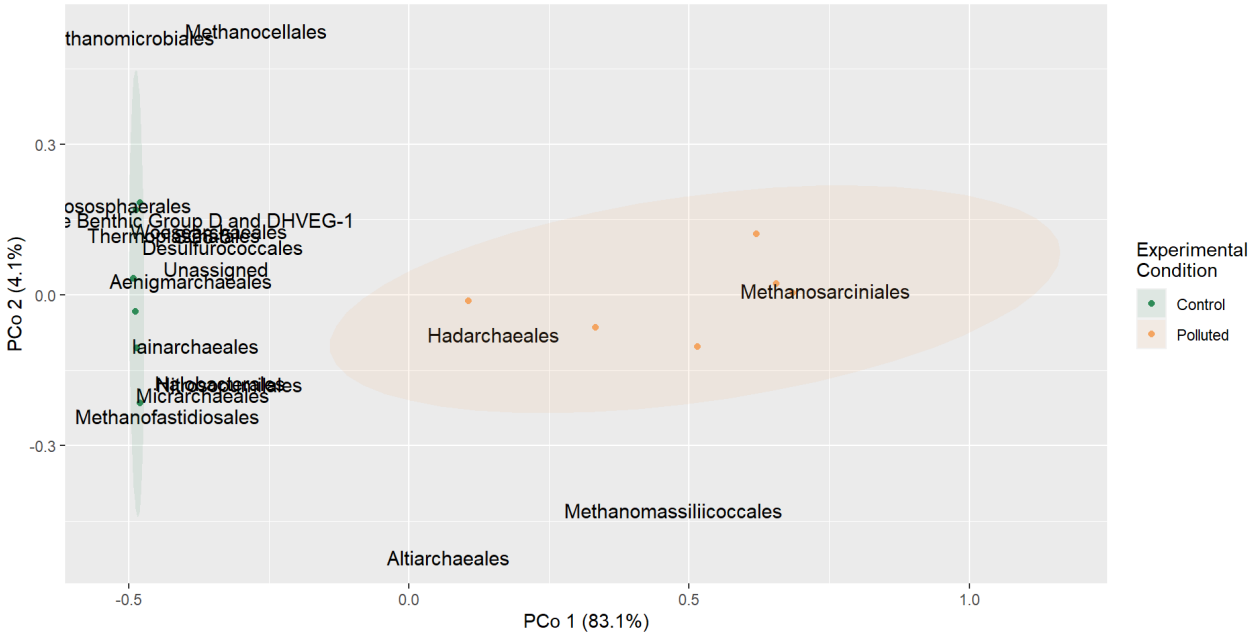

Figure 18: PCoA of the pollution experiment based on the archaeal sequencing data. The loadings of each archaeal order are indicated by text labels. PCo1 and PCo2 are the principal coordinates explaining most of the variation in the data. The 95% confidence intervals of the sample polluted and control samples are indicated with coloured ellipses and form distinct clusters with no overlap. PCo1 explains 83.1 % of the variation in the data, and is also responsible for most of the separation of the two clusters. *Methanosarciniales* correlates 99.9 % with PCo1, while all other phyla correlate < 20 % with PCo1. None of the archaeal classes correlate strongly with PCo2, which explains 4.2 % of the variation.

3.4.7 AOA decreased in relative abundance in the polluted microcosm.

The order *Nitrosopumilales*, which is affiliated with AOA, displayed an increasing sequence relative abundance in the control sediments during the last two weeks of the experiment (Figure 19). Interestingly, this was not the case for the Oslo Fjord and Cref microcosms, where the median relative abundance of *Nitrosopumilales* decreased after two weeks (Figure 10). In contrast to the control, the polluted sediments displayed a reduction in sequence relative abundance of *Nitrosopumilales* (Figure 19), accompanied by the enrichment of *Methanosarciniales* (Figure 17B).

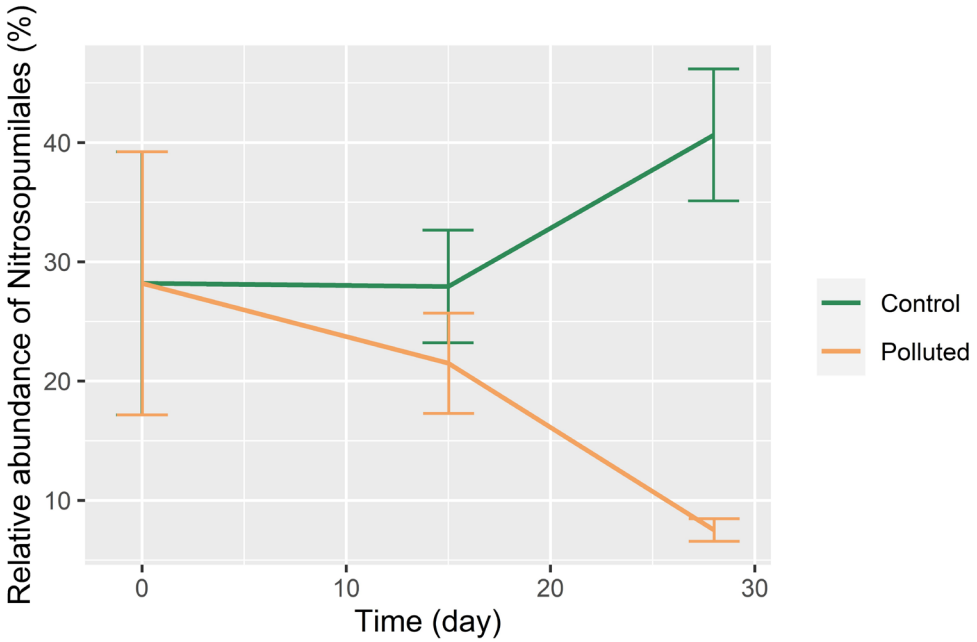

Figure 19: The mean relative abundances of *Nitrosopumilales* in the pollution experiment microcosms over time. The relative abundances were determined in triplicate sediment samples using Nanopore 16S rRNA sequencing. Standard deviations are indicated with error bars to indicate the variation among the triplicate samples.

3.4.8 *Gammaproteobacteria* increased in relative abundance in the polluted sediments.

Gammaproteobacteria seemed to be the most abundant bacterial class in both microcosms, according to the Nanopore 16S rRNA sequencing results. However, the relative abundance of *Gammaproteobacteria* was higher in the polluted sediments than in the control sediments after two and four weeks of incubation (Wilcoxon p = 0.02, Figure 20). Accordingly, a PCoA indicated that the polluted and control sediments differed in bacterial composition, and that most of the variation was attributed to *Gammaproteobacteria*. The difference between the control and polluted sediments increased as the taxonomic rank decreased (Appendix Figure A30).

The relative sequence abundance of four genera belonging to the *Gammaproteobacteria* differed in the polluted and control sediments. Specifically, *Methylophaga* (family *Methylophagaceae*, order *Nitrosococcales*) and *Methylosphaera* (family *Methylomonadaceae*, order *Methylococcales*) seemed to occur in larger relative abundances in the polluted sediments (Wilcoxon p = 0.004 and 0.002, respectively), while *Corallomonas* and *Neptuniibacter* (both belonging to the family *Nitrincolaceae*, order *Methylococcales*) occurred in a larger relative abundance in the control sediments (Appendix Figures A27-A29). However, most of the sequences were not assigned a genus.

Bacteroidia also differed in sequence relative abundance between the polluted and control sediments (Wilcoxon p = 0.02) and seemed to be slightly more abundant in the control sediments (Figure 20). However, this difference was not found in any detected members of the *Bacteroidia* at lower taxonomic ranks (Appendix Figures A27-A29). On the other hand, the genus *Sulfurimonas*, which belongs to the class *Campylobacteria,* was more abundant in the polluted microcosm sediments than the control.

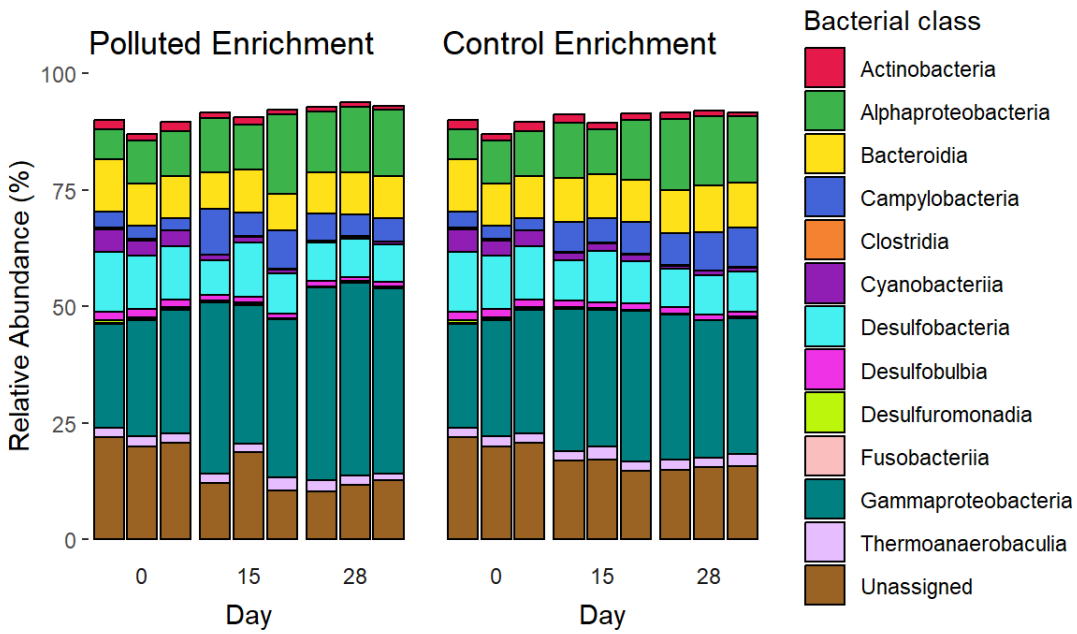

Figure 20: The 13 most abundant bacterial classes in the pollution experiment microcosms, according to the Nanopore sequencing results. It is worth noticing that 10-22 % of the sequences were not assigned a bacterial class. *Gammaproteobacteria* was the most abundant class in the polluted and control sediments, surpassing the relative abundance of unassigned sequences. Furthermore, *Gammaproteobacteria* and *Bacteroidia* displayed different abundances in the polluted and control microcosms at 15 and 28 days (Wilcoxon $p = 0.02$ for both).

4 Discussion

4.1 Were AOA affected by methanol?

4.1.1 Cref-20-S displayed signs of ammonia-oxidising activity.

While the concentration of nitrate was below the detection limit in the Oslo Fjord microcosms after four weeks of incubation (Figure 6B), it increased throughout the four weeks in the Cref microcosms (Figure 6A). This was especially the case for the sediments that were diluted with sand and incubated at 20˚C, Cref-20-S. Although the absence of nitrate in the Oslo Fjord microcosms could have been a result of nitrate-consuming processes, and not necessarily attributable to the absence of nitrifiers, the lack of observable signs of nitrification led to us rejecting the Oslo Fjord microcosms as possible inoculums for the pollution experiment. In contrast, the accumulation of nitrate in the Cref microcosms was interpreted as a sign of increased nitrifying activity, including the activity of AOA. Hence, the sediment from Cref-20-S was used as the inoculum in the pollution experiment.

4.1.2 AOB were more abundant than AOA.

Whereas the relative abundance of the AOA *Nitrosopumilales* increased in the control microcosm over time, it decreased in the polluted microcosm (Figure 19). The same trend was displayed by AOA at all taxonomic levels (Figures 17 and Appendix Figures A19-A21). However, the concentration of ammonium decreased at a substantially faster rate in the polluted microcosm than the control microcosm (Figure 14A), suggesting that AOA were not the primary drivers behind the ammonia-oxidation in the polluted microcosm.

The copy number of the bacterial and archaeal *amoA* genes implied that AOB were more abundant than AOA in the control and polluted microcosm (Figure 16). AOB can have up to three copies of the *amoA* gene in their genomes (Norton et al., 2002), while AOA seem to have a single copy (Walker et al., 2010). However, the genomic copy number variation is not enough to account for the observed difference in copy number between the archaeal and bacterial *amoA* genes (Figure 16). Hence, it may seem that most of the observed ammonium oxidation in the polluted and the control microcosm are attributable to AOB rather than AOA.

4.1.3 The absolute abundance of AOA did not decrease when exposed to methanol.

Nitrosopumilales was not the only archaeal order displaying a decreasing relative abundance in the polluted microcosm. A decrease in sequence relative abundance was also observed for all the other detected archaeal orders, except for *Methanosarciniales*, which was substantially enriched (Figure 17B). When excluding *Methanosarciniales*, the relative abundance of all the other archaeal orders correlated 99 % between the polluted and the control microcosm. The correlation decreased to -0.021 % when including *Methanosarciniales*, implying that the decrease in sequence relative abundance of other archaea may be attributable to the substantial enrichment of *Methanosarciniales*, rather than a decrease in absolute abundance. Hence, the abundance of AOA might not have been affected by the simulated pollution.

4.1.3 Methylotrophic and methanotrophic microorganisms were enriched in the presence of methanol.

Methanosarciniales (class *Methanosarcinia*) displayed a striking increase over time in the polluted microcosm (Figure 17B). *Methanosarciniales* are methylotrophic methanogens converting methanol to methane and carbon dioxide (Fischer et al., 2021), and were likely enriched due to the methanol added to the polluted microcosm. The order went from representing < 1 % of the total archaeal sequences in the inoculum to > 70 % in the polluted microcosm sediments after four weeks of incubation, while continuing to represent a minor part of the archaeal community in the control sediments (Figure 17B). Furthermore, the PCoA indicated that *Methanosarciniales* was the primary contributor to the clustering of the polluted microcosm samples and the control microcosm samples (Figure 18). Hence, in terms of archaeal composition, *Methanosarciniales* seemed to be the primary difference between the polluted and control microcosm.

The increase in bacterial 16S rRNA copy number over time (Figure 16) indicated that some bacteria were enriched. According to the sequencing results, *Gammaproteobacteria* was the only bacterial class to be enriched in the polluted microcosm (Figure 17). However, at lower taxonomic ranks, most of the sequences affiliated with the *Gammaproteobacteria* were not assigned a taxonomy. Nevertheless, the gammaproteobacterial orders *Methylococcales* and *Nitrosococcales* were largely responsible for the different bacterial composition in the polluted and control microcosm (Appendix Figure A30). At the genus level, two gammaproteobacterial genera were enriched in the polluted microcosm, namely *Methylosphaera* (order

Methylococcales) and *Methylophaga* (order *Nitrosococcales*) (Appendix Figure A29). All known species affiliated with the *Methylophaga* are heterotrophs that use methanol as a carbon and energy source, and most of them can reduce nitrate to nitrite (Boden, 2012; Fischer et al., 2021). The members of *Methylococcales* are methanotrophs and can grow on methanol (Bowman, 2014; Chistoserdova & Lidstrom, 2013). Hence, analogously to the archaeal *Methanosarcinia*, the enrichment of *Methylophaga* and *Methylococcales* might be directly attributable to methanol.

4.1.4 The consumption of ammonium may be attributable to methanotrophs and AOB.

Because AOA and AOB oxidise ammonium to nitrite, we expected to observe a decrease in the concentration of ammonium and an increase in in the concentration of nitrite, in the presence of metabolically active AOA. Indeed, the concentration of ammonium decreased in both microcosms and nitrite was recorded during the first days of the experiment (Figure 14). However, while the concentration of ammonium decreased slowly in the control microcosm, the polluted microcosm displayed a rapid decrease reaching the lower limit of detection after only eleven days of incubation. These observations imply that ammonia-oxidising activity occurred at a higher rate in the polluted microcosm than the control microcosm. Moreover, nitrite was detected exclusively when the concentration of ammonium peaked. Hence, the accumulation of nitrite seemed to be dependent on the availability of ammonium, which strongly points towards ammonia oxidation taking place.

As previously discussed, it seems that AOB might have been responsible for most of the ammonium consumption. AOB are affiliated with the *Gammaproteobacteria* and *Alphaproteobacteria*, which were both among the most abundant bacterial classes in the control and polluted sediments (Figure 20). *Gammaproteobacteria* increased in relative abundance in the polluted microcosm over time, while the bacterial *amoA* gene was equally present in the control and polluted microcosm and did not seem to increase over time (Figure 16). This raises the question of why ammonium was consumed at a higher rate in the polluted microcosm than the control microcosm. One possible explanation could be that the gene copy number does not provide information about the actual activity taking place. Although the AOB seemed to be as abundant in the polluted and the control microcosm, we do not know if the AOB were more actively oxidising ammonia in one of the microcosms. This problem could have been avoided by using real-time qPCR of *amoA* transcripts. Another possible explanation could be related to

the methanotroph *Methylococcales*, which was enriched in the polluted sediments but barely present in the control sediments. Some methanotrophs can carry out heterotrophic oxidation of ammonia to nitrite (Bock & Wagner, 2013; Fischer et al., 2021; Nyerges & Stein, 2009). Although we do not know if this is the case for *Methylococcales*, the possible association between methylotrophs and ammonia oxidation in the presence of methanol might be an interesting subject for further investigation.

4.1.5 Nitrate and nitrite might have been consumed by *Nitrospira* and *Desulfobacteria*.

Although 15 mg L^{-1} of nitrate was added to the polluted microcosm at the first day of the experiment, and repeatedly added in lower amounts upon each sampling, nitrate was never detected in the liquid medium. The absence of detectable nitrate does not necessarily imply the absence of nitrite-oxidisers. Indeed, nitrite was detected only in low concentrations in short periods of time, despite the signs of considerable ammonia-oxidising activity (Figure 14). The consistently low concentrations of nitrite observed in both microcosms may indicate the presence of nitrite oxidisers, which was confirmed by the detection of the nitrite-oxidising genus *Nitrospira* in both microcosms (Appendix Figure A29). Another possibility is that nitrite and nitrate were reduced. For example, *Desulfobacteria*, which was among the most sequence abundant bacterial classes in the control and polluted microcosms (Figure 20), can carry out nitrate and nitrite reduction as a respiratory strategy (Bourceau et al., 2023; Nie et al., 2021). Hence, several microorganisms might have contributed to the consumption of nitrate and nitrite.

4.1.6 Nitrification, methane oxidation, and fermentation might have lowered the pH.

After each sampling and pH recording, the pH was adjusted to 8-8.2. However, the recorded pH values after 2-3 days of incubation never surpassed pH 7.5, neither in the liquid medium nor in the sediments (Figure 15-C and 15-D). This observation indicates the occurrence of microbial activity producing acidic compounds, such as nitrification or fermentation. As time passed and the remaining amount of ammonium decreased, the difference between the adjusted pH and the recorded pH became smaller, hence the apparent increase in the system pH (Figure 15-C and 15-D). That is, assuming that the decreasing pH can be attributed to nitrifying activity, the decreasing concentration of available ammonium led to a lower rate of ammonia-oxidising activity, which is inextricably linked to the production of acidic by-products (Munn,

2019). Essentially, it seems that the system pH might have been tightly connected to the ammonia-oxidising activity in the microcosms.

On the second day of incubation, the liquid and sediment pH were lower in the polluted microcosm than the control microcosm. Assuming that the decreasing pH is attributable to nitrifying activity, this observation corresponds well to the fast consumption of ammonium observed in the polluted microcosm during the first days of the experiment (Figure 14A), further supporting the assumption that the rate of nitrification was higher in the polluted sediments during the first days of the experiment. Furthermore, after the second day of incubation, the liquid pH in the control microcosm was consistently lower compared to the polluted sediments (Figure 15D), while little difference was observed in the sediment pH (Figure 15C). Hence, as also suggested by the slow decrease in the concentration of ammonium observed in the control microcosm until day 20 (Figure 14B), the nitrifying activity might have continued for much longer in the control microcosm than the polluted microcosm.

The pH might also have decreased because of fermentative activity. In this case, available organic compounds are oxidised anaerobically to provide electrons for energy production (Munn, 2019). Although fermentative activity might have contributed to reducing the system pH, it is unlikely that fermentation was the main driver behind the difference in pH between the polluted and control microcosms (Figure 15D), because we assumed that the available amount of fermentation substrates was similar in the polluted and control microcosms.

Lastly, methanol can be oxidised by sulphate-reducing microorganisms. This reaction produces the acidic by-product H^+ (Fischer et al., 2021), which might have contributed to decreasing the pH in the polluted microcosm. Therefore, methanol oxidation might have been the primary driver behind the decreasing pH in the polluted sediments, especially after most of the ammonium was consumed.

4.1.7 The difference in liquid and sediment ORP indicates that oxygen might have been available and consumed.

The recorded sediment ORP was higher in the polluted microcosm than the control until day 4 (Figure 15A). Yet, the sediment ORPs in both microcosms were below 0 mV, implying anoxic conditions. Owing to their roles as potential electron acceptors, both nitrite and nitrate can promote oxidative conditions in the absence of oxygen (Søndergaard, 2009). The fact that

nitrite accumulated in the polluted microcosms during the first days of incubation (Figure 14A) indicates that ammonia-oxidising activity might have contributed to the initially elevated ORP.

Unlike the sediment ORP, the liquid ORP generally remained above 0 mV in both microcosms, indicating oxidative conditions in the liquid part of the microcosm. This is logical, because, unlike the sediments, the liquid medium was in direct contact with the microaerophilic space during the incubation and with the air during sampling, allowing oxygen to diffuse into the medium. The large difference in ORP between the sediments and the liquid medium suggests that most of the oxygen was consumed either in the liquid environment or in the interface between the liquid and the sediments. Hence, nitrification, which is an aerobic process, might have taken place in the surface sediments. Moreover, the liquid ORP was higher in the control microcosm than the polluted microcosm (Figure 15B), indicating that oxygen was consumed at a higher rate in the polluted microcosm. This might have been a result of the higher rate of ammonia oxidation as suggested by the rapid decrease in ammonium (Figure 14A).

4.1.8 Whether AOA are affected by methanol pollution is still uncertain.

It was recently shown that methanol and methane competitively inhibit the ammonia monooxygenase (AMO) enzyme of a soil AOA (Oudova-Rivera et al., 2023). To the writer's knowledge, sensitivity to methanol has not yet been investigated for marine AOA, which can have other adaptations than terrestrial AOA. On the other hand, the effect of methanol on the AMO enzyme was observed *in vitro*, while little is still known about the dynamics of methanol *in situ.* In marine bottom sediments, methanol could be consumed by methylotrophs before it reaches concentrations that inhibit the archaeal AMO. However, we did not monitor the concentration of methanol in the sediments. Furthermore, the rapid ammonium consumption observed in the polluted microcosm might be attributable to methanotrophic bacteria and AOB, making it more difficult to assess the activity of AOA. Hence, we cannot conclude on whether methanol affected AOA.

4.2 Were AOA enriched?

4.2.1 The ammonia-oxidising activity might be attributed to AOB.

The ammonia-oxidising order *Nitrosospumilales* (class *Nitrososphaeria*) was the archaeal order with the highest relative sequence abundance in all the Oslo Fjord microcosms, representing up to 75 % of the 16S rRNA sequences, in comparison to 30 % in the Cref microcosms (Figure 9). The relative sequence abundance of *Nitrosopumilales* seemed to increase in the Oslo Fjord microcosms and the Cref-20 microcosm during the first two weeks of incubation, indicating that we initially succeeded in enriching the AOA (Figure 10). However, after four weeks of incubation, the relative abundance of *Nitrosopumilales* had decreased in all the microcosms, indicating that the conditions were no longer optimal for its growth.

The AOA *Nitrososphaeria* accounted for up to 75 % of the archaeal 16S rRNA sequences in the microcosms (Figure 9). Despite this, we detected a substantially higher number of bacterial than archaeal *amoA* sequences in all the microcosms (Figure 7), suggesting that there were more AOB than AOA present there. However, the number of AOB seemed vanishingly low in comparison to the total number of bacteria (Figure 7). This was also reflected in the sequencing results (Appendix Figures A12 and A16), revealing that the AOB order *Nitrosococcales* was among the 13 most sequence abundant bacterial orders, although it accounted for less than 3 % of the bacterial 16S rRNA sequences in the microcosm sediments. However, the abundances generated with the 16S rRNA sequences are not comparable across domains, because archaeal and bacterial sequences were targeted and sequenced separately. While the Nanopore sequencing generated a total number of 14.8 million bacterial reads, only 5.17 million archaeal reads were generated. Although the sequence abundance of each domain could be interpreted in the light of primer coverage and the number of target sequences per genome, the considerable difference between the archaeal and bacterial 16S rRNA sequence abundance also indicates that, of the two domains, the bacteria dominated in the microcosm sediments. Taken together with the fact that the bacterial *amoA* was more abundant than the archaeal *amoA* in all the microcosms, the low relative abundance of AOB in comparison to other bacteria is most likely a result of the vast diversity and large number of bacteria. In conclusion, it seems that the AOB were much more abundant than the AOA in the microcosm sediments.

Other observations also suggest that AOB, rather than AOA, might have been the primary ammonia-oxidisers in the microcosms. Several AOB are affiliated with the *Alphaproteobacteria* and *Gammaproteobacteria* (Abeliovich, 2006; Bock & Wagner, 2013), all of which were among the most abundant bacterial phyla in the microcosms (Figure 12). Nevertheless, most of the bacterial 16S rRNA were not assigned a taxonomy at lower taxonomic ranks (figures A27-A29), which might have resulted in AOB being underrepresented in our results. Moreover, previous findings indicate that AOA, in contrast to AOB, are adapted to environments depleted in ammonium (Martens-Habbena et al., 2009) and that their growth can be inhibited by ammonia concentrations in the millimolar range (Park et al., 2010; Qin et al., 2014). Consequently, the observed accumulation of ammonium suggest that the microcosms might have provided better breeding grounds for AOB than AOA (Figure 6). Lastly, the AOA-affiliated genus *Nitrosopumilus* has displayed ammonia oxidation arrest in the presence of various organic compounds (Könneke et al., 2005; Qin et al., 2016). The low ORPs observed in the microcosms of the present project suggest the presence of organic matter (Godson et al., 2022). Although we do not know which organic compounds were present in our microcosms, this observation might suggest that the presence of some organic compounds could have contributed to disfavouring the growth of AOA.

4.2.2 Ammonia might have accumulated due to ammonification.

Because AOA and AOB carry out the first step of nitrification, involving the oxidation of ammonium to nitrite, we assumed that the concentration of ammonium would decrease in the presence of metabolically active ammonia oxidisers. However, the net observed concentration of ammonium increased in all the microcosms (Figure 6). The increasing ammonium concentrations do not necessarily indicate that nitrification did not take place. Rather, they may infer that some microbial activity produced at least as much ammonium as was consumed. The three main microbial sources of ammonium are nitrogen fixation, ammonification, and dissimilatory nitrate reduction to ammonia (DNRA) (Hutchins & Capone, 2022), and all three processes might have occurred in the microcosms. However, ammonium accumulation by DNRA requires nitrate, which was not initially available in the microcosms, while nitrification requires dinitrogen, which was not monitored during the present project. Ammonification, on the other hand, involves returning organic nitrogen from dead biomass to the inorganic pool by decomposition (Munn, 2019). Inoculating the sediments in a liquid medium could have stressed the sedimentary microbial community, because the artificial seawater medium might not have

replicated the exact conditions of the original fjord environment. Hence, adaptations to the new conditions might have been required to survive, potentially leading to the death of microorganisms not being able to adapt. Moreover, dead macroorganisms were observed in the Oslo Fjord microcosms after two weeks of incubation (Appendix Figure A4-A), potentially contributing to the source of organic nitrogen available for decomposition and resulting ammonium accumulation. The initial adaptation and resulting death of macro- and microorganisms might have led to the generally steep increase in ammonium concentrations during the first two weeks of incubation. In contrast, the decrease or more gentle increase observed at four weeks might have been a result of the microorganisms' adaptation to their new environment followed by a lower death rate (Figure 6).

4.2.3 Nitrite-oxidising activity might have taken place.

We also expected to detect nitrite in the case of ammonia-oxidising activity. However, nitrite was not detected at any time in any microcosm (Figure 6). The absence of detectable nitrite can be attributed to the nitrite-oxidising activity carried out by other microorganisms in the sediments, as indicated by the accumulation of nitrate observed in all the microcosms after two weeks of incubation (Figure 6). Nitrite-oxidising bacteria are affiliated with the *Alphaproteobacteria* and *Gammaproteobacteria* (Abeliovich, 2006), which were among the most abundant bacterial classes in all the microcosms (Figure 12). Additionally, the genus *Nitrospira*, which has both nitrite-oxidising and complete ammonia-oxidising (comammox) members (Sakoula et al., 2021), was detected in all the microcosms (Appendix Figures A14 and A18). Thus, several observations indicate that the second step of nitrification might have taken place in the microcosms.

4.2.4 *Desulfobacteria* and other microorganisms might have consumed nitrite and nitrate.

The concentration of nitrate had decreased to below the detection limit in the Oslo Fjord microcosms after four weeks (Figure 6B), indicating the presence of nitrate- or nitrite-consuming microbes. Nitrate is an energetically favourable electron acceptor in environments with little or no oxygen, which seemed to be the case in the microcosm sediments, considering the negative ORPs recorded (Figure 6). *Desulfobacteria*, which was the most sequence abundant bacterial class in all the microcosms (Figure 12), was recently found to harbour DNRA-associated genes and to carry out nitrate and nitrite reduction as a respiratory strategy (Bourceau et al., 2023; Nie et al., 2021). On the other hand, the relative abundance of

Desulfobacteria was higher in the Cref microcosms, where nitrate accumulated, than the Oslo Fjord microcosms, where no nitrate was detected. In contrast, *Cyanobacteria*, which are known to assimilate nitrate (Tee et al., 2020), were more abundant in the Oslo Fjord microcosms than the Cref microcosms (Appendix Figures A11 and A15). However, it is unlikely that they were metabolically active in the microcosms, considering the dark conditions. Hence, the consumption of nitrite or nitrate in the Oslo Fjord sediments might be attributable to some of the other microorganisms in the sediments or in the liquid medium.

4.2.5 The pH and ORP indicated that nitrification was carried out.

The ORP might have been connected to the presence of nitrate. Nitrate serves as an alternative electron acceptor under anaerobic conditions (Bourceau et al., 2023), and its presence can increase the sediment ORP (Søndergaard, 2009). Indeed, the microcosm displaying the steepest increase in nitrate concentration was the one inoculated with diluted Cref sediments and incubated at 20˚C (Cref-20-S). This nitrate accumulation took place during the last two weeks of the incubation. Simultaneously, Cref-20-S also displayed a steep increase in sediment ORP (Figure 6A), which might have been induced by the increasing presence of nitrate as a potential electron acceptor. In contrast, no nitrate was detected in any of the Oslo Fjord microcosms after four weeks of incubation, and the Oslo Fjord microcosms displayed relatively gentle, if any, increases in sediment ORP during the last two weeks of incubation (Figure 6B).

The pH recordings also support that nitrification took place in the microcosms. Both steps of nitrification involve proton turnover (Munn, 2019) and, therefore, the consistent decrease in pH observed in all the microcosms (Figure 6) could be an indication of nitrifying activity. However, there are several other microbial processes with a proton turnover, as well as processes generating organic acids, such as fermentation. Therefore, the pH is not a valid argument for nitrification alone but must be seen in context with the other chemical recordings and molecular analyses.

4.2.6 The sediments might have been anoxic.

Although most of our observations suggest that nitrification took place in the microcosms, the negative sediment ORP recorded (Figure 6) indicates that the microcosm sediments were anoxic. Nitrification is a strictly aerobic process and cannot occur in anoxic environments. However, it was recently shown that the AOA *Nitrosopumilus maritimus* SCM1 can produce its own oxygen when exposed to anoxic environments (Kraft et al., 2022). If this was the case

in our microcosms, the amount of produced oxygen might have been to small and local to be detected. Another explanation for the discrepancy between the ORP and the other observations could be the presence of an oxic-anoxic transition zone. Oxygen might have been available in the liquid part of the microcosm and consumed by AOA and other microbes living on the sediment surface, resulting in little or no penetration of oxygen through the sediments. Because the ORP meter was sunk 1-2 cm into the sediments when recording sediment ORPs, we did not obtain information about the possible availability of oxygen in the top millimetre layers of the sediments. Measuring the liquid ORP close to the sediment surface could have provided more information about potential oxygen gradients.

4.3 Archaeal primers might be biased due to limited sequence databases.

4.3.1 Two qPCR primer pairs were used to monitor AOA.

Various short-range primers targeting the archaeal 16S rRNA and *amoA* genes (Appendix Table A1) were evaluated for their abilities to detect AOA. Out of the four tested, none of the primer pairs targeting the archaeal *amoA* gene performed flawlessly (Appendix Figure A1, Appendix Table A2). Specifically, two primer pairs did not produce amplicons, while a third pair seemed to produce primer-dimers. The primer pair Cren-amoA-Q-F/Cren-amoA-mod-R was selected for the qPCR analyses of the microcosm sediments because it seemed to target AOA with high specificity, without targeting unwanted sequences from the bacterial controls. The same applied to the MCGI-554r/MCGI-391f pair, which targets the 16S rRNA gene of AOA (Wuchter et al., 2006). Both primer pairs were used to monitor AOA by qPCR during the present project.

Most of the short-range primer pairs targeting the archaeal 16S rRNA displayed either poor coverage of sedimentary AOA or poor specificity to archaea (Appendix Table A2). The poor coverage may be a result of the primer design. Primers easily become highly specific to the sequences used to design them, especially when the design is based on a limited selection of sequences, in terms of diversity and number. Because the covered diversity in archaeal databases is subject to our limited knowledge of the archaeal domain (Baker et al., 2020), it is reasonable to assume that archaeal primers also suffer from poor coverage of archaea not represented in the database.

4.3.2 Three long-range primer pairs displayed high coverage of the archaeal domain.

While the *in vitro* primer evaluation indicated that the forward primer Arch-21F was more specific to archaea than SSU1ArF, the *in silico* evaluation revealed that the forward primers differed substantially in terms of coverage. That is, Arch-21F covered only 5.9% of the archaeal domain (Appendix Table A4) and <25% of any archaeal phylum (Figure 4), while SSU1ArF covered 75.6 % of the archaea (Appendix Table A4) and most archaeal phyla with >50% (Figure 4). This illustrates the importance of evaluating the primers thoroughly before using them for analyses. Moreover, the reverse primers displayed ≈97% coverage of the archaeal domain (Appendix Table A4) and all archaeal phyla except *Iainarchaeota* ≈100%, resulting in the forward primer being the limiting factor in terms of covering the archaeal domain.

The Arch-1017R reverse primer was used to make the archaeal 16S rRNA library for the Nanopore sequencing, despite its low coverage of *Iainarchaeota* (Figure 4). This was primarily because Arch-1017R targeted fewer bacterial and eukaryotic sequences than the other evaluated reverse primers and, hence, was the most archaea-specific of the reverse primers (Appendix Table A4). In contrast, SSU1000ArR displayed a better coverage of *Iainarchaeota* (Figure 4), at the price of slightly lower specificity to archaea (Appendix Table A4). We chose to emphasise specificity rather than coverage of *Iainarchaeota*, which are not affiliated with the AOA. However, the SSU1000ArR reverse primer is a promising primer for future research aiming to cover the archaeal diversity at the price of slightly less specificity to archaea.

The long-range reverse primers that were evaluated using SILVA TestProbe covered the exact same 14 archaeal phyla as the forward primer SSU1ArF (Figure 4). Interestingly, these 14 phyla are the only archaeal phyla represented in the SILVA SSU r138.1 database (accessed 14.07.2023 from https://www.arb-silva.de/browser/). This observation indicates that the four primers in question may be biased toward a limited selection of archaeal sequences available for primer design. As previously mentioned, primers are more effective at targeting sequences closely related to the sequences used for the primer design. The issue with primer bias was recently assessed using reverse-transcription of SSU rRNA molecules to sequence the 16S rRNA genes from various environmental samples (Karst et al., 2018). The experiment resulted in more full-length archaeal 16S rRNA sequences than are available in the SILVA database, which illustrates the potentially severe consequences of using methods dependent on primers. Furthermore, their findings illustrate the weakness in methods relying on databases. Although

databases may harbour only high-quality sequences, their coverage of the archaeal domain may not reflect the actual diversity of archaea. Thus, the archaeal taxa detected in the microcosms from the present project might as well be biased against actual archaeal diversity, due to primer bias and database bias.

4.4 Future aspects

It was recently shown that the ammonia monooxygenase enzyme of a terrestrial AOA was competitively inhibited by methane and methanol (Oudova-Rivera et al., 2023). In contrast, our results indicate that the abundance of AOA was not affected by methanol and nitrate pollution (Figure 16), possibly because the sediments subjected to methanol and nitrate displayed an enrichment of methylotrophic bacteria and archaea that might have consumed the methanol (Figures 17 and 20). Monitoring the methanol concentration could have contributed to better understand the dynamics of the compounds and whether it accumulated.

A PCoA of the microbial composition in the polluted and control sediment suggested that the methylotrophs were accountable for most of the variation between the two sediments (Figures 18 and appendix A30). Nevertheless, the ammonia oxidation seemed to occur at a higher rate in the polluted microcosm (Appendix Figure 14A), indicating that there might be an association between methylotrophs and ammonia-oxidation. We do not have the evidence to conclude on this, but previous findings indicate that some methanotrophs can carry out heterotrophic oxidation of ammonia to nitrite (Bock & Wagner, 2013; Fischer et al., 2021; Nyerges & Stein, 2009). Nevertheless, monitoring mRNA transcripts of the bacterial and archaeal *amoA* could have provided insights into whether AOA and AOB were metabolically active.

The number of sequenced archaeal reads was approximately three times lower than the number of bacterial reads. This might reflect that bacteria were more abundant than bacteria in our enrichments. This is contradictory to previous findings reporting that the Archaea is the dominant prokaryotic domain in marine sediments (Biddle et al., 2006; Lipp et al., 2008). However, as previously discussed, the low abundance of archaea relative to bacteria might be a result of primer bias. Furthermore, some methods of DNA extraction are less efficient for archaea than bacteria (Roopnarain et al., 2017), resulting in an underestimation of archaea in subsequent molecular analyses. Although the extraction efficiency was not controlled for

archaea in the present project, this might have been a contributing factor to the low number of archaeal reads relative to bacterial reads.

The number of Nanopore reads that were not assigned a taxonomy increased with decreasing taxonomic rank. In other words, the taxonomic resolution was relatively poor. This made it difficult to assess the microbial diversity at lower taxonomic ranks, which could have provided more detailed information about the metabolic potential of the microbes in the sediments. The poor taxonomic resolution might have been a result of the read quality, which was designated a Qscore 10 indicating a 1/10 error rate. Employing another sequencing technology, such as the more time consuming and expensive Illumina sequencing technology, could contribute to a higher taxonomic resolution. Another possible explanation for the poor taxonomic resolution is that our knowledge about sedimentary microorganisms is limited (Orcutt et al., 2011). As a result, the sequences that were not assigned a taxonomy might have originated from yet unknown lineages.

During the microcosm experiment, we diluted parts of the sediment samples with sterile sand before inoculating them in the liquid medium, because we hypothesised that sedimentary AOA may require space and available sediments for potential aggregation to thrive. Microcosms with diluted and undiluted sediments were incubated at two different temperatures, because we wanted to assess if the temperature influenced the enrichment of AOA. However, neither the microcosm temperature nor diluting the sediments with sterile sand seemed to affect the enrichment of *Nitrosopumilales* (Figure 11). On the other hand, diluting the sediments with sterile sand might have positively influenced the survival of *Nitrosopumilales*. That is, while the overall relative abundance of *Nitrosopumilales* decreased during the last two weeks of incubation, it remained slightly higher in the diluted sediments than the undiluted sediments (Figure 11). Although this difference was not supported by the Wilcoxon rank sum test, it may suggest that the diluted sediments provide some benefit for the survival of AOA, perhaps by reducing the abundance of, and thereby the competition with, other microbes in the sediments. Hence, the effect of sediment dilution on the survival of AOA in a microcosm might be an interesting subject for further investigation of the interaction of AOA with other microorganisms.

In previous studies, the microcosm and isolation of sedimentary AOA was done in a liquid medium, and the sediments were discarded after the primary inoculation (Könneke et al., 2005;

Park et al., 2010). We hypothesised that sedimentary AOA might have better chances to survive by keeping the sediments in the microcosms and possibly by providing sterile sediments as a part of the medium. During the initial microcosm experiments, we did not successfully enrich AOA (Figures 7 and 10). On the other hand, AOA seemed to be enriched in the control sediments during the pollution experiment (Figure 19), although this was not supported by the qPCR analysis (Figure 16). In contrast to the initial Cref and Oslo Fjord microcosms, the microcosms from the pollution experiment were supplied with fresh medium and pH adjustments with 2-3 days interval. Our results suggest that the enrichment of AOA in a medium partially composed of sediments might be possible, but that adjusting the pH regularly and supply the microcosm with fresh medium regularly may be favourable.

Another difference between the initial microcosms and the control microcosm from the pollution experiment is the dynamics of ammonium. The initial Cref and Oslo Fjord microcosms displayed an accumulation of ammonium (Figure 6), suggesting that a vast number of microorganisms might not have survived the transition to laboratory conditions. In contrast, the inoculum used in the pollution experiment had already been subjected to laboratory conditions for four weeks, which might have given the microorganisms time to adapt. Indeed, the ammonium levels did not increase in the pollution experiment microcosms (Figure 6), indicating a lower decomposition and ammonification rate. To decrease the potential stress attributed to the artificial conditions in a microcosm, and thus potentially reducing the extent of necessary adaptations to the new environment, the artificial seawater medium could have been substituted with natural seawater. Future microcosms attempts might consider allowing the microcosms to go on for longer than four weeks, thereby allowing the sedimentary microorganisms to adapt before being enriched. During the adaptation period, close monitoring of ammonium may be helpful, so that measures can be taken to reduce the concentration of ammonium.

The medium used during the present project contained 0.2 mM ammonium, which might have been too much to avoid the enrichment of AOB. Previous findings indicate that AOB have a higher affinity threshold to ammonia compared to AOA (Martens-Habbena et al., 2009). Specifically, AOB have displayed ammonia affinity thresholds in the range of 1-140 µM (Bollmann A, 2002; Prosser, 2004). In contrast, AOA have displayed exponential growth with as little as <10 nM ammonium (Martens-Habbena et al., 2009) and inhibited growth at > 1-4

mM ammonium (Park et al., 2010; Qin et al., 2014). However, in the pollution experiment microcosms, the MGI 16S rRNA and bacterial *amoA* genes produced copy number curves with strikingly similar shapes (Figure 16), suggesting that AOA and AOB might have thrived in the same sediment microenvironments. Although the concentration of ammonium in the microcosms from the present study never surpassed 1 mM (Figure 6), the accumulation of ammonium, which was potentially attributable to ammonification, might have contributed to enriching AOA and AOB simultaneously. Furthermore, the bacterial *amoA* gene was detected in substantially higher numbers than the archaeal *amoA* gene in all the microcosms in the present study, including the inoculums (Figures 7 and 16), indicating that AOB might have started out with an advantageous abundance in the case of a competition. Hence, further attempts to enrich AOA might consider using a lower concentration of ammonium in the liquid medium, to subject the AOB to an even stronger selection pressure.

Bicarbonate was used as the buffer and the carbon source for chemolithoautotrophy in the microcosms. However, supposing that chemolithoautotrophic activity consumed some of the bicarbonate for carbon fixation, the buffer capacity of bicarbonate was likely reduced over time. Furthermore, the consistent decrease in pH observed in our microcosms also indicates that a stronger buffering system may be beneficial. Hence, a buffering system other than bicarbonate, such as the HEPES buffer (Martens-Habbena et al., 2009), could be more suitable for microcosms of sedimentary AOA.

4.5 Strengths and weaknesses

The combination of DNA-based and chemical methods represents one of the strengths of the present study. While DNA-based methods provided an insight into the microbial composition of the sediments, the measurements of pH, ORP, and nitrogen species provided useful information about the nitrifying activity, as well as other potential metabolic activities, occurring in the sediments.

Despite AOA being the organisms of major interest in the present project, the microcosm approach adapted in the present project enabled the observation of AOA in a context allowing interactions with other sedimentary microorganisms. Our approach resulted in the unexpected observation of methylotrophic archaea and bacteria being enriched when exposed to methanol,

and the possibility of methylotrophs contributing to the oxidation of ammonium. Nevertheless, microcosms are, at best, simplified versions of the ecosystem of interest. Therefore, our findings must be interpreted in this context, and a future *in situ* revision of our findings might provide a more correct picture of the processes and interactions taking place in the presence of methanol.

While the sequencing results indicated that the relative abundance of AOA decreased over time in the polluted microcosm, the qPCR results suggested that the abundance of AOA did not change during the experiment. However, the precision of the DNA-based methods was relatively poor, as displayed by the large standard deviations associated with the mean copy number of the AOA marker genes (Figure 16) and the mean relative sequence abundance (Figure 19). The poor precision might be a result of the sediments samples being taken in triplicates from a non-homogenous medium. Sediments can potentially display local differences in microbial composition within the same microcosm. Another explanation might be the technical variation in DNA yield from the extraction, which was not investigated during the present project.

Although DNA quantification and sequencing techniques are useful tools to assess the microbial composition and metabolic potential in environmental samples, DNA alone does not tell the whole story. The presence of a gene, such as the *amoA* gene, does not necessarily imply that the gene is expressed or that the enzyme it encodes is active or even functioning. Therefore, a major weakness in the present study is the use of DNA-based techniques to infer the microbial processes taking place in the microcosms. RNA-based or proteomics-based methods could have provided a more nuanced overview of the activity and interactions taking place in the microcosms.

The primer-dependent methods used in the present project also represent a weakness. Although the primers were carefully chosen based on thorough evaluations, there will always be a bias associated with the use of primers. As previously discussed, primers are biased towards the sequences used to design them, which might result in a failure to detect yet unknown organisms. Furthermore, primer-based methods require the use of PCR, which is highly susceptible to contamination due to its ability to exponentially amplify the present target genes. The primer-associated weaknesses can be solved using a metagenomic approach (Escobar-Zepeda et al., 2015), thus avoiding the use of primers.

Lastly, the present project illustrates a weakness related to our limited knowledge about archaea. The SILVA SSU database release 138.1, which was used to assign taxonomies to the sequences generated in the present project, contains nearly two million bacterial 16S rRNA sequences. In contrast, the number of archaeal sequences is barely 70,000 (accessed 17.08.23 from https://www.arb-silva.de/). The large difference between the number of bacterial and archaeal sequences reflects our limited knowledge about archaea. It was also reflected in our results, where the number of archaeal taxa detected in the sediments was considerably lower than the observed bacterial diversity. Furthermore, the number of archaeal sequences that were not assigned a taxonomy in the present project was considerably lower than the number of unassigned bacterial sequences. This might be a result of the combined primer bias and limited number of sequences available in the database, which might have resulted in us overlooking several yet unknown archaea. Hence, as long as our knowledge about archaea remains sparse, our understanding of archaeal communities may be biased against the yet unknown diversity.

4.6 Conclusion

The results of the present project indicate that the organic emissions from wastewater treatment plants might contribute to the enrichment of methylotrophic methanogens and, consequently, increasing the emissions of methane. Methane is a greenhouse gas that contributes to global warming, and methane emissions from aquatic ecosystems increases with anthropogenic impact (Rosentreter et al., 2021). In times where global warming represents one of our biggest challenges, strategies to reduce the anthropogenic contribution to the emission of greenhouse gases can be of great value. Our findings suggest that further investigations of the impact of methanol pollution and purified wastewater on marine sediments might be beneficial to our understanding of anthropogenic greenhouse gas emissions. However, our experiment should be reproduced using multiple sediment samples in multiple replicates to evaluate the reliability of our findings. Moreover, *in situ* analyses of sediments impacted by purified wastewater will also contribute to draw any conclusions on the impact of purified wastewater on sedimentary microorganisms.

Whether marine AOA are affected by methanol pollution remains unclear. We did observe signs of ammonia-oxidising activity, but we were unable to attribute it to AOA. While the relative abundance of AOA decreased in the presence of methanol, there were little signs of an

absolute decrease in their abundance. Altogether, we did not observe a direct inhibition of AOA by methanol. Our results rather suggest that methylotrophs might contribute to keeping the concentration of methanol too low to have an inhibitory effect on AOA. Moreover, it seems that ammonia oxidation might have occurred at a faster rate in polluted sediments than control sediments, implying a potential connection between methanol and ammonium metabolisms. These observations represent interesting topics for further investigation.

While signs of nitrifying activity were observed during our attempt to enrich AOA, the qPCR results revealed that AOA did not increase in abundance. Nevertheless, the experience acquired from the project might be of use for future attempts in enriching AOA. That is, the concentration of ammonium might be of great importance to the competition between AOA and AOB, while the use of natural seawater as the liquid medium might contribute to keeping the accumulation of ammonium to a minimum. Moreover, regular monitoring and supply of fresh medium can contribute to enriching AOA. Although enriching AOA in a medium composed of sediments and liquid medium makes it difficult to quantify the AOA due to the inhomogeneity of the sediments, chemical monitoring has proven useful to detect nitrifying activity. Lastly, the use of primer-dependent methods does not come without bias, especially for archaea, which are poorly represented in the sequence databases.

We found three promising long-range primer pairs targeting the archaeal 16S rRNA gene. However, the restricted selection of archaeal sequences available in databases might have introduced some bias in our perception of the archaeal composition of the sediments. The primer coverage might be biased towards the sequences used to design the primers, while database shortcomings might result in low taxonomic resolution when assigning taxonomies to the sequences. Hence, primer-independent methods can be of great value to further research.

Two of the evaluated qPCR primers displayed a satisfactory detection of sedimentary AOA. However, the short-range primer pairs were only evaluated *in vitro* using DNA extractions from a restricted selection of sediments. Therefore, the primer specificity may be biased towards AOA specific to these sediments, while other AOA are potentially not covered by the primer pairs. Evaluating the qPCR primers *in silico* could have provided a better understanding of our results and potential biases related to their coverage and specificity.

References

Abeliovich, A. (2006). The Nitrite Oxidizing Bacteria. In M. Dworkin, S. Falkow, E. Rosenberg, K.-H. Schleifer, & E. Stackebrandt (Eds.), *The Prokaryotes: Volume 5: Proteobacteria: Alpha and Beta Subclasses* (pp. 861-872). Springer New York. https://doi.org/10.1007/0-387-30745-1_41

Apprill, A., McNally, S., Parsons, R., & Weber, L. (2015). Minor revision to V4 region SSU rRNA 806R gene primer greatly increases detection of SAR11 bacterioplankton. *Aquatic Microbial Ecology*, *75*(2), 129-137. https://www.int-res.com/abstracts/ame/v75/n2/p129-137/

Arrigo, K. R. (2005). Marine microorganisms and global nutrient cycles. *Nature*, *437*(7057), 349-355. https://doi.org/10.1038/nature04159

Bahram, M., Anslan, S., Hildebrand, F., Bork, P., & Tedersoo, L. (2019). Newly designed 16S rRNA metabarcoding primers amplify diverse and novel archaeal taxa from the environment. *Environ Microbiol Rep*, *11*(4), 487-494. https://doi.org/10.1111/1758-2229.12684

Baker, B. J., De Anda, V., Seitz, K. W., Dombrowski, N., Santoro, A. E., & Lloyd, K. G. (2020). Diversity, ecology and evolution of Archaea. *Nature Microbiology*, *5*(7), 887-900. https://doi.org/10.1038/s41564-020-0715-z

Baker, G. C., Smith, J. J., & Cowan, D. A. (2003). Review and re-analysis of domain-specific 16S primers. *J Microbiol Methods*, *55*(3), 541-555. https://doi.org/10.1016/j.mimet.2003.08.009

Bar-On, Y. M., Phillips, R., & Milo, R. (2018). The biomass distribution on Earth. *Proceedings of the national academy of sciences*, *115*(25), 6506-6511. https://doi.org/doi:10.1073/pnas.1711842115

Biddle, J. F., Lipp, J. S., Lever, M. A., Lloyd, K. G., Sørensen, K. B., Anderson, R., Fredricks, H. F., Elvert, M., Kelly, T. J., Schrag, D. P., Sogin, M. L., Brenchley, J. E., Teske, A., House, C. H., & Hinrichs, K.-U. (2006). Heterotrophic Archaea dominate sedimentary subsurface ecosystems off Peru. *Proceedings of the national academy of sciences*, *103*(10), 3846-3851. https://doi.org/doi:10.1073/pnas.0600035103

Bock, E., & Wagner, M. (2013). Oxidation of Inorganic Nitrogen Compounds as an Energy Source. In E. Rosenberg, E. F. DeLong, S. Lory, E. Stackebrandt, & F. Thompson (Eds.), *The Prokaryotes: Prokaryotic Physiology and Biochemistry* (pp. 83-118). Springer Berlin Heidelberg. https://doi.org/10.1007/978-3-642-30141-4_64

Boden, R. (2012). Emended description of the genus Methylophaga Janvier et al. 1985. *International Journal of Systematic and Evolutionary Microbiology*, *62*(Pt_7), 1644-1646. https://doi.org/https://doi.org/10.1099/ijs.0.033639-0

Bollmann A, B.-G. M., Laanbroek HJ. (2002). Growth at Low Ammonium Concentrations and Starvation Response as Potential Factors Involved in Niche Differentiation among Ammonia-Oxidizing Bacteria. *Applied and Environmental Microbiology*, *68*(10), 4751-4757. https://doi.org/doi:10.1128/AEM.68.10.4751-4757.2002

Bourceau, O. M., Ferdelman, T., Lavik, G., Mussmann, M., Kuypers, M. M. M., & Marchant, H. K. (2023). Simultaneous sulfate and nitrate reduction in coastal sediments. *ISME Communications*, *3*(1), 17. https://doi.org/10.1038/s43705-023-00222-y

Bowman, J. P. (2014). The Family Methylococcaceae. In E. Rosenberg, E. F. DeLong, S. Lory, E. Stackebrandt, & F. Thompson (Eds.), *The Prokaryotes: Gammaproteobacteria* (pp. 411-440). Springer Berlin Heidelberg. https://doi.org/10.1007/978-3-642-38922-1_237

Brochier-Armanet, C., Boussau, B., Gribaldo, S., & Forterre, P. (2008). Mesophilic crenarchaeota: proposal for a third archaeal phylum, the Thaumarchaeota. *Nature Reviews Microbiology*, *6*(3), 245-252. https://doi.org/10.1038/nrmicro1852

Bråte, J., Logares, R., Berney, C., Ree, D. K., Klaveness, D., Jakobsen, K. S., & Shalchian-Tabrizi, K. (2010). Freshwater Perkinsea and marine-freshwater colonizations revealed by pyrosequencing and phylogeny of environmental rDNA. *Isme j*, *4*(9), 1144-1153. https://doi.org/10.1038/ismej.2010.39

Bustin, S. A., Benes, V., Garson, J. A., Hellemans, J., Huggett, J., Kubista, M., Mueller, R., Nolan, T., Pfaffl, M. W., Shipley, G. L., Vandesompele, J., & Wittwer, C. T. (2009). The MIQE Guidelines: Minimum Information for Publication of Quantitative Real-Time PCR Experiments. *Clinical Chemistry*, *55*(4), 611-622. https://doi.org/10.1373/clinchem.2008.112797

Callahan, B. J., McMurdie, P. J., Rosen, M. J., Han, A. W., Johnson, A. J. A., & Holmes, S. P. (2016). DADA2: High-resolution sample inference from Illumina amplicon data. *Nature Methods*, *13*(7), 581-583. https://doi.org/10.1038/nmeth.3869

Cavicchioli, R., Ripple, W. J., Timmis, K. N., Azam, F., Bakken, L. R., Baylis, M., Behrenfeld, M. J., Boetius, A., Boyd, P. W., Classen, A. T., Crowther, T. W., Danovaro, R., Foreman, C. M., Huisman, J., Hutchins, D. A., Jansson, J. K., Karl, D. M., Koskella, B., Mark Welch, D. B., . . . Webster, N. S. (2019). Scientists' warning to humanity: microorganisms and climate change. *Nature Reviews Microbiology*, *17*(9), 569-586. https://doi.org/10.1038/s41579-019-0222-5

Chistoserdova, L., & Lidstrom, M. E. (2013). Aerobic Methylotrophic Prokaryotes. In E. Rosenberg, E. F. DeLong, S. Lory, E. Stackebrandt, & F. Thompson (Eds.), *The Prokaryotes: Prokaryotic Physiology and Biochemistry* (pp. 267-285). Springer Berlin Heidelberg. https://doi.org/10.1007/978-3-642-30141-4_68

D'Hondt, S., Inagaki, F., Zarikian, C. A., Abrams, L. J., Dubois, N., Engelhardt, T., Evans, H., Ferdelman, T., Gribsholt, B., Harris, R. N., Hoppie, Bryce W., Hyun, J.-H., Kallmeyer, J., Kim, J., Lynch, J. E., McKinley, Claire C., Mitsunobu, S., Morono, Y., Murray, R. W., . . . Ziebis, W. (2015). Presence of oxygen and aerobic communities from sea floor to basement in deep-sea sediments. *Nature Geoscience*, *8*(4), 299-304. https://doi.org/10.1038/ngeo2387

Danovaro, R., Molari, M., Corinaldesi, C., & Dell'Anno, A. (2016). Macroecological drivers of archaea and bacteria in benthic deep-sea ecosystems. *Science Advances*, *2*(4), e1500961.

De León, K. B., Gerlach, R., Peyton, B. M., & Fields, M. W. (2013). Archaeal and bacterial communities in three alkaline hot springs in Heart Lake Geyser Basin, Yellowstone National Park. *Front Microbiol*, *4*, 330. https://doi.org/10.3389/fmicb.2013.00330

DeLong, E. F. (1992). Archaea in coastal marine environments. *Proceedings of the national academy of sciences*, *89*(12), 5685-5689. https://doi.org/doi:10.1073/pnas.89.12.5685

Doxey, A. C., Kurtz, D. A., Lynch, M. D. J., Sauder, L. A., & Neufeld, J. D. (2015). Aquatic metagenomes implicate Thaumarchaeota in global cobalamin production. *The ISME journal*, *9*(2), 461-471. https://doi.org/10.1038/ismej.2014.142

Elser, J. J., Bracken, M. E. S., Cleland, E. E., Gruner, D. S., Harpole, W. S., Hillebrand, H., Ngai, J. T., Seabloom, E. W., Shurin, J. B., & Smith, J. E. (2007). Global analysis of nitrogen and phosphorus limitation of primary producers in freshwater, marine and terrestrial ecosystems. *Ecology Letters*, *10*(12), 1135-1142. https://doi.org/https://doi.org/10.1111/j.1461-0248.2007.01113.x

Escobar-Zepeda, A., Vera-Ponce de León, A., & Sanchez-Flores, A. (2015). The Road to Metagenomics: From Microbiology to DNA Sequencing Technologies and Bioinformatics. *Front Genet*, *6*, 348. https://doi.org/10.3389/fgene.2015.00348

Fischer, P. Q., Sánchez-Andrea, I., Stams, A. J. M., Villanueva, L., & Sousa, D. Z. (2021). Anaerobic microbial methanol conversion in marine sediments. *Environmental Microbiology*, *23*(3), 1348-1362. https://doi.org/https://doi.org/10.1111/1462-2920.15434

Forurensningsforskriften. (2004). *Forskrift om begrensning av forurensning*. (FOR-2004-06-01-931). Norway: Ministry of Climate and Environment Retrieved from https://lovdata.no/dokument/SF/forskrift/2004-06-01-931

Gantner, S., Andersson, A. F., Alonso-Sáez, L., & Bertilsson, S. (2011). Novel primers for 16S rRNA-based archaeal community analyses in environmental samples. *Journal of Microbiological Methods*, *84*(1), 12-18. https://doi.org/https://doi.org/10.1016/j.mimet.2010.10.001

Godson, P. S., Vincent, S. G. T., & Krishnakumar, S. (2022). *Ecology and Biodiversity of Benthos*. Elsevier.

Higuchi, R., Fockler, C., Dollinger, G., & Watson, R. (1993). Kinetic PCR analysis: real-time monitoring of DNA amplification reactions. *Biotechnology (N Y)*, *11*(9), 1026-1030. https://doi.org/10.1038/nbt0993-1026

Hong, J. K., Kim, H. J., & Cho, J. C. (2014). Novel PCR primers for the archaeal phylum Thaumarchaeota designed based on the comparative analysis of 16S rRNA gene sequences. *PLoS One*, *9*(5), e96197. https://doi.org/10.1371/journal.pone.0096197

Hooper, A. B., & Terry, K. T. (1973). Specific Inhibitors of Ammonia Oxidation in Nitrosomonas. *Journal of Bacteriology*, *115*(2), 480-485. https://doi.org/doi:10.1128/jb.115.2.480-485.1973

Hutchins, D. A., & Capone, D. G. (2022). The marine nitrogen cycle: new developments and global change. *Nature Reviews Microbiology*, *20*(7), 401-414. https://doi.org/10.1038/s41579-022-00687-z

Jensen, M. M., Thamdrup, B., & Dalsgaard, T. (2007). Effects of Specific Inhibitors on Anammox and Denitrification in Marine Sediments. *Applied and Environmental Microbiology*, *73*(10), 3151-3158. https://doi.org/doi:10.1128/AEM.01898-06

Kalyuhznaya, M. G., Martens-Habbena, W., Wang, T., Hackett, M., Stolyar, S. M., Stahl, D. A., Lidstrom, M. E., & Chistoserdova, L. (2009). Methylophilaceae link methanol oxidation to denitrification in freshwater lake sediment as suggested by stable isotope probing and pure culture analysis. *Environmental microbiology reports*, *1*(5), 385-392. https://doi.org/https://doi.org/10.1111/j.1758-2229.2009.00046.x

Karner, M. B., DeLong, E. F., & Karl, D. M. (2001). Archaeal dominance in the mesopelagic zone of the Pacific Ocean. *Nature*, *409*(6819), 507-510. https://doi.org/10.1038/35054051

Karst, S. M., Dueholm, M. S., McIlroy, S. J., Kirkegaard, R. H., Nielsen, P. H., & Albertsen, M. (2018). Retrieval of a million high-quality, full-length microbial 16S and 18S rRNA gene sequences without primer bias. *Nature Biotechnology*, *36*(2), 190-195. https://doi.org/10.1038/nbt.4045

King, G. M., Klug, M. J., & Lovley, D. R. (1983). Metabolism of Acetate, Methanol, and Methylated Amines in Intertidal Sediments of Lowes Cove, Maine. *Applied and Environmental Microbiology*, *45*(6), 1848-1853. https://doi.org/doi:10.1128/aem.45.6.1848-1853.1983

Kraft, B., Jehmlich, N., Larsen, M., Bristow, L., Könneke, M., Thamdrup, B., & Canfield, D. (2022). Oxygen and nitrogen production by an ammonia-oxidizing archaeon. *Science (New York, N.Y.)*, *375*, 97-100. https://doi.org/10.1126/science.abe6733

Kräutler, B. (2005). Vitamin B12: chemistry and biochemistry. *Biochem Soc Trans*, *33*(Pt 4), 806-810. https://doi.org/10.1042/bst0330806

Könneke, M., Bernhard, A. E., de la Torre, J. R., Walker, C. B., Waterbury, J. B., & Stahl, D. A. (2005). Isolation of an autotrophic ammonia-oxidizing marine archaeon. *Nature*, *437*(7058), 543-546. https://doi.org/10.1038/nature03911

Lane, D. J. (1991). 16S/23S rRNA sequencing. In E. Stackebrandt & M. Goodfellow (Eds.), *Nucleic acid techniques in bacterial systematics* (pp. 115-175). John Wiley and Sons.

Law, K. P., He, W., Tao, J., & Zhang, C. (2021). Characterization of the Exometabolome of Nitrosopumilus maritimus SCM1 by Liquid Chromatography–Ion Mobility Mass Spectrometry [Original Research]. *Frontiers in Microbiology*, *12*. https://doi.org/10.3389/fmicb.2021.658781

Li, M., & Gu, J.-D. (2013). Community structure and transcript responses of anammox bacteria, AOA, and AOB in mangrove sediment microcosms amended with ammonium and nitrite. *Applied Microbiology and Biotechnology*, *97*(22), 9859-9874. https://doi.org/10.1007/s00253-012-4683-y

Lipp, J. S., Morono, Y., Inagaki, F., & Hinrichs, K.-U. (2008). Significant contribution of Archaea to extant biomass in marine subsurface sediments. *Nature*, *454*(7207), 991-994. https://doi.org/10.1038/nature07174

Liu, Y., & Whitman, W. B. (2008). Metabolic, Phylogenetic, and Ecological Diversity of the Methanogenic Archaea. *Annals of the New York Academy of Sciences*, *1125*(1), 171-189. https://doi.org/https://doi.org/10.1196/annals.1419.019

Lu, H., Chandran, K., & Stensel, D. (2014). Microbial ecology of denitrification in biological wastewater treatment. *Water research*, *64*, 237-254. https://doi.org/https://doi.org/10.1016/j.watres.2014.06.042

Magi, A., Semeraro, R., Mingrino, A., Giusti, B., & D'aurizio, R. (2018). Nanopore sequencing data analysis: state of the art, applications and challenges. *Briefings in bioinformatics*, *19*(6), 1256-1272.

Martens-Habbena, W., Berube, P. M., Urakawa, H., de la Torre, J. R., & Stahl, D. A. (2009). Ammonia oxidation kinetics determine niche separation of nitrifying Archaea and Bacteria. *Nature*, *461*(7266), 976-979. https://doi.org/10.1038/nature08465

Mincer, T. J., Church, M. J., Taylor, L. T., Preston, C., Karl, D. M., & DeLong, E. F. (2007). Quantitative distribution of presumptive archaeal and bacterial nitrifiers in Monterey Bay and the North Pacific Subtropical Gyre. *Environ Microbiol*, *9*(5), 1162-1175. https://doi.org/10.1111/j.1462-2920.2007.01239.x

Mullis, K. B., & Faloona, F. A. (1987). Specific synthesis of DNA in vitro via a polymerase-catalyzed chain reaction. *Methods in enzymology*, *155*, 335-350. https://doi.org/10.1016/0076-6879(87)55023-6

Munn, C. B. (2019). *Marine microbiology: ecology & applications*. CRC Press.

Nie, S., Zhang, Z., Mo, S., Li, J., He, S., Kashif, M., Liang, Z., Shen, P., Yan, B., & Jiang, C. (2021). Desulfobacterales stimulates nitrate reduction in the mangrove ecosystem of a subtropical gulf. *Science of The Total Environment*, *769*, 144562. https://doi.org/https://doi.org/10.1016/j.scitotenv.2020.144562

Nogales, B., Lanfranconi, M. P., Piña-Villalonga, J. M., & Bosch, R. (2011). Anthropogenic perturbations in marine microbial communities. *FEMS Microbiology Reviews*, *35*(2), 275-298. https://doi.org/10.1111/j.1574-6976.2010.00248.x

Norton, J. M., Alzerreca, J. J., Suwa, Y., & Klotz, M. G. (2002). Diversity of ammonia monooxygenase operon in autotrophic ammonia-oxidizing bacteria. *Arch Microbiol*, *177*(2), 139-149. https://doi.org/10.1007/s00203-001-0369-z

Norwegian Ministry of Climate and Environment. (2021). *Helhetlig tiltaksplan for en ren og rik Oslofjord*.

Nyberg, U., Aspegren, H., Andersson, B., Jansen, J. l. C., & Villadsen, I. S. (1992). Full-Scale Application of Nitrogen Removal with Methanol as Carbon Source. *Water Science and Technology*, *26*(5-6), 1077-1086. https://doi.org/10.2166/wst.1992.0549

Nyerges, G., & Stein, L. Y. (2009). Ammonia cometabolism and product inhibition vary considerably among species of methanotrophic bacteria. *FEMS Microbiology Letters*, *297*(1), 131-136. https://doi.org/10.1111/j.1574-6968.2009.01674.x

Oksanen, J., Blanchet, F. G., Friendly, M., Kindt, R., Legendre, P., McGlinn, D., & Wagner, H. (2017). vegan: community ecology package. R package version 2.4–4.2. In.

Orcutt, B. N., Sylvan, J. B., Knab, N. J., & Edwards, K. J. (2011). Microbial Ecology of the Dark Ocean above, at, and below the Seafloor. *Microbiology and molecular biology reviews*, *75*(2), 361-422. https://doi.org/doi:10.1128/mmbr.00039-10

Oren, A., & Garrity, G. M. (2021). Valid publication of the names of forty-two phyla of prokaryotes. *International Journal of Systematic and Evolutionary Microbiology*, *71*(10). https://doi.org/https://doi.org/10.1099/ijsem.0.005056

Orsi, W. D. (2018). Ecology and evolution of seafloor and subseafloor microbial communities. *Nature Reviews Microbiology*, *16*(11), 671-683. https://doi.org/10.1038/s41579-018-0046-8

Oudova-Rivera, B., Wright, C. L., Crombie, A. T., Murrell, J. C., & Lehtovirta-Morley, L. E. (2023). The effect of methane and methanol on the terrestrial ammonia-oxidizing archaeon 'Candidatus Nitrosocosmicus franklandus C13'. *Environmental Microbiology*, *25*(5), 948-961. https://doi.org/https://doi.org/10.1111/1462-2920.16316

Park, B.-J., Park, S.-J., Yoon, D.-N., Schouten, S., Sinninghe Damsté, J. S., & Rhee, S.-K. (2010). Cultivation of autotrophic ammonia-oxidizing archaea from marine sediments in coculture with sulfur-oxidizing bacteria. *Applied and Environmental Microbiology*, *76*(22), 7575-7587.

Park, J. Y., & Yoo, Y. J. (2009). Biological nitrate removal in industrial wastewater treatment: which electron donor we can choose. *Appl Microbiol Biotechnol*, *82*(3), 415-429. https://doi.org/10.1007/s00253-008-1799-1

Pelaz, L., Gómez, A., Letona, A., Garralón, G., & Fdz-Polanco, M. (2018). Nitrogen removal in domestic wastewater. Effect of nitrate recycling and COD/N ratio. *Chemosphere*, *212*, 8-14. https://doi.org/https://doi.org/10.1016/j.chemosphere.2018.08.052

Pepper, I. L., Gerba, C. P., Gentry, T. J., & Maier, R. M. (2011). *Environmental microbiology*. Academic press.

Pepper, I. L., & Pillai, S. D. (1994). Detection of Specific DNA Sequences in Environmental Samples Via Polymerase Chain Reaction. In *Methods of Soil Analysis* (pp. 707-726). https://doi.org/https://doi.org/10.2136/sssabookser5.2.c34

Pettersen, R., Ormaasen, I., Angell, I. L., Keeley, N. B., Lindseth, A., Snipen, L., & Rudi, K. (2022). Bimodal distribution of seafloor microbiota diversity and function are associated with marine aquaculture. *Marine Genomics*, *66*, 100991. https://doi.org/https://doi.org/10.1016/j.margen.2022.100991

Prosser, J. I. (2004). Nitrogen in Soils - Nitrification. In *Encyclopedia of Soils in the Environment* (Vol. 4, pp. 31-39). https://doi.org/10.1016/B0-12-348530-4/00512-9

Qin, W., Amin, S. A., Martens-Habbena, W., Walker, C. B., Urakawa, H., Devol, A. H., Ingalls, A. E., Moffett, J. W., Armbrust, E. V., & Stahl, D. A. (2014). Marine ammonia-oxidizing archaeal isolates display obligate mixotrophy and wide ecotypic variation. *Proc Natl Acad Sci U S A*, *111*(34), 12504-12509. https://doi.org/10.1073/pnas.1324115111

Qin, W., Martens-Habbena, W., Kobelt, J. N., & Stahl, D. A. (2016). Candidatus Nitrosopumilus. In *Bergey's Manual of Systematics of Archaea and Bacteria* (pp. 1-9). John wiley & Sons, Inc. https://doi.org/https://doi.org/10.1002/9781118960608.gbm01290

Quast, C., Pruesse, E., Yilmaz, P., Gerken, J., Schweer, T., Yarza, P., Peplies, J., & Glöckner, F. O. (2013). The SILVA ribosomal RNA gene database project: improved data processing and web-based tools. *Nucleic Acids Res*, *41*(Database issue), D590-596. https://doi.org/10.1093/nar/gks1219

R Core Team. (2022). *R: A language and environment for statistical computing*. . In (Version v2022.07.2+576) R Foundation for Statistical Computing. https://www.R-project.org/

Reysenbach, A., & Pace, N. (1995). In P. A. Robb FT (Ed.), *Archaea: a laboratory manual* (pp. 101-107). Cold Spring Harbor Press.

Roopnarain, A., Mukhuba, M., Adeleke, R., & Moeletsi, M. (2017). Biases during DNA extraction affect bacterial and archaeal community profile of anaerobic digestion samples. *3 Biotech*, *7*(6), 375. https://doi.org/10.1007/s13205-017-1009-x

Rosentreter, J. A., Borges, A. V., Deemer, B. R., Holgerson, M. A., Liu, S., Song, C., Melack, J., Raymond, P. A., Duarte, C. M., Allen, G. H., Olefeldt, D., Poulter, B., Battin, T. I., & Eyre, B. D. (2021). Half of global methane emissions come from highly variable aquatic ecosystem sources. *Nature Geoscience*, *14*(4), 225-230. https://doi.org/10.1038/s41561-021-00715-2

Rotthauwe, J. H., Witzel, K. P., & Liesack, W. (1997). The ammonia monooxygenase structural gene amoA as a functional marker: molecular fine-scale analysis of natural ammonia-oxidizing populations. *Appl Environ Microbiol*, *63*(12), 4704-4712. https://doi.org/10.1128/aem.63.12.4704-4712.1997

Ruijter, J. M., Ramakers, C., Hoogaars, W. M. H., Karlen, Y., Bakker, O., van den Hoff, M. J. B., & Moorman, A. F. M. (2009). Amplification efficiency: linking baseline and bias in the analysis of quantitative PCR data. *Nucleic Acids Research*, *37*(6), e45-e45. https://doi.org/10.1093/nar/gkp045

Ruprecht, J. E., Birrer, S. C., Dafforn, K. A., Mitrovic, S. M., Crane, S. L., Johnston, E. L., Wemheuer, F., Navarro, A., Harrison, A. J., Turner, I. L., & Glamore, W. C. (2021). Wastewater effluents cause microbial community shifts and change trophic status. *Water research*, *200*, 117206. https://doi.org/https://doi.org/10.1016/j.watres.2021.117206

Ruscalleda Beylier, M., Balaguer, M. D., Colprim, J., Pellicer-Nàcher, C., Ni, B. J., Smets, B. F., Sun, S. P., & Wang, R. C. (2011). 6.27 - Biological Nitrogen Removal from Domestic Wastewater. In M. Moo-Young (Ed.), *Comprehensive Biotechnology (Second Edition)* (pp. 329-340). Academic Press. https://doi.org/https://doi.org/10.1016/B978-0-08-088504-9.00533-X

Sakoula, D., Koch, H., Frank, J., Jetten, M. S. M., van Kessel, M. A. H. J., & Lücker, S. (2021). Enrichment and physiological characterization of a novel comammox Nitrospira indicates ammonium inhibition of complete nitrification. *The ISME journal*, *15*(4), 1010-1024. https://doi.org/10.1038/s41396-020-00827-4

Sintes, E., Bergauer, K., De Corte, D., Yokokawa, T., & Herndl, G. J. (2013). Archaeal amoA gene diversity points to distinct biogeography of ammonia-oxidizing Crenarchaeota in the ocean. *Environmental Microbiology*, *15*(5), 1647-1658. https://doi.org/https://doi.org/10.1111/j.1462-2920.2012.02801.x

Smith, V. H., Tilman, G. D., & Nekola, J. C. (1999). Eutrophication: impacts of excess nutrient inputs on freshwater, marine, and terrestrial ecosystems. *Environmental Pollution*, *100*(1), 179-196. https://doi.org/https://doi.org/10.1016/S0269-7491(99)00091-3

Stahl, D. A., Flesher, B., Mansfield, H. R., & Montgomery, L. (1988). Use of phylogenetically based hybridization probes for studies of ruminal microbial ecology. *Appl Environ Microbiol*, *54*(5), 1079-1084. https://doi.org/10.1128/aem.54.5.1079-1084.1988

Statistisk sentralbyrå. (2023). *11342: Areal og befolkning, etter region, statistikkvariabel og år*. Retrieved September 16 from https://norskvann.no/avlopsdirektiv-norsk-vanns-horingsinnspill-til-miljodirektoratet-om-eus-forslag-til-revidert-avlopsdirektiv/

Søndergaard, M. (2009). Redox Potential. In G. E. Likens (Ed.), *Encyclopedia of Inland Waters* (pp. 852-859). Academic Press. https://doi.org/https://doi.org/10.1016/B978-012370626-3.00115-0

Takai, K., & Horikoshi, K. (2000). Rapid detection and quantification of members of the archaeal community by quantitative PCR using fluorogenic probes. *Appl Environ Microbiol*, *66*(11), 5066-5072. https://doi.org/10.1128/aem.66.11.5066-5072.2000

Tee, H. S., Waite, D., Payne, L., Middleditch, M., Wood, S., & Handley, K. M. (2020). Tools for successful proliferation: diverse strategies of nutrient acquisition by a benthic cyanobacterium. *The ISME journal*, *14*(8), 2164-2178. https://doi.org/10.1038/s41396-020-0676-5

Treusch, A. H., Leininger, S., Kletzin, A., Schuster, S. C., Klenk, H. P., & Schleper, C. (2005). Novel genes for nitrite reductase and Amo-related proteins indicate a role of uncultivated mesophilic crenarchaeota in nitrogen cycling. *Environ Microbiol*, *7*(12), 1985-1995. https://doi.org/10.1111/j.1462-2920.2005.00906.x

Walker, C. B., de la Torre, J. R., Klotz, M. G., Urakawa, H., Pinel, N., Arp, D. J., Brochier-Armanet, C., Chain, P. S., Chan, P. P., Gollabgir, A., Hemp, J., Hügler, M., Karr, E. A., Könneke, M., Shin, M., Lawton, T. J., Lowe, T., Martens-Habbena, W., Sayavedra-Soto, L. A., . . . Stahl, D. A. (2010). Nitrosopumilus maritimus genome reveals unique mechanisms for nitrification and autotrophy in globally distributed marine crenarchaea. *Proc Natl Acad Sci U S A*, *107*(19), 8818-8823. https://doi.org/10.1073/pnas.0913533107

Wei, S., Cui, H., Zhang, Y., Su, X., Dong, H., Chen, F., & Zhu, Y. (2019). Comparative evaluation of three archaeal primer pairs for exploring archaeal communities in deep-sea sediments and permafrost soils. *Extremophiles*, *23*(6), 747-757. https://doi.org/10.1007/s00792-019-01128-1

Whitman, W. B., Oren, A., Chuvochina, M., da Costa, M. S., Garrity, G. M., Rainey, F. A., Rossello-Mora, R., Schink, B., Sutcliffe, I., Trujillo, M. E., & Ventura, S. (2018). Proposal of the suffix –ota to denote phyla. Addendum to 'Proposal to include the rank of phylum in the International Code of Nomenclature of Prokaryotes'. *International Journal of Systematic and Evolutionary Microbiology*, *68*(3), 967-969. https://doi.org/https://doi.org/10.1099/ijsem.0.002593

Wick, R. R., Judd, L. M., & Holt, K. E. (2019). Performance of neural network basecalling tools for Oxford Nanopore sequencing. *Genome Biology*, *20*(1), 129. https://doi.org/10.1186/s13059-019-1727-y

Wickham, H. (2016). *ggplot2: Elegant Graphics for Data Analysis*. In Springer-Verlag https://ggplot2.tidyverse.org

Widdel, F., & Bak, F. (1992). Gram-Negative Mesophilic Sulfate-Reducing Bacteria. In A. Balows, H. G. Trüper, M. Dworkin, W. Harder, & K.-H. Schleifer (Eds.), *The Prokaryotes: A Handbook on the Biology of Bacteria: Ecophysiology, Isolation, Identification, Applications* (pp. 3352-3378). Springer New York. https://doi.org/10.1007/978-1-4757-2191-1_21

Wu, Y., Ke, X., Hernández, M., Wang, B., Dumont, M. G., Jia, Z., & Conrad, R. (2013). Autotrophic Growth of Bacterial and Archaeal Ammonia Oxidizers in Freshwater Sediment Microcosms Incubated at Different Temperatures. *Applied and Environmental Microbiology*, *79*(9), 3076-3084. https://doi.org/doi:10.1128/AEM.00061-13

Wuchter, C., Abbas, B., Coolen, M. J., Herfort, L., van Bleijswijk, J., Timmers, P., Strous, M., Teira, E., Herndl, G. J., Middelburg, J. J., Schouten, S., & Sinninghe Damsté, J. S. (2006). Archaeal nitrification in the ocean. *Proc Natl Acad Sci U S A*, *103*(33), 12317-12322. https://doi.org/10.1073/pnas.0600756103

Yilmaz, P., Parfrey, L. W., Yarza, P., Gerken, J., Pruesse, E., Quast, C., Schweer, T., Peplies, J., Ludwig, W., & Glöckner, F. O. (2014). The SILVA and "All-species Living Tree Project (LTP)" taxonomic frameworks. *Nucleic Acids Res*, *42*(Database issue), D643-648. https://doi.org/10.1093/nar/gkt1209

Yu, Y., Lee, C., Kim, J., & Hwang, S. (2005). Group-specific primer and probe sets to detect methanogenic communities using quantitative real-time polymerase chain reaction. *Biotechnol Bioeng*, *89*(6), 670-679. https://doi.org/10.1002/bit.20347

Zeng, J., Zhao, D., Yu, Z., Huang, R., & Wu, Q. L. (2014). Temperature Responses of Ammonia-Oxidizing Prokaryotes in Freshwater Sediment Microcosms. *PLoS One*, *9*(6), e100653. https://doi.org/10.1371/journal.pone.0100653

Zhang, W., Ki, J.-S., & Qian, P.-Y. (2008). Microbial diversity in polluted harbor sediments I: Bacterial community assessment based on four clone libraries of 16S rDNA. *Estuarine, Coastal and Shelf Science*, *76*(3), 668-681. https://doi.org/https://doi.org/10.1016/j.ecss.2007.07.040

Zorz, J., Li, C., Chakraborty, A., Gittins, D. A., Surcon, T., Morrison, N., Bennett, R., MacDonald, A., & Hubert, C. R. J. (2023). SituSeq: an offline protocol for rapid and remote Nanopore 16S rRNA amplicon sequence analysis. *ISME Commun*, *3*(1), 33. https://doi.org/10.1038/s43705-023-00239-3

Appendix

Protocol for gel electrophoresis

To make a 1% gel, 1g of UltraPure™ agarose (Thermo Fischer Scientific, USA) was used per 100 mL of 1% Tris/Acetate/EDTA (TAE) buffer. Accordingly, 2% gels were made using 2g of agarose per 100 mL of 1% TAE buffer. The agarose was dissolved in the buffer using a microwave, and the gel was allowed to cool down to approximately 60˚C before 3 µl of PeqGREEN DNA/RNA dye (VWR, Germany) was added per 50 mL of gel. Gels with PeqGREEN were stored for up to one week in a water bath at 60˚C.

The liquid gel with PeqGREEN was poured into a gel tray with combs. Bubbles were pushed towards the edges of the gel tray using a pipette tip. The gel was allowed to set for approximately 15 minutes before it was transferred to an electrophoresis unit and loaded with 4 µl of the 100bp DNA ladder RTL (Solis BioDyne, Estonia) and 6 µl of the DNA samples. Non-purified amplicons containing HOT FIREPol Blend Master Mix RTL (Solis BioDyne, Estonia) were loaded directly. qPCR amplicons were mixed 1:5 (v/v) with 6×Gel Loading Dye Purple no SDS (New England BioLabs, USA) before loading. The gels were run at 80V for 30-45 min, depending on the size of the DNA fragments and the gel concentration. The DNA bands were visualised using trans UV on a Gel Doc™ XR imaging system (Bio-Rad, USA).

Short-range primer evaluation

Candidate qPCR primer pairs (table A1) were used to amplify the Tromsø Cref sediment extraction (Table 2) using gradient PCR with annealing temperatures between 54.5°C and 65.0°C, to determine their optimal annealing temperatures. Two of the primer pairs targeting the archaeal *amoA* did not produce amplicons (Figures A1B, A1D). All the primer pairs targeting the archaeal 16S rRNA seemed promising for further testing.

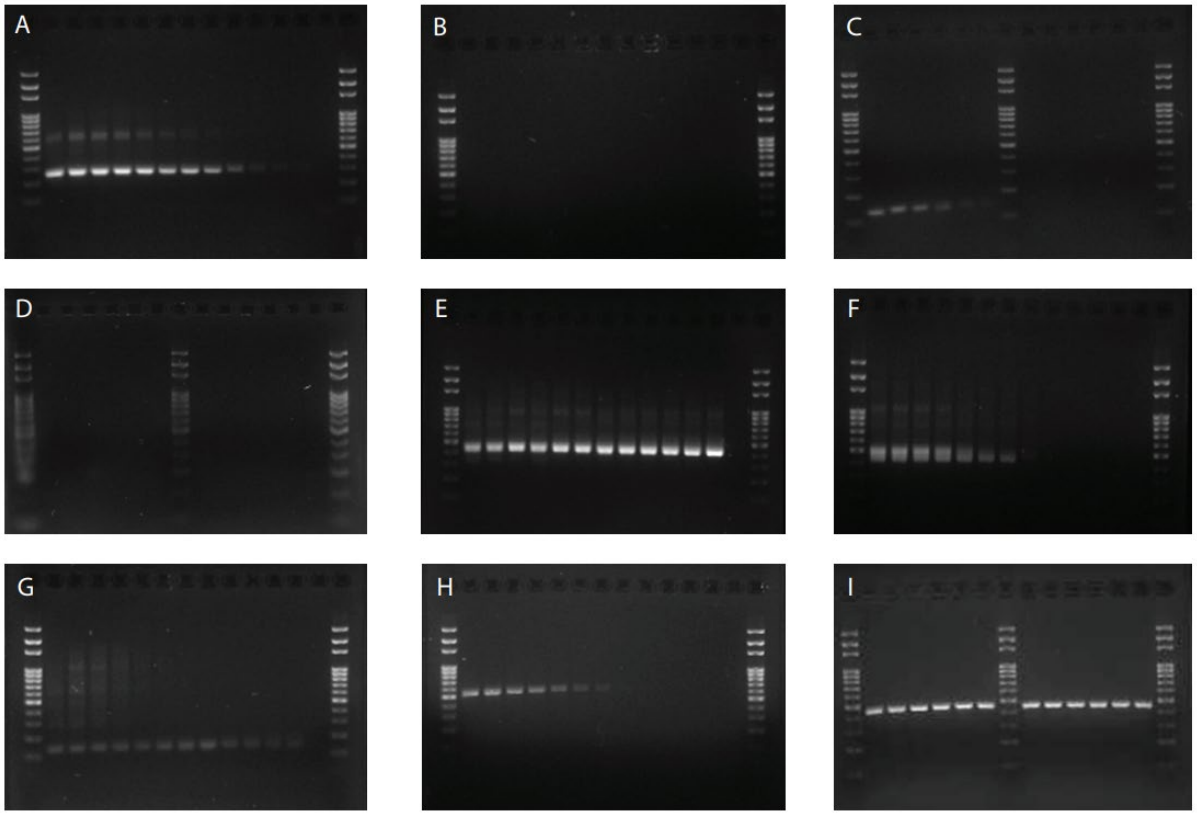

Figure A1: Gel electrophoresis of gradient PCR products from short-range qPCR primer pairs targeting the archaeal 16S rRNA and *amoA* genes. All reactions contained the same template, namely the extraction from the Cref sediments. The temperature gradient went from 54.5˚C on the left to 65.0˚C on the right on all plates, and the PCR products were loaded on the gel accordingly. Each gel was loaded with gradient PCR products from one primer pair represented with a letter (A-I). **A:** Arch-amoA-for/Arch-amoA-rev produced two different PCR products. **B:** Arch-amoA-for/Arch-amoA-rev-New did not produce amplicons. **C:** Cren-amoA-Q-F/Cren-amoA-mod-R produced amplicons at annealing temperatures below 60˚C. **D:** Arch-amo-196F/Arch-amo-227R did not produce amplicons. **E:** Arch-519F/Arch-915R produced amplicons at all annealing temperatures. **F:** 340F/806rB seemed to produce multiple PCR products. **G:** MCGI-391F/MCGI-554R produced amplicons at annealing temperatures above 60˚C. **H:** SSU1ArF/SSU520ArR produced amplicons at annealing temperatures below 60˚C. **I:** THAUM-494F/Arch-915R produced amplicons at all annealing temperatures.

The primer pairs that produced amplicon during gradient PCR were tested using qPCR at their optimal annealing temperatures (Table 3), which were determined from the gradient PCR results (Figure A1).

The three AOA-specific primer pairs Arch-amoA-for/Arch-amoA-rev, Cren-amoA-Q-F/Cren-amoA-mod-R and MCGI-391F/MCGI-554R seemed to detect *Nitrosopumilus* and related AOA without targeting unwanted bacterial or eukaryotic sequences (Appendix Table A2). Arch-amoA-for/Arch-amoA-rev and MCGI-391F/MCGI-554R both displayed a shoulder in their melting peak plots, indicating primer dimers, but primer dimers were detected by gel electrophoresis only among the *amoA* amplicons.

The remaining primer pairs targeting the archaeal 16S rRNA were unspecific to marine AOA, because they targeted DNA sequences in templates where we knew that marine AOA were absent (table A2). Furthermore, the amplification curves resulting from the Arch-519F/Arch-915R pair were nearly identical to those resulting from the bacterial primer pair 341f/806r. Therefore, their raw C_q values were plotted to assess their correlation. The raw C_q values correlated with a Pearson correlation coefficient of 95 % (figure A2), indicating that Arch-519F/Arch-915R may target bacteria.

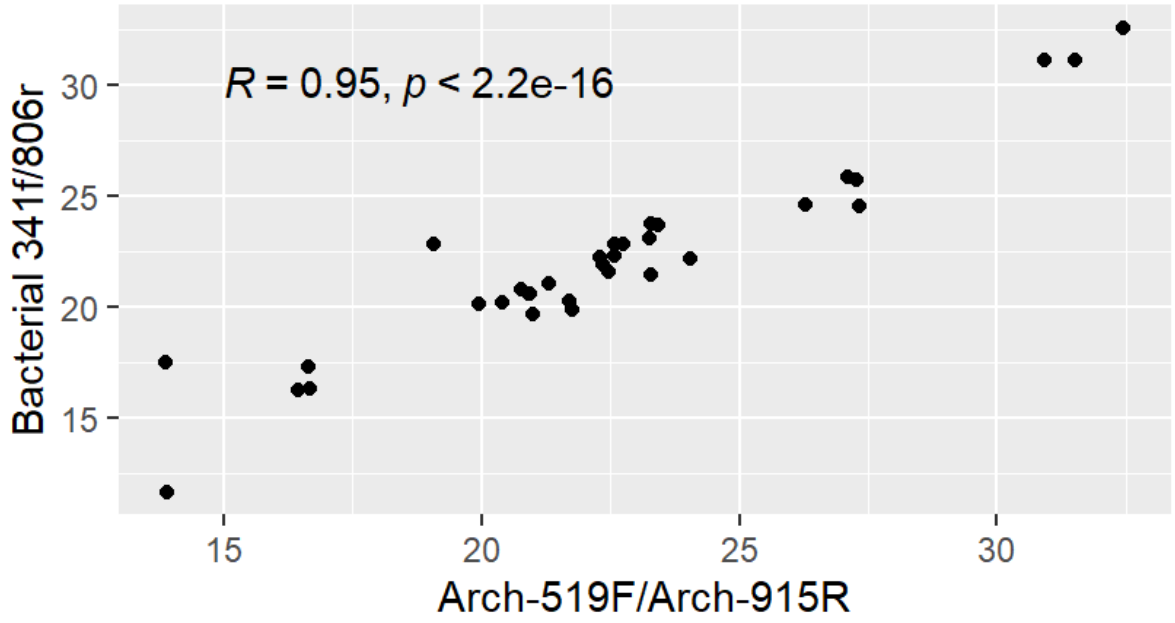

Figure A2: Scatter plot of the C_q values resulting from qPCR with the Arch-519F/Arch-915R (x coordinate) and bacterial 341f/806r (y coordinate) primer pairs targeting the archaeal and bacterial 16S rRNA genes, respectively. The plot shows a linear relationship between the C_q values from the different primer pairs. Each point represents the C_q values produced by each primer pair with the same template. The Pearson correlation coefficient (R) and p value (p) are displayed in the upper left corner.

Table A1: The short-range primers used in the present study. All the listed archaeal primers were evaluated thoroughly using gradient PCR and qPCR, with the aim to find suitable primer pairs for qPCR analyses of sedimentary AOA. The bacterial and eukaryotic primer pairs listed were used during qPCR analyses.

Use	Target	Direction	Primer name	Sequence (5'-3')	Reference
Short-range primer evaluation	Archaeal *amoA*	Forward	Arch-Amoa-for	CTGAYTGGGCYTGGACATC	(Wuchter et al., 2006)
			Cren-AmoA-Q-F	GCARGTMGGWAAETTCTAYAA	(Mincer et al., 2007)
			Arch-amo-196F	GGWGTKCCRGGRACWGCMAC	(Treusch et al., 2005)
		Reverse	Arch-Amoa-rev	TTCTTCTTTGTTGCCCAGTA	(Wuchter et al., 2006)
			Arch-Amoa-rev-New	TTCTTCTTCGTCGCCCAATA	(Sintes et al., 2013)
			Cren-AmoA-mod-R	AAGCGGCCATCCATCTGTA	(Mincer et al., 2007)
			Arch-amo-227R	CRATGAAGTCRTAHGGRTADC	(Treusch et al., 2005)
	Archaeal 16S rRNA	Forward	Arch-519F	CAGCCGCCGCGGTAA	(Novogene, UK)
			SSU1ArF	TCCGGTTGATCCYGCBRG	(Bahram et al., 2019)
			MCGI-391f	AAGGTTARTCCGAGTGRTTTC	(Wuchter et al., 2006)
			340f	CCCTAYGGGGYGCASCAG	(Gantner et al., 2011)
			THAUM-494F	GAATAAGGGGTGGGCAAGT	(Hong et al., 2014)
		Reverse	MCGI-554r	TGACCACTTGAGGTGCTG	(Wuchter et al., 2006)
			806rB	GGACTACNVGGGTWTCTAAT	(Apprill et al., 2015)
			SSU520ArR	GCTACGRRYGYTTTARRC	(Bahram et al., 2019)
			Arch-915R	GTGCTCCCCCGCCAATTCCT	(Novogene, UK)
qPCR	Bacterial 16S rRNA	Forward	341f	CCTACGGGRBGCASCAG	(Yu et al., 2005)
		Reverse	806r	GGACTACYVGGGTATCTAAT	
	Bacterial *amoA*	Forward	amoA-1F	GGGGTTTCTACTGGTGGT	(Rotthauwe et al., 1997)
		Reverse	amoA-2R	CCCCTCKGSAAAGCCTTCTTC	
	Eukaryotic 18S rRNA	Forward	3NDF	GGCAAGTCTGGTGCCAG	(Bråte et al., 2010)
		Reverse	V4_Euk_R2	ACGGTATCTRATCRTCTTCG	

Table A2: Results from the qPCR evaluation of short-range primers targeting the archaeal 16S rRNA and *amoA*. The table provides an overview of the results from the melting curve analyses and gel electrophoreses of the qPCR products resulting from the combinations of different primer pairs (rows) and templates (columns). Melting peaks (T_m) were obtained from the melting curve analyses following the qPCR. The amplicon lengths were assessed using gel electrophoresis. Some primer and template combinations resulted in multiple products and melt peaks, in which case the corresponding values are separated with a semi colon. The templates are color-coded, where green indicates that *Nitrosopumilus* has previously been detected in the templates, yellow indicates that *Nitrosopumilus* is either absent or present in low numbers, orange corresponds to templates where no archaeal DNA is present, while blue represents negative controls where no template DNA has been added on purpose. More information about the templates can be found in the Methods section.

	Template											
Primer pair	DigiMiBa high diversity		DigiMiBa low diversity		Cref		C1		Zymo community standard		Negative control	
	Length (bp)	**T_m (˚C)**	**Length (bp)**	**T_m (˚C)**	**Length (bp)**	**T_m (˚C)**	**Length (bp)**	**T_m (˚C)**	**Length (bp)**	**T_m (˚C)**	**Length (bp)**	**T_m (˚C)**
Arch-amoA-for/ Arch-amoA-rev	100; 250	74; 82	100	74	100; 250	74; 82	100; 600	74; 87	100	74	100	74
Cren-amoA-Q-F/ Cren-amoA-mod-R	150	83			150	83	150	83				
Arch-519F/ Arch915R	500	88	500	84	500	88	500	88	500	88	500	88
340F/ 806rB	500	87	500	87	500	87	500	87	500	89		
MCGI-391F/ MCGI-554R	150	84			150	84	150	84				
SSU1ArF/ SSU520ArR					500	87	500	87				
THAUM-494F/ Arch-915R	500	86			500	86	500	86	300; 900	77; 89		

Long-range primer evaluation

Because the Nanopore sequencing technology enables the sequencing of long amplicons, and we wished to use this technology to assess the archaeal diversity in our sediment samples, efforts were made to find suitable long-range primer pairs targeting the archaeal 16S rRNA in sediments. Promising primers were gathered from the literature (table A3), combined by the author, and first assessed using gradient PCR and gel electrophoresis.

After determining the primer pairs' general performance and optimal annealing temperatures, the primer pairs performing satisfactorily were tested further using regular PCR with various templates. In addition to the Cref template, two control templates containing little or no archaea were used to test the primer pairs' target specificity *in vitro*. All SSU1ArF primer combinations produced amplicons with the template containing only bacteria and eukaryotes, although in lower amounts than with the Cref template (figures A3A, A3B, A3C). Contrarily, the Arch-21F primer combinations produced amplicons exclusively with the Cref template (figures A3D, A3E, A3F).

The coverage and specificity of the five promising long-range primers were tested using the SILVA TestProbe 3.0 probe evaluation tool. From the *in vitro* analysis, the Arch-21F forward primer seemed more specific to archaea than the SSU1ArF forward primer (figure A3). However, the *in-silico* testing using SILVA TestProbe revealed that the only difference in specificity between the two forward primers was that SSU1ArF covers 0.3 % of the eukaryotic domain, while Arch-21F covers 0 % of eukaryotes (table A4). None of the forward primers targeted any bacteria. On the other hand, the SSU1ArF covered 75.6 % of the archaeal domain, which was considerably better than Arch-21F, that only covered 5.9 % (table A4). In contrast, the three reverse primers had almost identical performance in terms of coverage and specificity.

Table A3: The long-range primers used in the present study. All the listed archaeal primers were evaluated thoroughly using gradient PCR, regular PCR with different templates, as well as *in silico* using SILVA TestProbe and RStudio, with the aim to find suitable primer pairs for Nanopore sequencing of the 16S rRNA gene from sedimentary archaea. The bacterial primer pair listed was used for Nanopore sequencing of bacterial 16S rRNA genes.

Use	Target	Direction	Primer name	Sequence (5'-3')	Reference
Long-range primer evaluation	Archaeal 16S rRNA	Forward	SSU1ArF	TCCGGTTGATCCYGCBRG	(Bahram et al., 2019)
			Arch-21F	TTCCGGTTGATCCYGCCGGA	(DeLong, 1992)
			Arch-349F	GYGCASCAGKCGMGAAW	(Takai & Horikoshi, 2000)
			THAUM-494F	GAATAAGGGGTGGGCAAGT	(Hong et al., 2014)
		Reverse	Arch-1000R	GGCCATGCACYWCYTCTC	(Gantner et al., 2011)
			SSU1000ArR	GGCCATGCAMYWCCTCTC	(Bahram et al., 2019)
			Arch-1017R	GGCCATGCACCWCCTCTC	(Reysenbach & Pace, 1995)
	Universal 16S rRNA		AU1204R	TTMGGGGCATRCNKACCT	(De León et al., 2013)
			U1392R	ACGGGCGGTGTGTRC	(Stahl et al., 1988)
			U1492R	GGYTACCTTGTTACGACTT	(Lane, 1991)
Nanopore sequencing	Bacterial 16S rRNA	Forward	Mangala-F1	TCCTACGGGAGGCAGCAG	(Genetic analysis, Norway)
		Reverse	16SUR	CGGTTACCTTGTTACGACTT	

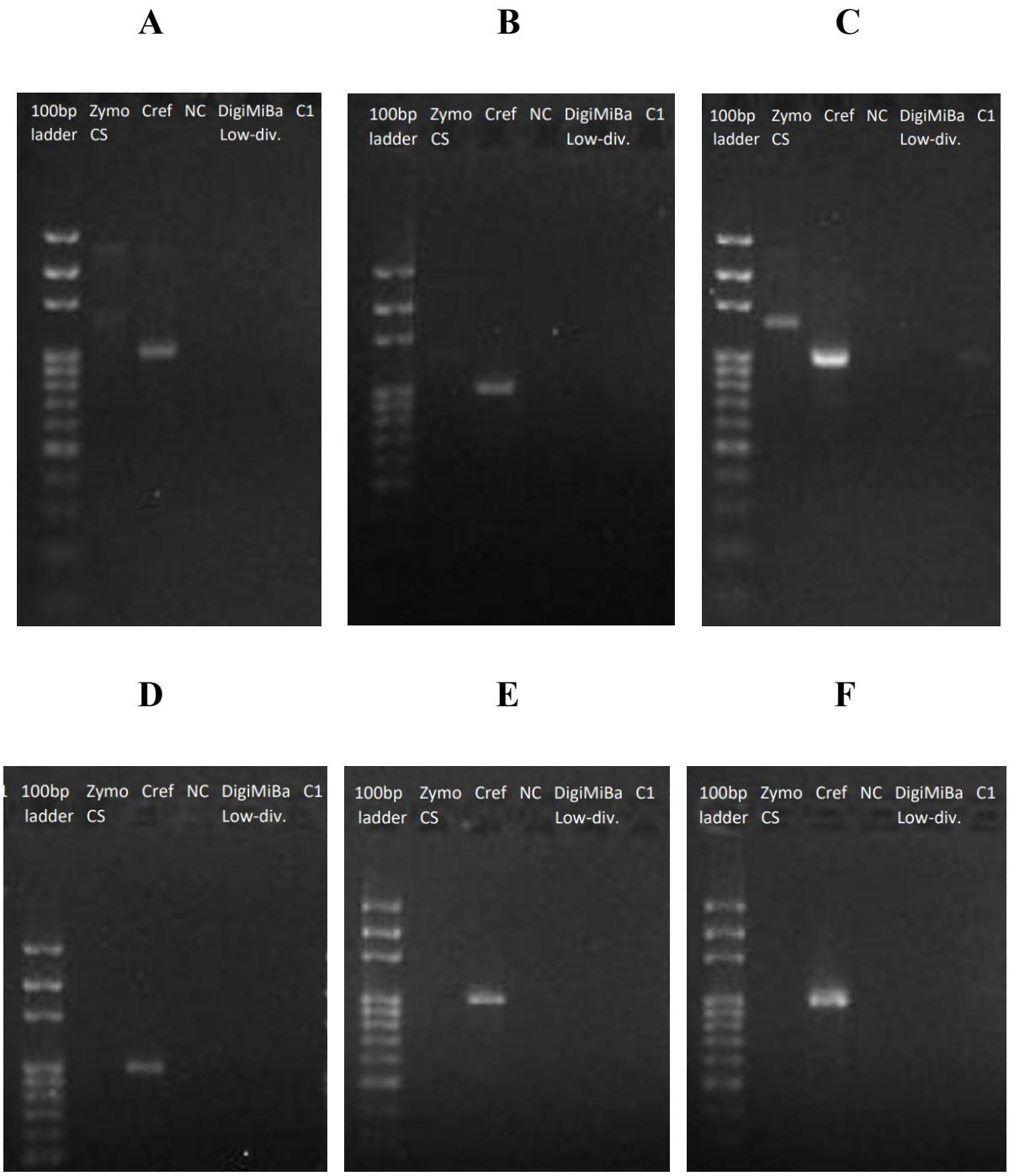

Figure A3: Gel results from long-range primer evaluation using regular PCR. All amplicons were produced using an annealing temperature of 55˚C and the same templates: the Cref sediment extraction served as an archaeal positive control, the C1 sediment and the Zymo Community Standard (Zymo CS) extractions served as bacterial positive controls, and nuclease-free water was used as a negative control (NC). **A:** The SSU1ArF/SSU1000ArR primer pair targeted archaea and bacteria. **B:** The SSU1ArF/Arch-1000R primer pair targeted archaea and bacteria. **C:** The SSU1ArF/Arch-1017 primer pair targeted archaea and bacteria. **D:** The Arch-21F/SSU1000ArR primer pair only targeted archaea. **E:** The Arch-21F/Arch-1000R primer pair only targeted archaea. **F:** The Arch-21F/Arch-1017R primer pair only targeted archaea.

Table A4: Long-range primers targeting the archaeal 16S rRNA gene and their coverages of the bacterial, archaeal, and eukaryotic domains, according to the SILVA TestProbe 3.0 evaluation results. The five primer pairs evaluated performed satisfactorily in terms of stable production of only one PCR product when the Cref sediment extraction was used as a template. However, the SSU1ArF produced amplicons with a template consisting of bacterial and eukaryotic DNA, which was not the case for Arch-21F. According to SILVA TestProbe, the forward primers differed mostly in archaeal coverage, which was considerably better when using the SSU1ArF forward primer. On the other hand, the reverse primers did not differ much in terms of coverage of any domain.

Primer name	**Direction**	**Coverage of the archaeal domain (%)**	**Coverage of the bacterial domain (%)**	**Coverage of the eukaryotic domain (%)**
SSU1ArF	Forward	75.6	0	0.3
Arch-21F	Forward	5.9	0	0
Arch-1000R	Reverse	97.3	3.1	80.0
Arch-1017R	Reverse	97.2	3.1	77.8
SSU1000ArR	Reverse	97.4	3.6	77.9

qPCR analysis of the microcosm sediments

None of the archaeal primer pairs produced amplicons with the negative controls. However, they targeted the positive control composed of bacterial and eukaryotic genes, although these amplicons generally reached the amplification threshold relatively late compared to the samples. The archaeal amplicons of the MGI 16S rRNA and *amoA* genes generally reached the amplification threshold at later cycles than the bacterial and eukaryotic genes. Furthermore, the bacterial primer pairs had a higher amplification efficiency than the archaeal and eukaryotic primer pairs (Table A5).

Table A5: The raw data from the qPCR assays. C_q denotes the range of cycle quantification (C_q) numbers produced by each primer pair with the given template. The C_q values were determined using the common thresholds determined by LinRegPCR. E is the amplification efficiency and N_q is the threshold, both determined by LinRegPCR. All the templates were extractions from sediments, except for the negative and positive controls. The negative control was nuclease-free water, while the Zymo Community DNA, which is composed of bacterial and eukaryotic DNA, was used as a bacterial/eukaryotic control. The pollution experiment sediments were sampled from the polluted and control sediments in the pollution experiment, while the Cref and Oslo Fjord microcosm sediments were sampled from the microcosm experiments. The primer pairs used to target the MGI 16S rRNA gene was the MCGI-391f/MCGI-554r pair. The archaeal *amoA* gene was targeted using Cren-amoA-Q-for/Cren-amoA-mod-R. The bacterial 16S rRNA and *amoA* genes were targeted using 341f/806r and amoA-1F/amoA-2R, respectively. The eukaryotic 18S rRNA gene was targeted with the 3NDF/V4_Euk_R2 primer pair.

Target gene	Result	Cref microcosm	Oslo Fjord microcosm	Pollution experiment	Negative control	Bacterial/Eukaryotic control
MGI 16S rRNA	C_q	28-31	25-30	30-35	> 40	34*
	N_q	349	349	359	**	**
	E	1.86	1.86	1.81	**	**
Archaeal *amoA*	C_q	31-34	28-33	31-37	> 40	37*
	N_q	287	287	345	**	**
	E	1.76	1.76	1.78	**	**
Bacterial 16S rRNA	C_q	19-22	19-23	17-21	35-38	12
	N_q	511	511	388	**	**
	E	1.80	1.80	1.79	**	**
Bacterial *amoA*	C_q	25-29	25-29	25-30	> 40	28-30
	N_q	469	469	539	**	**
	E	1.82	1.82	1.84	**	**
Eukaryotic 18S rRNA	C_q	23-27	22-27	-	38	16-19
	N_q	455	455	-	**	**
	E	1.78	1.78	-	**	**

* No target present in template.

** The same as described for the microcosm and pollution experiment samples, which were amplified on separate plates with individual control samples per plate.

The white substance observed in the Oslo Fjord microcosms.

In the undiluted Oslo Fjord microcosm, dark spots were observed in the sediments after two weeks of incubation (Figure A4-A). The dark spots had disappeared by the fourth week. Furthermore, a white substance was observed in all the microcosms except OF-10-S after two weeks of incubation (Figure A4-B). The white substance was observed by microscope (Figure A4-C).

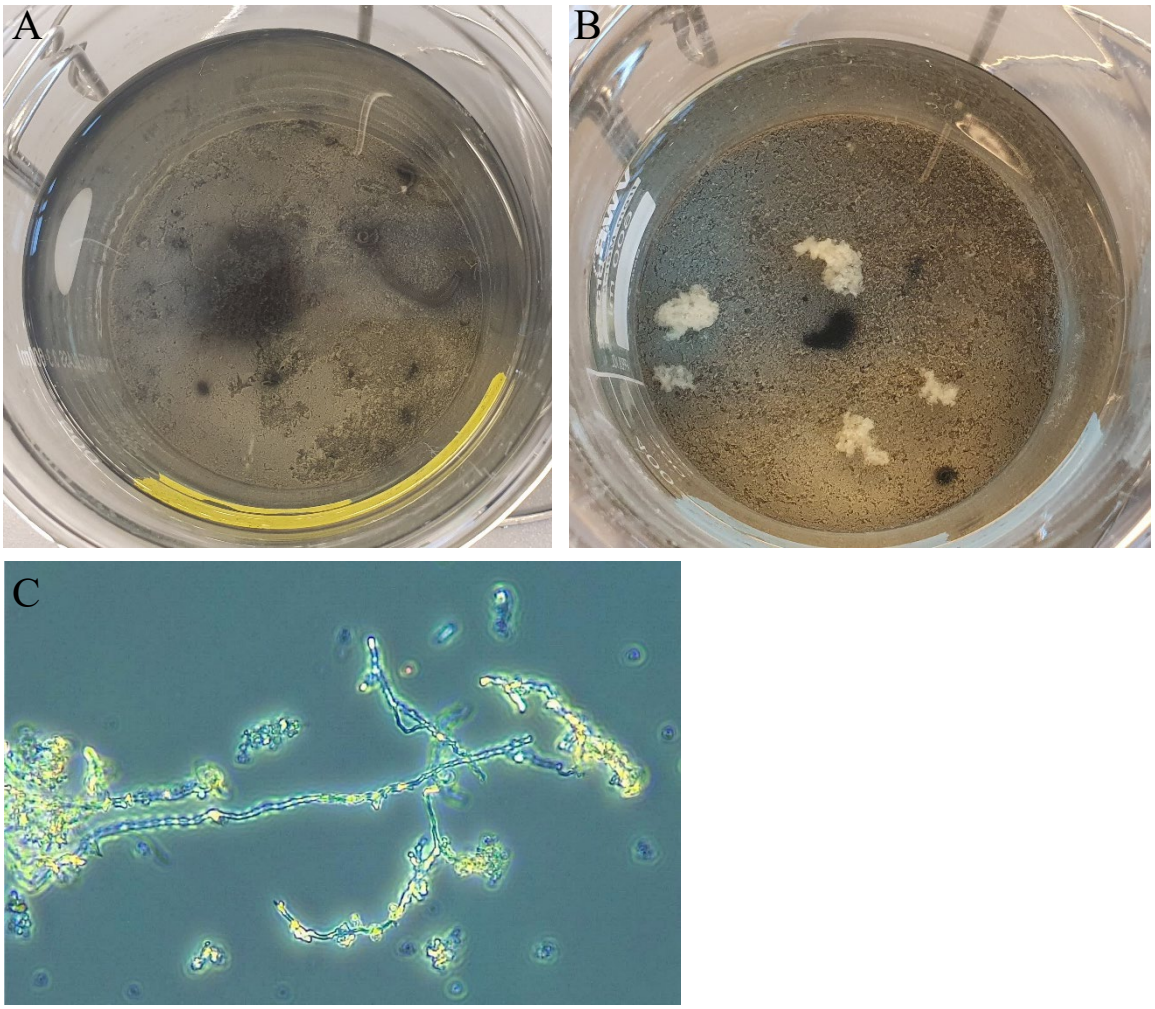

Figure A4: The sediments in the Oslo Fjord microcosms displayed some dark spots that seemed to appear around the cadavers of macroorganisms (A). White, cloud-like substances were observed in all the Oslo Fjord microcosms except OF-10-S after four weeks of incubation (B). These white substances were observed by light microscopy at 400 × magnification (C).

The Cref microcosms: archaeal sequence composition.

The microcosm sediments harboured various archaea. However, as the sequences were assigned lower taxonomic ranks, the number of unassigned taxa increased from 5 % at phylum level to 70-80 % at genus level (Figures A5-A7).

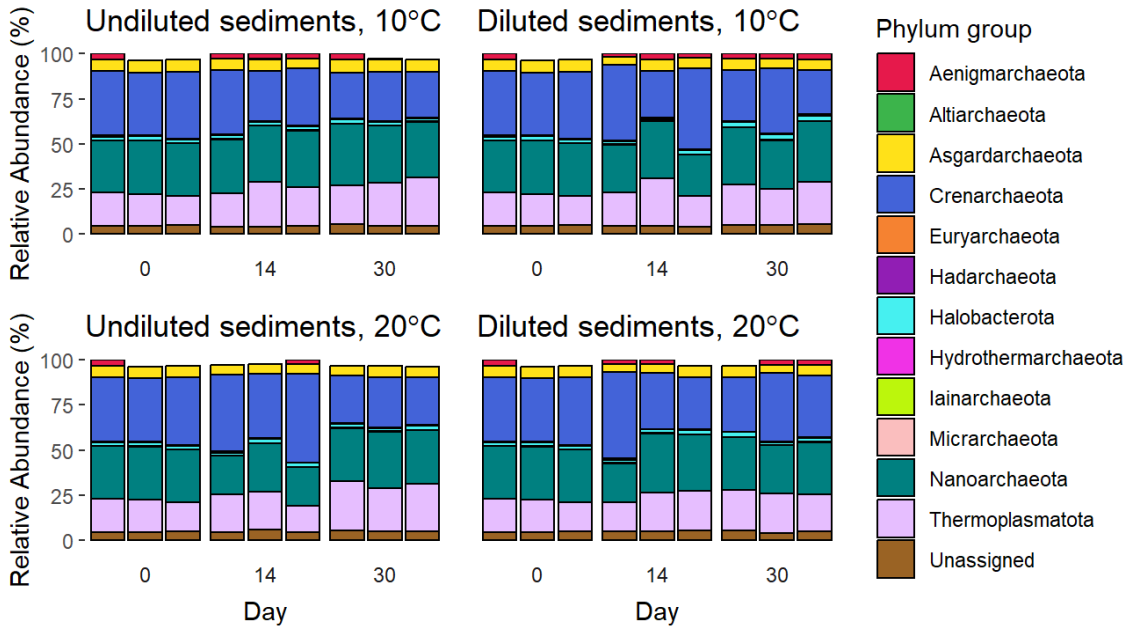

Figure A5: The top 13 archaeal phyla in the Cref microcosms according to the Nanopore 16S rRNA sequencing results. Sequences that could not be assigned to any phylum only represent approximately 5% of the archaeal sequences. *Crenarchaeota, Nanoarchaeota*, and *Thermoplasmatota* seem to be the dominant phyla in all the microcosms.

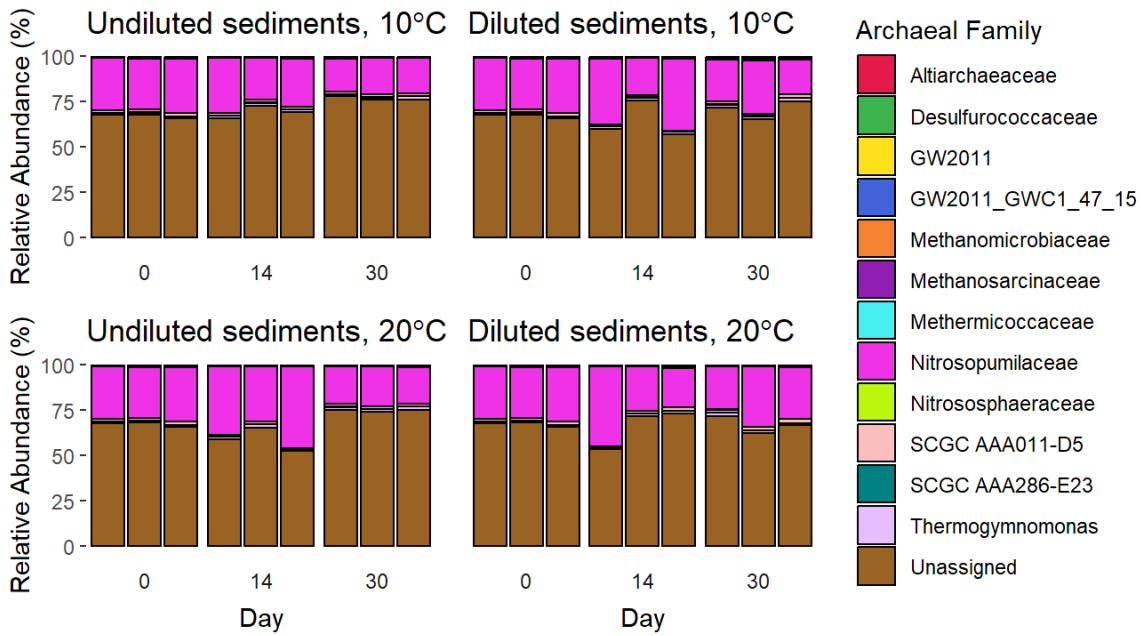

Figure A6: The top 13 archaeal families in the Cref microcosms according to the Nanopore 16S rRNA sequencing results. Sequences that could not be assigned to any family represent 55-80 % of the archaeal sequences. Aside from the unassigned sequences, *Nitrosopumilaceae* is relatively abundant.

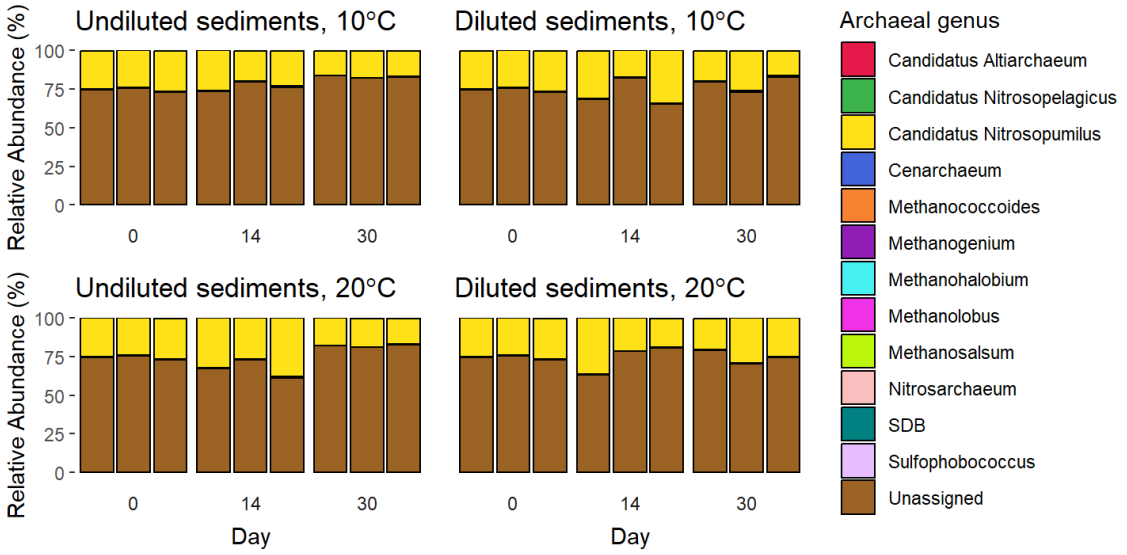

Figure A7: The top 13 archaeal genera in the Cref microcosms according to the Nanopore 16S rRNA sequencing results. Sequences that could not be assigned to any genus represent 60-80 % of the archaeal sequences. Aside from the unassigned sequences, *C.* Nitrosopumilus is relatively abundant.

The Oslo Fjord microcosms: Archaeal sequence composition.

The microcosm sediments harboured various archaea. However, as the sequences were assigned to lower taxonomic ranks, the number of unassigned taxa increased from approximately 5 % at phylum level to 45-60 % at genus level (Figures A8-A10).

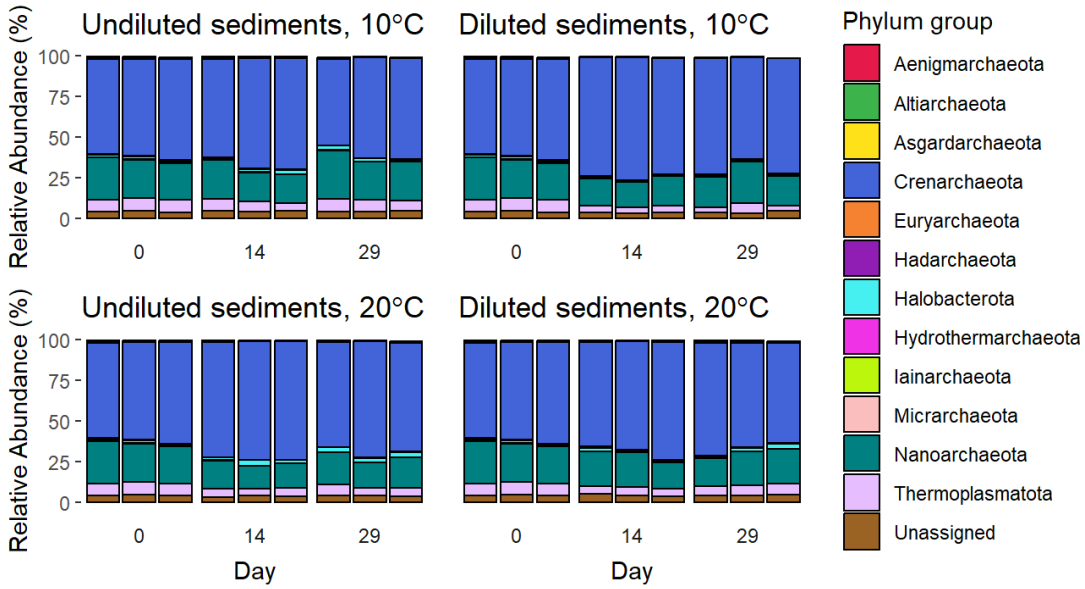

Figure A8: Top 13 archaeal phyla in the Oslo Fjord microcosm sediments according to the Nanopore 16S rRNA sequencing results. Sequences that could not be assigned to any phylum represent approximately 5 % of the archaeal sequences. *Crenarchaeota* seems to be the dominant phylum in all the microcosms, although a relatively high number of sequences were also assigned to *Nanoarchaeota*.

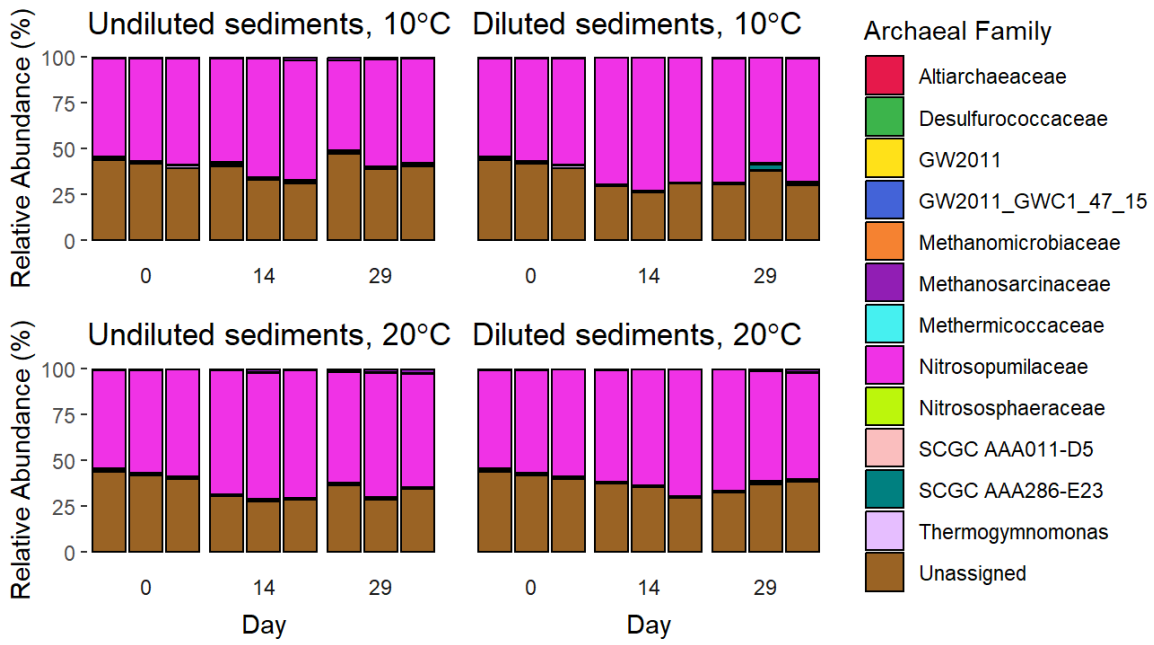

Figure A9: Top 13 archaeal families in the Oslo Fjord microcosm sediments according to the Nanopore 16S rRNA sequencing results. Sequences that could not be assigned to any family represent approximately 25-45 % of the archaeal sequences. *Nitrosopumilaceae* seems to be the dominant family in all the microcosms.

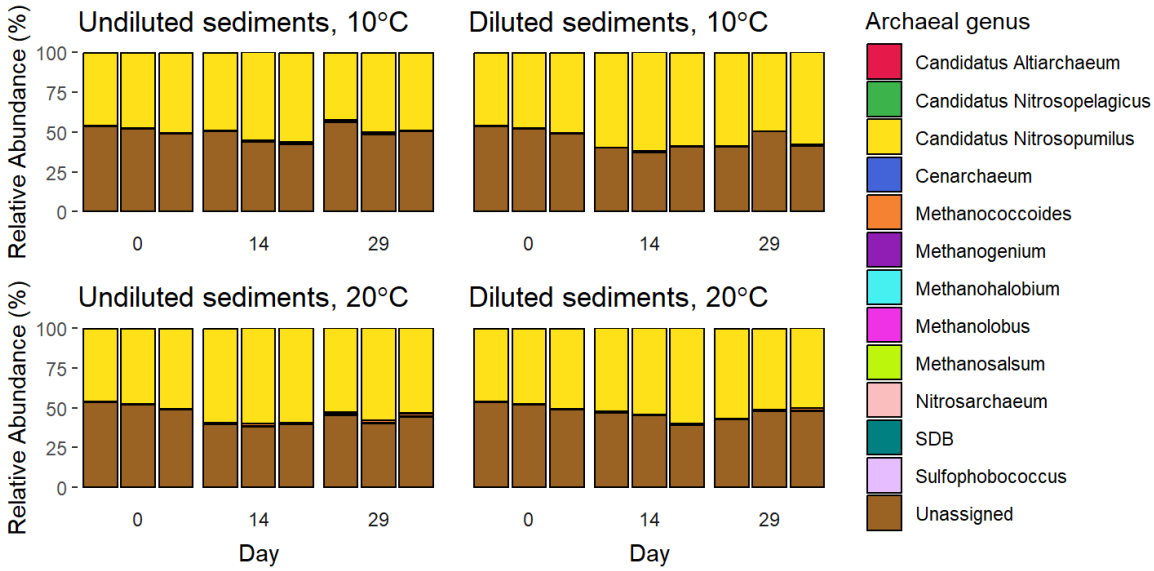

Figure A10: Top 13 archaeal genera in the Oslo Fjord microcosm sediments according to the Nanopore 16S rRNA sequencing results. Sequences that could not be assigned to any genus represent approximately 45-60 % of the archaeal sequences. Aside from the unassigned sequences, *C.* Nitrosopumilus seems to be the dominant genus in all the microcosms.

The Cref microcosms: Bacterial sequence composition.

The microcosm sediments harboured various bacteria. However, as the sequences were assigned lower taxonomic ranks, the number of unassigned taxa increased from 15-20 % at phylum level to 75-80 % at genus level (Figures A11-A14).

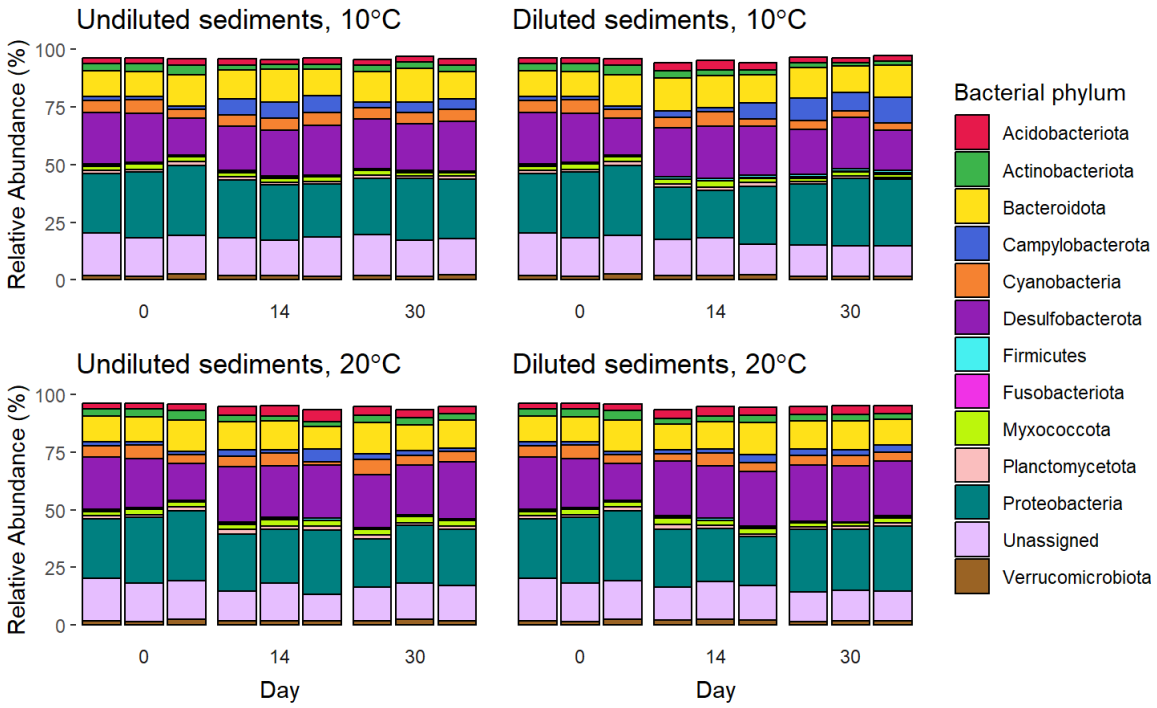

Figure A11: The 13 most abundant bacterial phyla in the Cref microcosms, according to the Nanopore sequencing results. *Bacteroidota, Desulfobacterota,* and *Proteobacteria* seem to be the most dominant bacterial phyla overall. The sequences that could not be assigned to any phylum represented less than 25% of the total number of bacteria at phylum level.

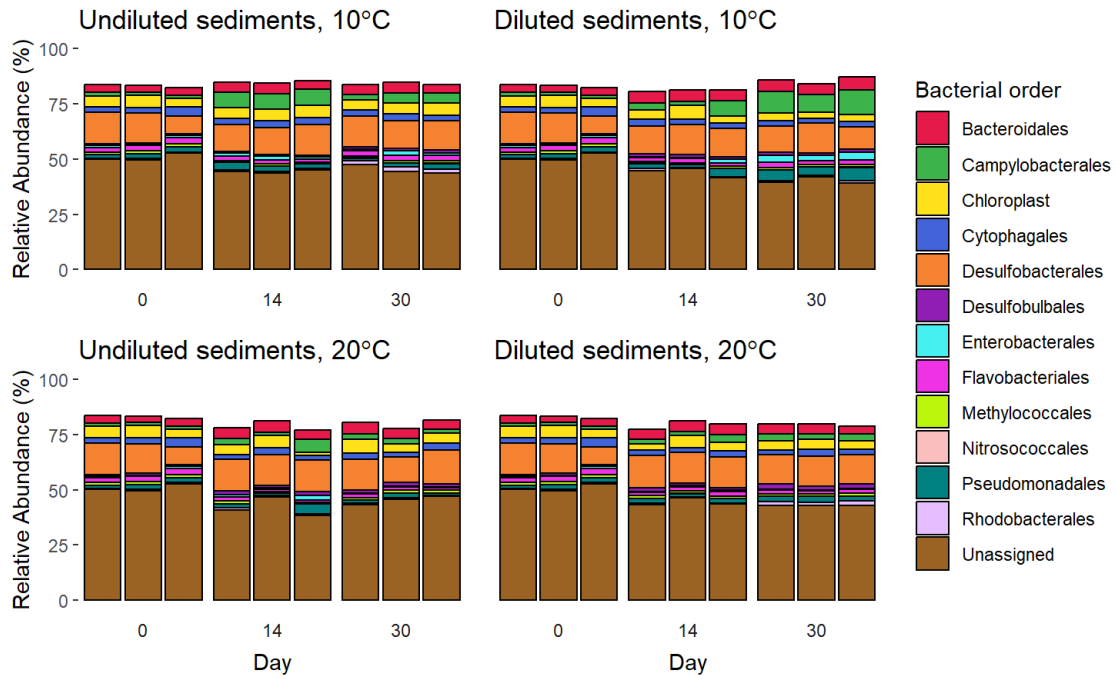

Figure A12: The 13 most abundant bacterial orders in the Cref microcosms, according to the Nanopore sequencing results. Sequences that could not be assigned to any bacterial order are dominant and represent more than half of the orders included in the figure. Aside from the unassigned sequences, *Desulfobacterales* seems to be the dominant bacterial order in all the microcosms.

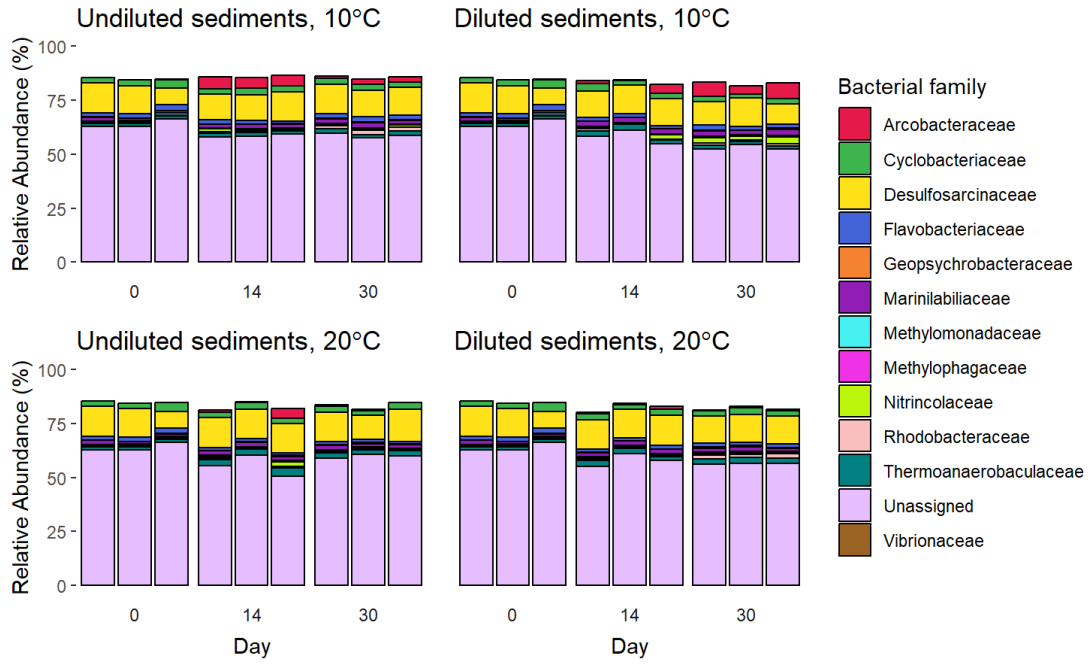

Figure A13: The 13 most abundant bacterial families in the Cref microcosms, according to the Nanopore sequencing results. Sequences that could not be assigned to any bacterial order are dominant and represent more than half of the bacterial sequences. Aside from the unassigned sequences, *Desulfosarcinaceae* and *Cyclobacteriaceae* seem to be the dominant bacterial families in all the microcosms.

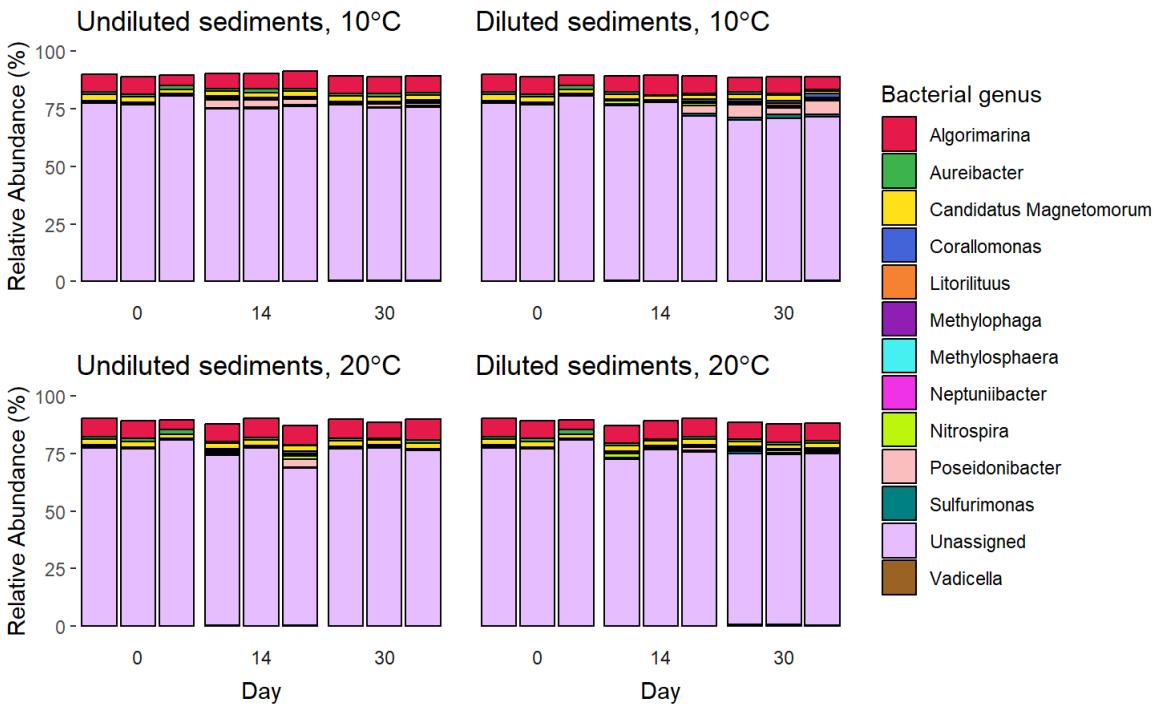

Figure A14: The 13 most abundant bacterial genera in the Cref microcosms, according to the Nanopore sequencing results. Sequences that could not be assigned to any bacterial order are dominant and represent >75% of the bacterial sequences. Aside from the unassigned sequences, *Algorimarina* seems to be the dominant bacterial order in all the microcosms.

The Oslo Fjord microcosms: Bacterial sequence composition.

The microcosm sediments harboured various bacteria. However, as the sequences were assigned to lower taxonomic ranks, the number of unassigned taxa increased from 5-15 % at phylum level to 60-85 % at genus level (A15-A18).

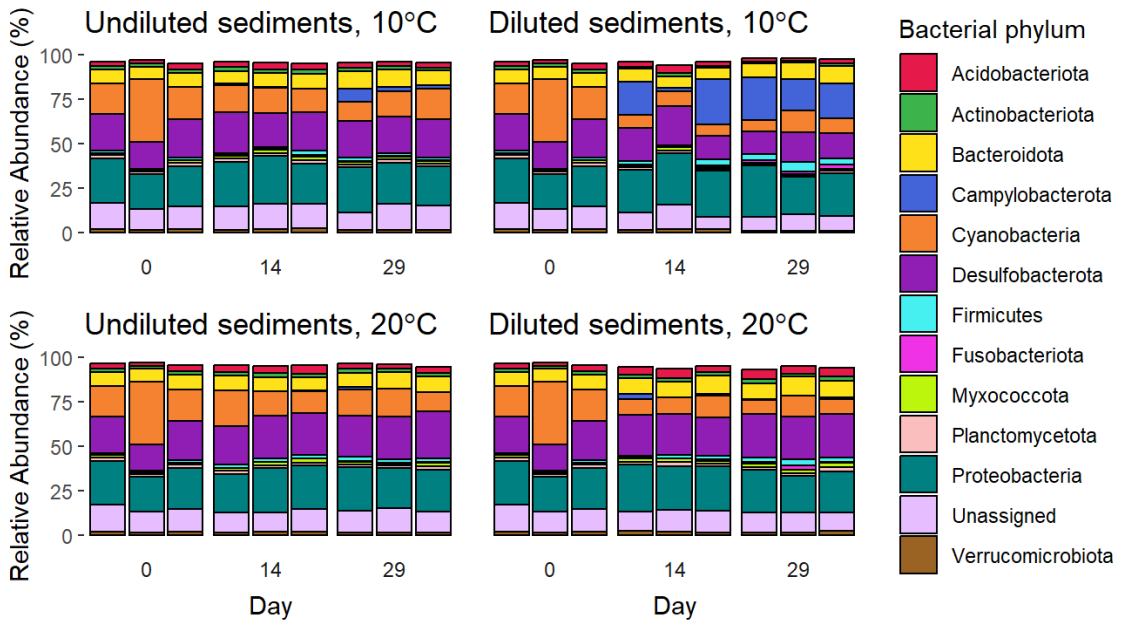

Figure A15: Top 13 bacterial phyla in the Oslo Fjord microcosm sediments according to the Nanopore 16S rRNA sequencing results. Sequences that could not be assigned to any phylum represent 5-15 % of the sequences. *Bacteroidota*, *Cyanobacteria*, *Desulfobacterota*, and *Proteobacteria* seem to be the dominant phyla in all microcosms. *Campylobacteria* were seemingly enriched in diluted sediments at 10˚C.

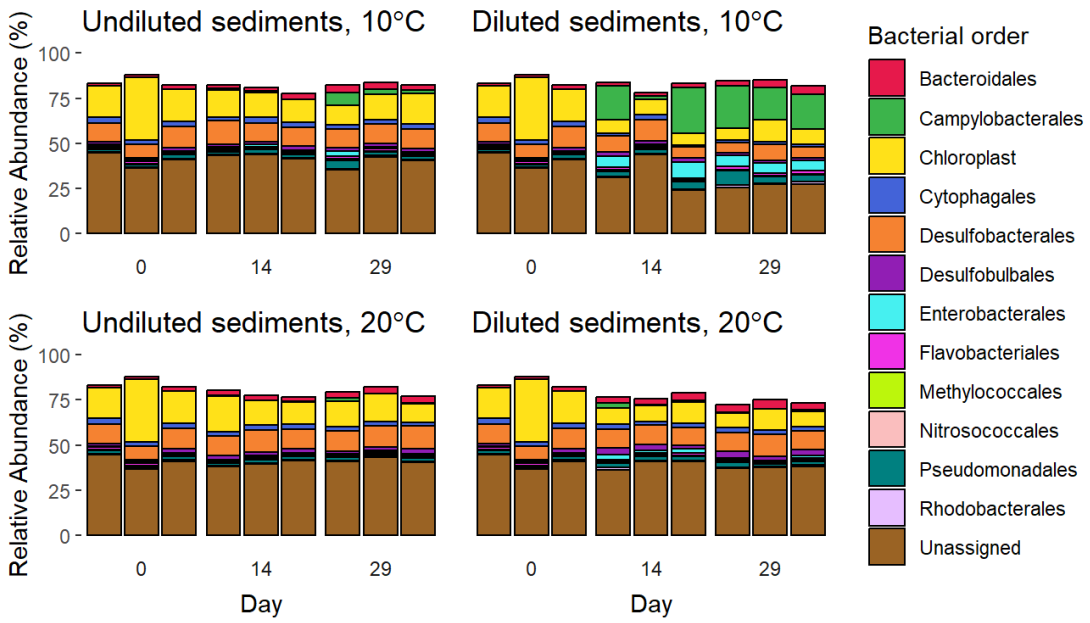

Figure A16: Top 13 bacterial orders in the Oslo Fjord microcosm sediments according to the 16S rRNA sequencing results. Sequences that could not be assigned to any order represent 25-45 % of the sequences. Aside from the unassigned sequences, *Chloroplast* and *Desulfobacterales* seem to be relatively abundant in all microcosms. However, after two weeks of microcosm, *Campylobacterales* and *Enterobacterales* were enriched in diluted sediments at 10˚C.

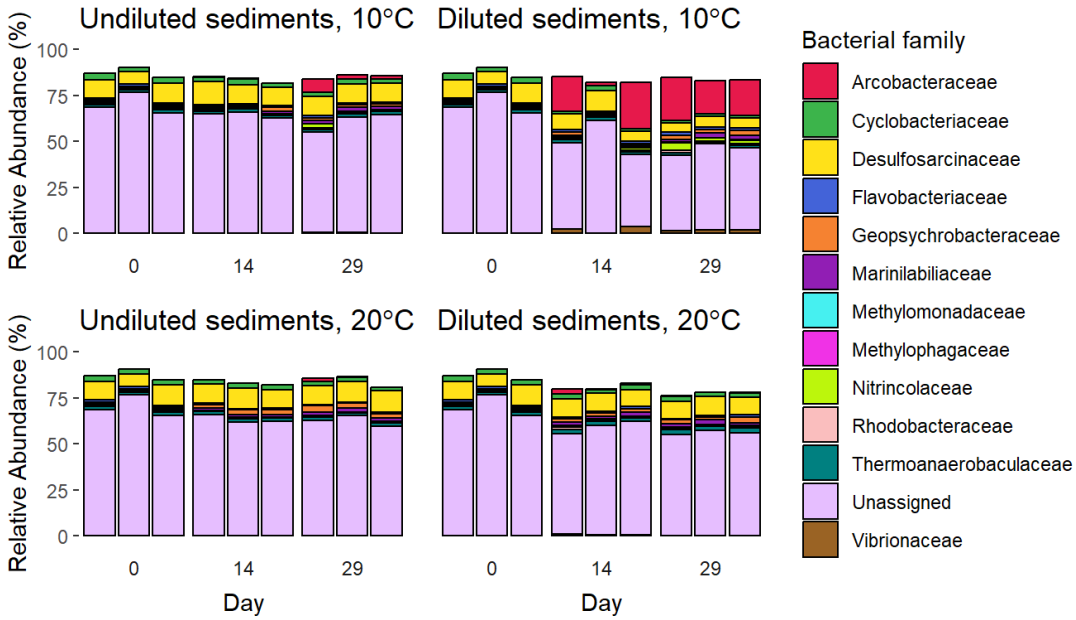

Figure A17: Top 13 bacterial families in the Oslo Fjord microcosm sediments according to the Nanopore 16S rRNA sequencing results. Sequences that could not be assigned to any family represent 50-80 % of the sequences. Aside from the unassigned sequences, *Desulfosarcinaceae* seems to be relatively abundant in all microcosms. However, *Arcobacteraceae* were enriched in diluted sediments at 10˚C.

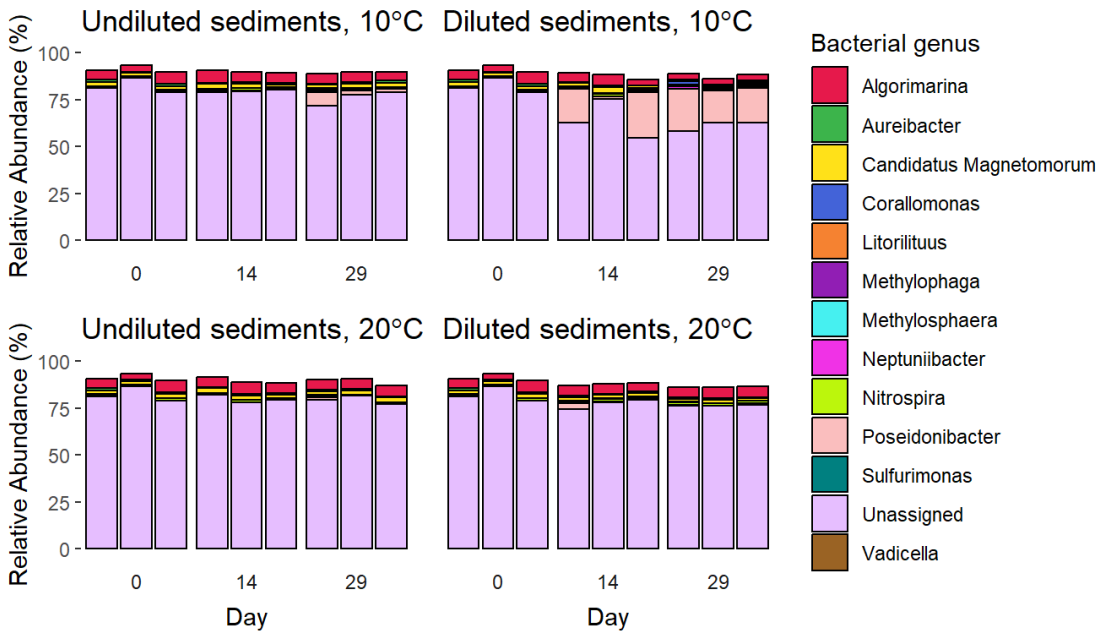

Figure A18: Top 13 bacterial genera in the Oslo Fjord microcosm sediments. Sequences that could not be assigned to any genus represent 60-85 % of the sequences. Aside from the unassigned sequeces, *Algomarina* was relatively abundant in all the microcosms. However, after two weeks of microcosm, *Poseidonibacter* were enriched in diluted sediments at 10˚C.

The pollution experiment: Descriptive figures of the archaeal sequence composition.

The control and polluted sediments harboured various archaea. However, the relative abundance of archaeal 16S rRNA sequences that were not assigned any taxon increased with decreasing taxonomic ranks, from approximately 1-5 % at phylum level to approximately 59-82 % at genus level (Figures A19-A21).

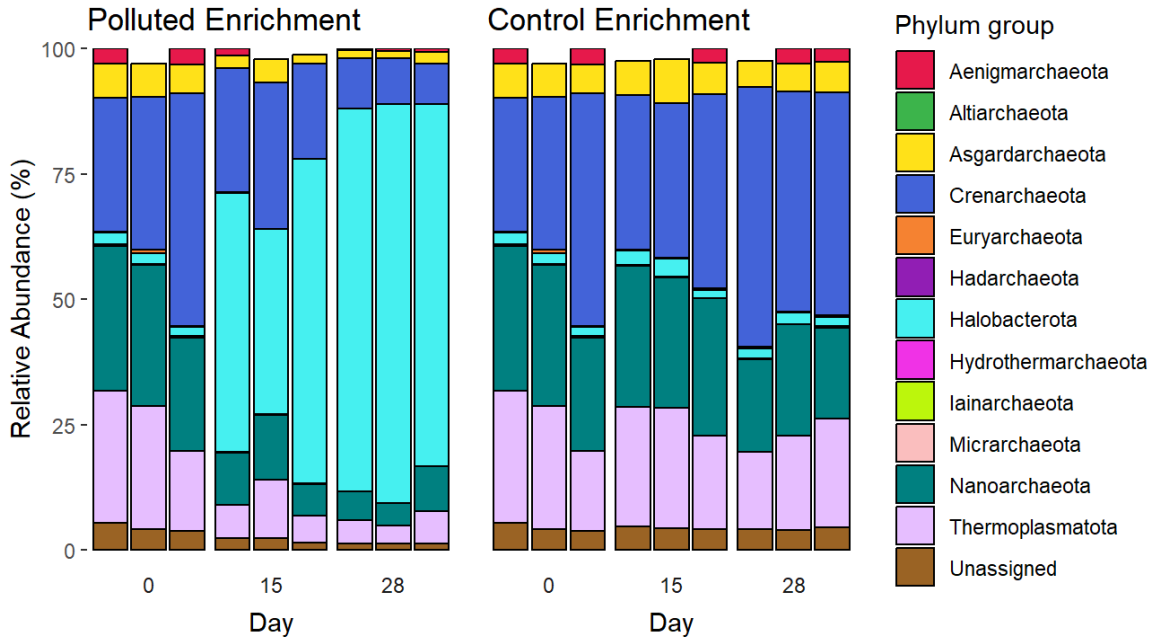

Figure A19: The 13 most abundant archaeal phyla in the pollution experiment microcosms, according to the Nanopore sequencing results. *Aenigmarchaeota, Asgardarchaeota, Crenarchaeota, Euryarchaeota, Halobacterota, Nanoarchaeota,* and *Thermoplasmatota* displayed different relative abundances in the polluted and control sediments (Wilcoxon $p < 0.05$). *Halobacterota* was seemingly enriched in the polluted sediments, while *Crenarchaeota* seemed to be enriched in the control sediments.

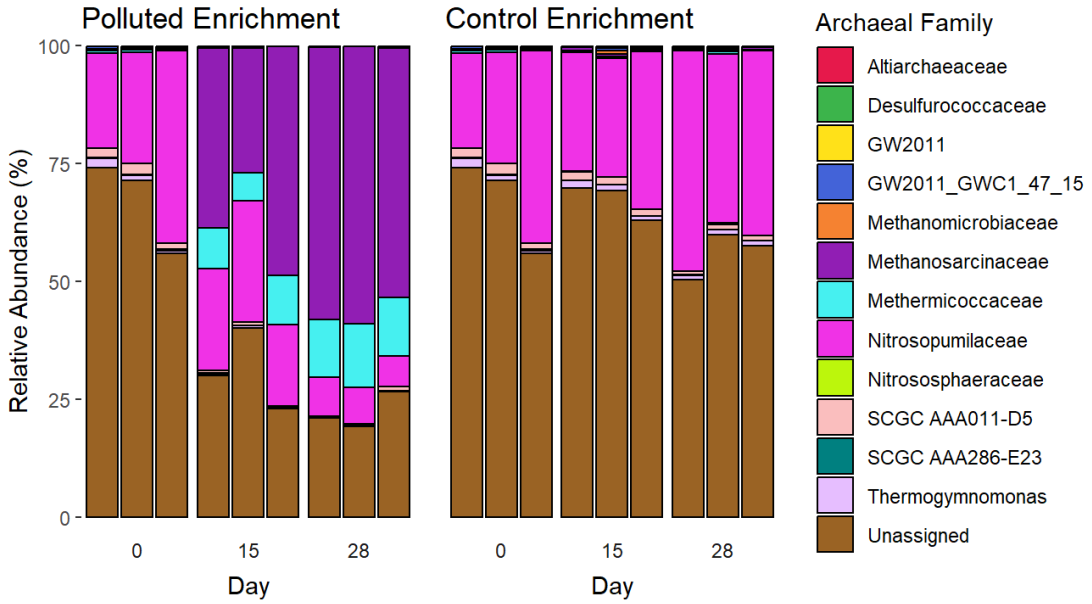

Figure A20: The 13 most abundant archaeal families in the pollution experiment microcosms, according to the Nanopore sequencing results. *Methanosarcinaceae, Methermicoccaceae, Nitrosopumilaceae,* and *Thermogymnomonas* displayed different relative abundances in the polluted and control sediments (Wilcoxon $p < 0.009$ for all). *Methanosarcinaceae* and *Methermicoccaceae* were seemingly enriched in the polluted sediments, while *Nitrosopumilaceae* seemed to be enriched in the control sediments.

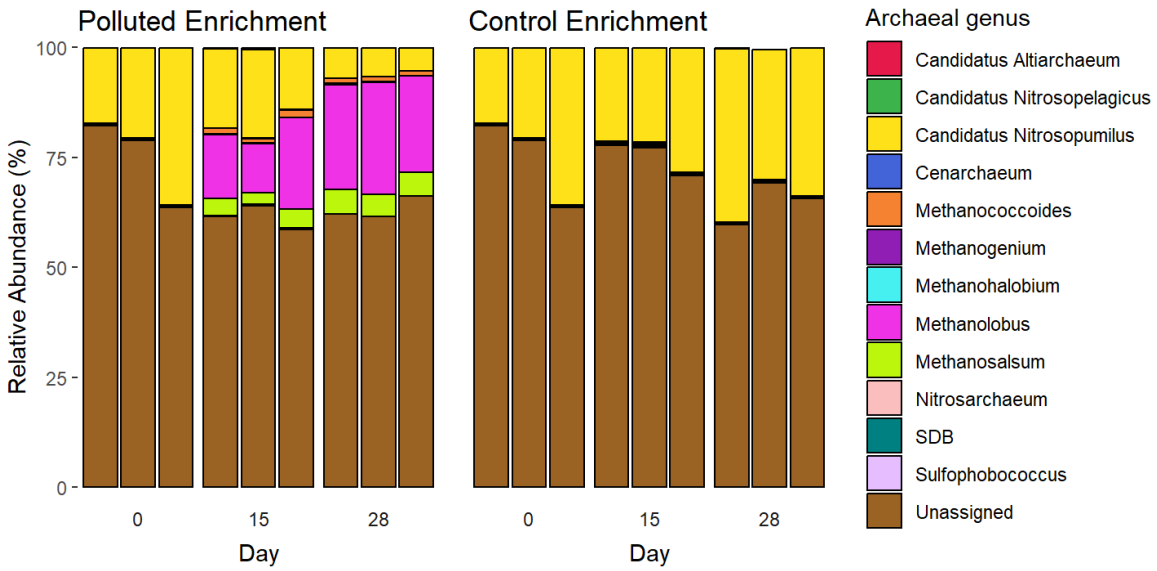

Figure A21: The 13 most abundant archaeal families in the pollution experiment microcosms, according to the Nanopore sequencing results. *Methanolobus, Methanohalobium, Methanococcoides, Methanosalsum, Cenarchaeum* and *Candidatus* Nitrosopumilus displayed different relative abundances in the polluted and control sediments (Wilcoxon $p < 0.009$ for all). *Methanolobus, Methanococcoides,* and *Methanosalsum* were seemingly enriched in the polluted sediments, while *Candidatus* Nitrosopumilus seemed to be enriched in the control sediments.

The pollution experiment: PCoA of the archaeal sequence composition.

The PCoA of the archaeal phyla in the pollution experiment indicates that the first principal coordinate explains 82.3 % of the variation and correlates 99.9 % with *Halobacterota* (Figure A22). This corresponds well to the observation that *Halobacterota* seems to be enriched in the polluted microcosm but is barely present in the control microcosm (Figure A19). Most of the remaining archaeal phyla were grouped around the control sample cluster (Figure A22). The same trend was observed at all taxonomic ranks (Figures A23-A25), indicating that *Methanolobus* and *Methanosalsum*, both belonging to the family *Methanosarcinaceae* and class *Methanosarcinia*, were the two genera responsible for most of the variation between the polluted and control sediments.

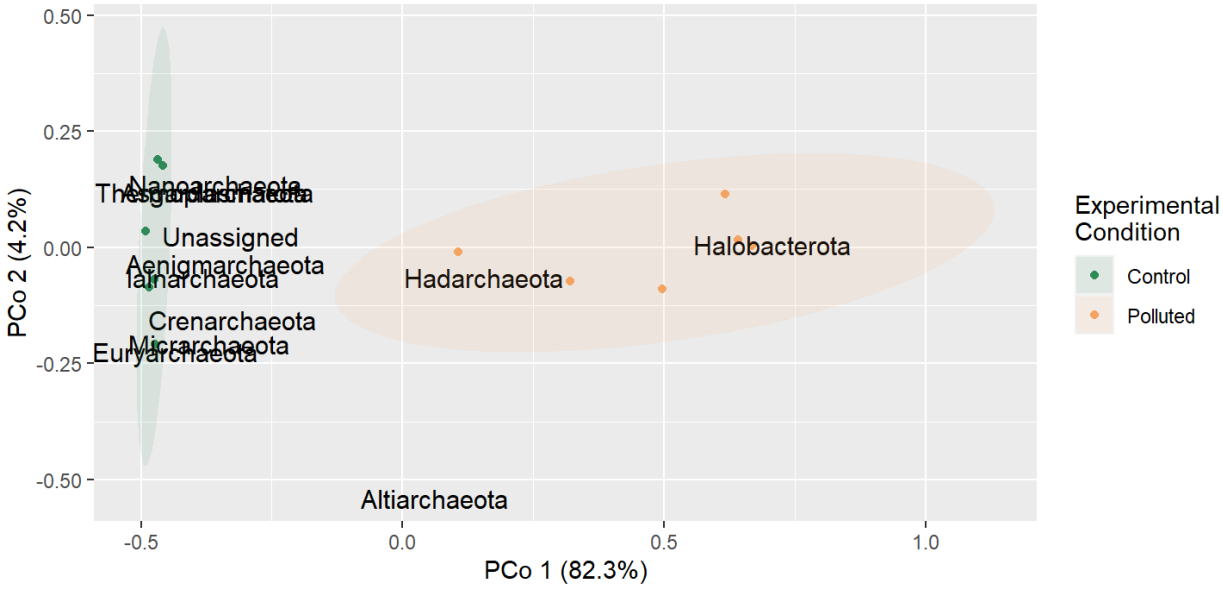

Figure A22: PCoA of the pollution experiment based on the archaeal sequencing data. The loadings of each archaeal phylum is indicated in text. The principal coordinates (PCo1 and PCo2) explaining most of the variation in the data are used as axes. The 95% confidence intervals of the sample groups (polluted and control) are indicated with coloured ellipses and form distinct clusters with no overlap. PCo1 explains 82.3% of the variation in the data, and is also responsible for most of the separation of the two clusters. *Halobacterota* correlates 99.9 % with PCo1.

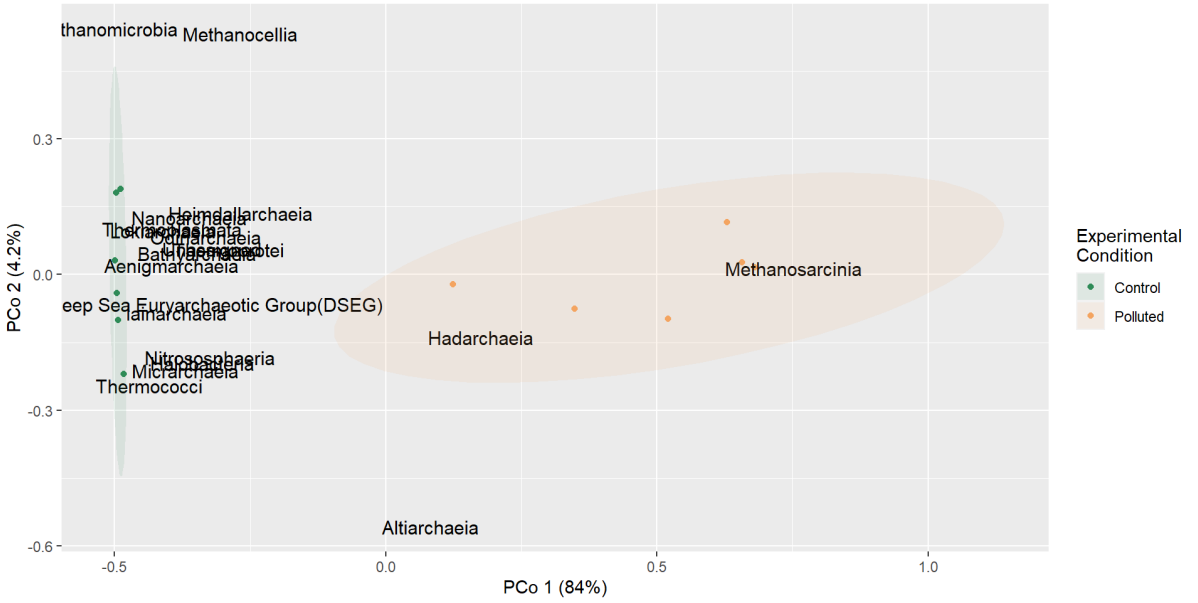

Figure A23: PCoA of the pollution experiment based on the archaeal sequencing data. The loadings of each archaeal class are indicated by text labels. PCo1 and PCo2 are the principal coordinates explaining most of the variation in the data. The 95% confidence intervals of the sample polluted and control samples are indicated with coloured ellipses and form distinct clusters with no overlap. PCo1 explains 84 % of the variation in the data, and is also responsible for most of the separation of the two clusters. *Halobacterota* correlates 99.8 % with PCo1, while all other phyla correlate < 8 % with PCo1. None of the archaeal classes correlate strongly with PCo2, which explains 4.2 % of the variation in the data.

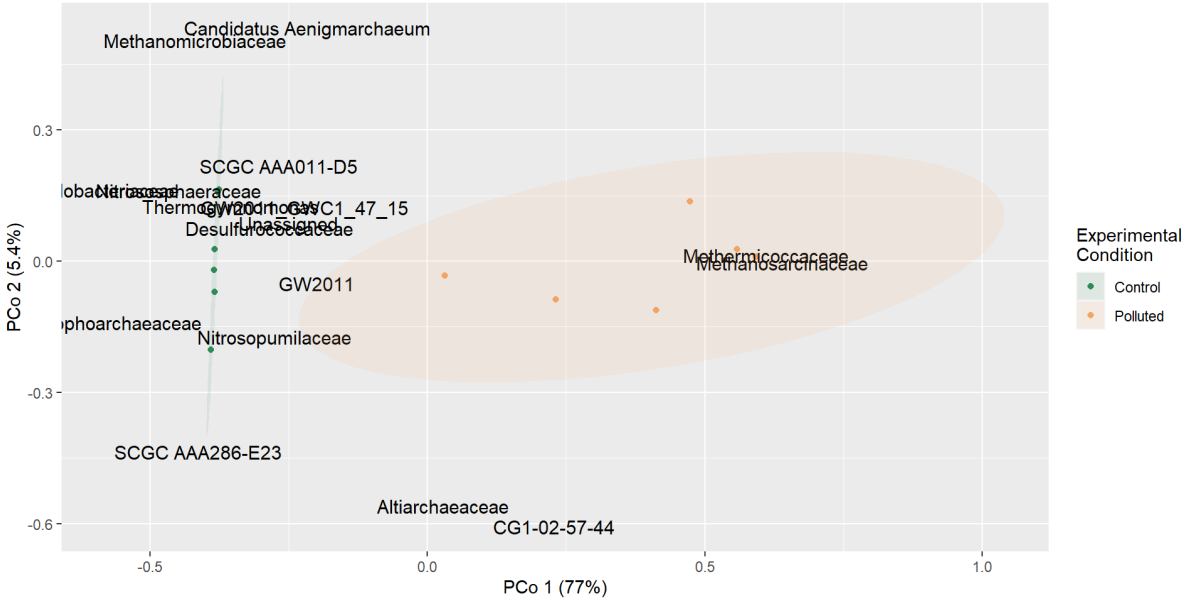

Figure A24: PCoA of the pollution experiment based on the archaeal sequencing data. The loadings of each archaeal family are indicated by text labels. PCo1 and PCo2 are the principal coordinates explaining most of the variation in the data. The 95% confidence intervals of the sample polluted and control samples are indicated with coloured ellipses and form distinct clusters with no overlap. PCo1 explains 77 % of the variation in the data, and is also responsible for most of the separation of the two clusters. PCo1 correlates 99.99 % with

Methanosarciniaceae and 99.98 % with *Methermicoccaceae*, while all other phyla correlate < 21 % with PCo1. None of the archaeal classes correlate strongly with PCo2, which explains 5.4 % of the variation in the data.

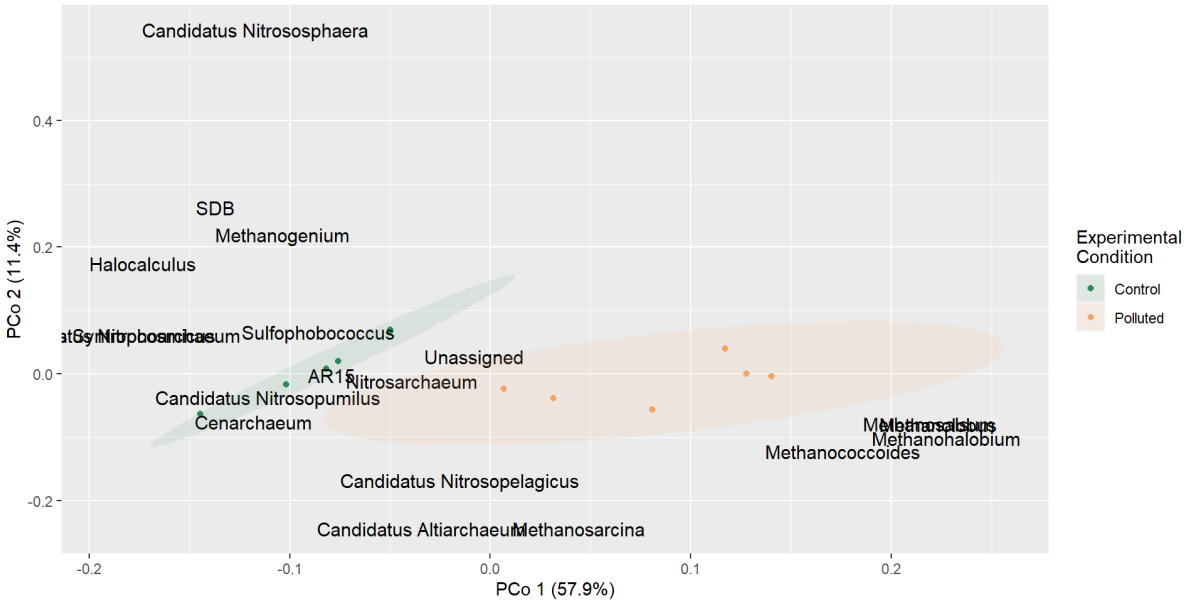

Figure A25: PCoA of the pollution experiment based on the archaeal sequencing data. The loadings of each archaeal genus are indicated by text labels. PCo1 and PCo2 are the principal coordinates explaining most of the variation in the data. The 95% confidence intervals of the sample polluted and control samples are indicated with coloured ellipses and form distinct clusters with no overlap. PCo1 explains 57.9 % of the variation in the data, and is also responsible for most of the separation of the two clusters. PCo1 correlates 97 % with *Methanolobus,* 96 % with *Methanosalsum,* and 85 % with *Methanohalobium* and *Methanococcoides,* while all other phyla correlate < 9 % with PCo1. The group of unassigned sequences correlates 90 % with PCo2, which explains 5.4 % of the variation in the data.

The pollution experiment: Descriptive figures of the bacterial sequence composition.

The control and polluted sediments harboured various bacteria. However, as the sequences were assigned to taxa at lower taxonomic ranks, the number of unassigned taxa increased from 7-13 % at phylum level to 57-62 % at genus level (Figures A26-A29).

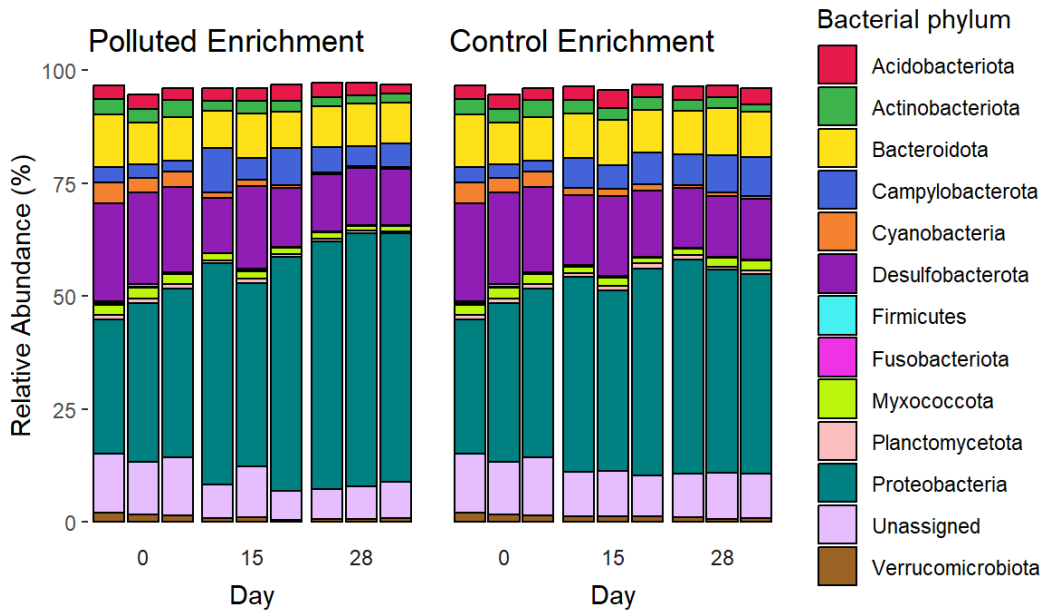

Figure A26: The 13 most abundant bacterial phyla in the pollution experiment microcosms, according to the Nanopore sequencing results. *Bacteroidota* ($p = 0.01$) and *Proteobacteria* ($p = 0.04$) were the only bacterial phyla displaying different abundances in the polluted and control microcosms at 15 and 28 days, according to the Wilcoxon rank sum test.

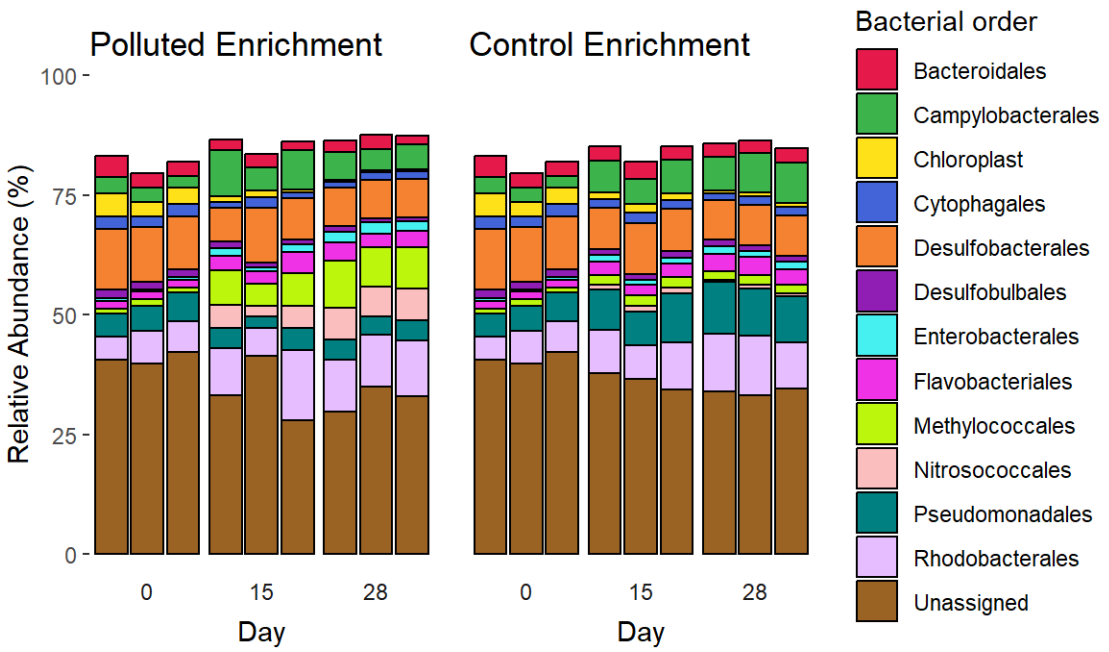

Figure A27: The 13 most abundant bacterial orders in the pollution experiment microcosms, according to the Nanopore sequencing results. A large portion of the reads were not assigned a class. *Methylococcales*, *Nitrosococcales,* and *Pseudomonadales* displayed different abundances in the polluted and control microcosms at 15 and 28 days, according to the Wilcoxon rank sum test (p = 0.002 for all).

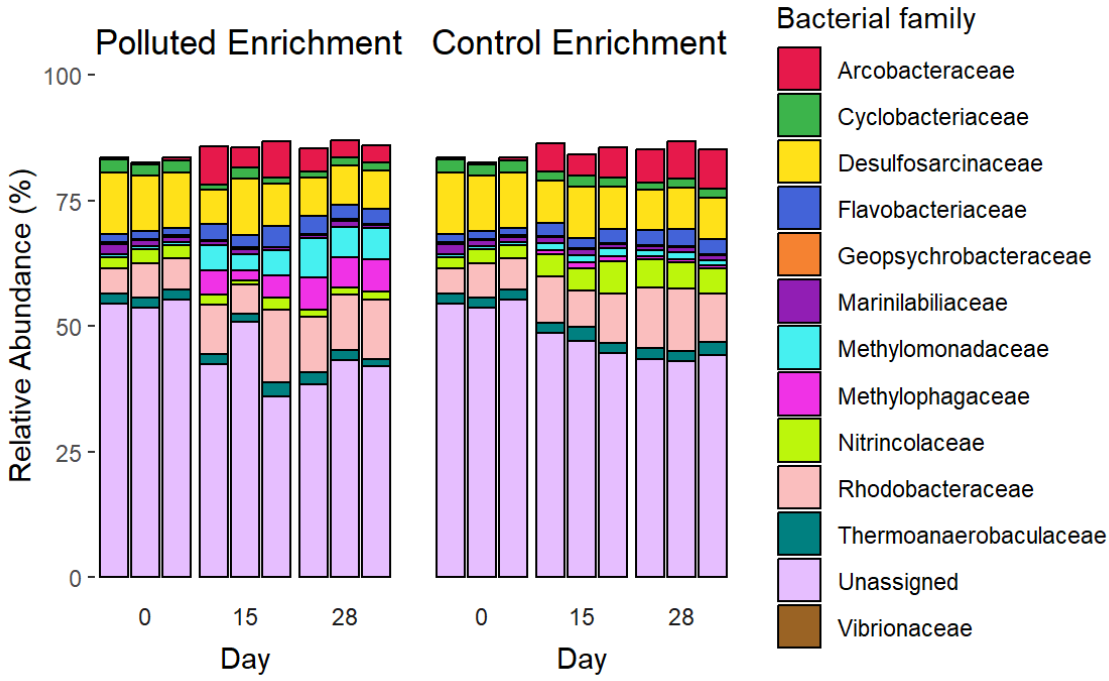

Figure A28: The 13 most abundant bacterial families in the pollution experiment microcosms, according to the Nanopore sequencing results. A large portion of the reads were not assigned a family. The *Methylomonadaceae*, *Methylophagaceae,* and *Nitrincolaceae* displayed different abundances in the polluted and control microcosms at 15 and 28 days, according to the Wilcoxon rank sum test (p = 0.002 for all).

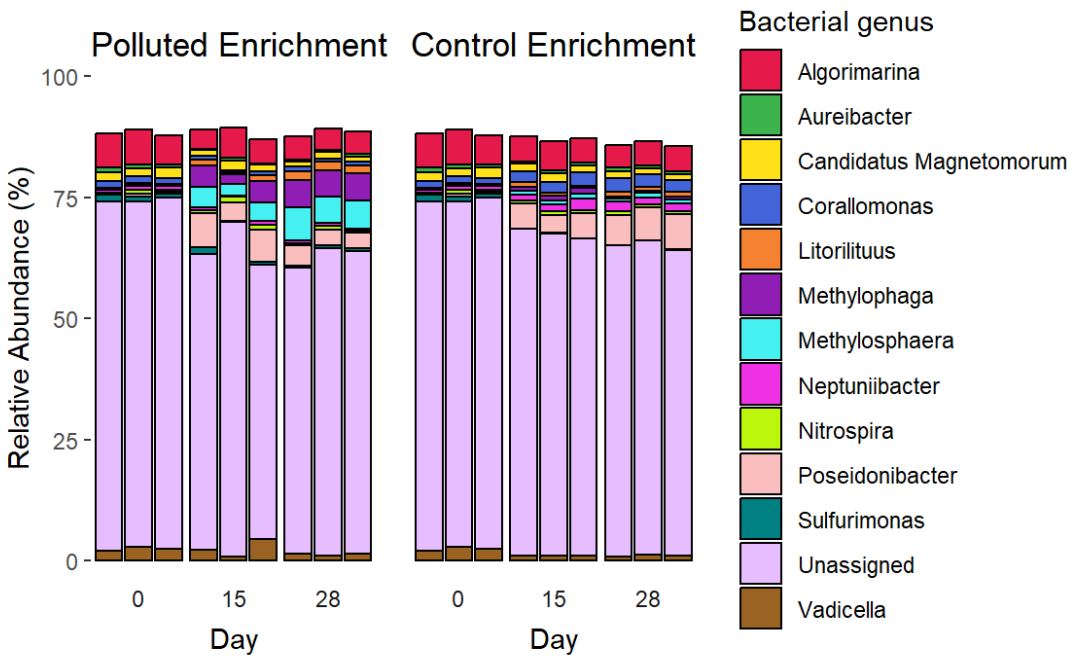

Figure A29: The 13 most abundant bacterial genera in the pollution experiment microcosms, according to the Nanopore sequencing results. A large portion of the reads were not assigned a genus. The genera *Corallomonas* (p = 0.002), *Methylosphaera* (p = 0.002), *Sulfurimonas* (p = 0.002), *Neptuniibacter* (p = 0.002), and *Methylpophaga* (p = 0.004) displayed different abundances in the polluted and control microcosms at 15 and 28 days, according to the Wilcoxon rank sum test.

The pollution experiment: PCoA of the bacterial sequence composition.

At phylum, class, and genus level, the 95 % confidence interval of the control sediment samples was largely covered by the 95 % confidence interval of the polluted sediments. However, at order and family level, the 95 % confidence intervals of the two microcosms were clearly separated. The bacterial families correlating the strongest with PCo1, which explained 45.9 % of the variation in the data, were *Marinobacteraceae* and *Methylococcaceae* (Figure A30). The bacterial loadings were not plotted because there were too many bacterial taxa to visualise.

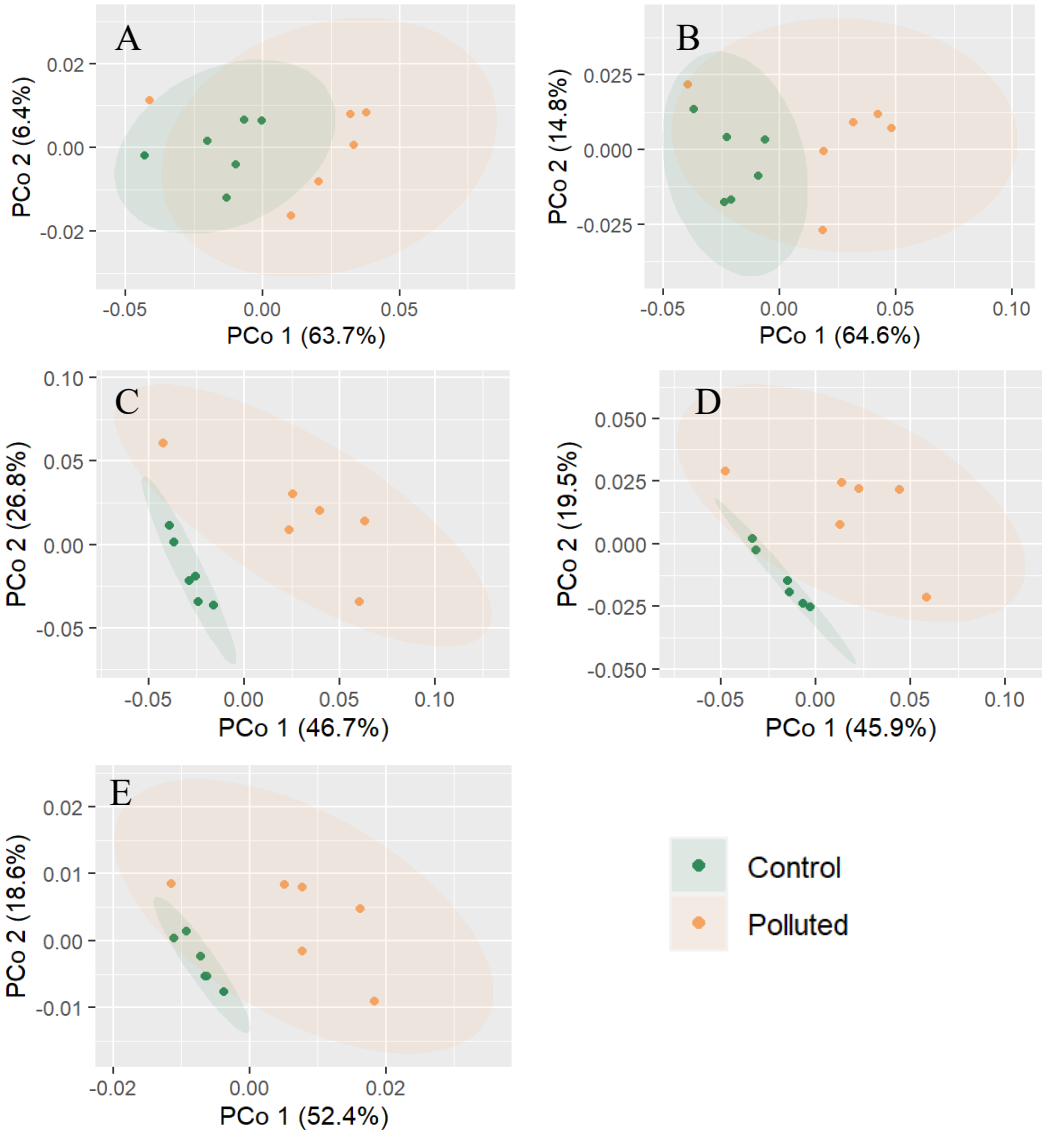

Figure A30: Plots of the principal coordinates explaining the most variation in bacterial abundances in the pollution experiment microcosms. The ellipses cover the 95 % confidence intervals (CI's) of the control samples (green) and the samples from the polluted microcosm (orange). Each plot display the principal coordinates at different taxonomic ranks of bacteria. Loadings are not included in the figure, but the most significant ones are mentioned below. **A: Phylum level**. PCo1 explains 63.7 % of the variation and correlates 0.99 with *Proteobacteria*. The control group CI is mostly covered by the CI of the polluted group. **B: Class level**. PCo1 explains 64.6 % of the variation and correates 0.96 with *Gammaproteobacteria*. The control group's CI is mostly covered by the polluted group's CI. **C: Order level**. The control group and the polluted group are clearly distinct when the variation is explained by PCo1 and PCo2, in which case PCo1 accounts for most of the grouping. PCo1 explains 46.7 % of the variation and correlates 0.89 with *Methylococcales* and *Nitrosococcales*. PCo2 explains 26.8 % of the variation and correlates 0.86 with *Desulfuromonadales.* **D: Family level.** The CI's of the control and polluted groups partially overlap when explained by PCo1 and PCo2. PCo1 explains 45.9 % of the variation and correlates 0.88 with *Marinobacteraceae* and 0.87 with *Methylococcaceae*. PCo2 explains 19.5% of the variation and does not correlate strongly with any particular bacterial family. **E: Genus level.** The CI's of the control and polluted groups partially overlap. PCo1 explains 52.4% of the variation and correlates > 0.9 with *Marinobacter*

and *Halarcobacter*, and > 0.8 with *Flavivirga, Methylophaga, Methylosphaera,* and *Arenitalea.* PCo2 explains 18.6% of the variation and does not correlate strongly with any particular genera.

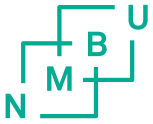

Norges miljø- og biovitenskapelige universitet
Noregs miljø- og biovitskapelege universitet
Norwegian University of Life Sciences

Postboks 5003
NO-1432 Ås
Norway